Rhenium(I) and -(V) Complexes of N-donor Heterocyclic Chelates

by

Ifeoma Ebinumoliseh

Submitted in the fulfilment
of the requirements for the degree of
Master of Science
in the School of Chemistry and Physics at the
University of KwaZulu-Natal

March 2016

Supervisors: **Dr. Alex B. Xulu** and **Dr. Irvin N. Booysen**

As the candidates' supervisors, we have approved this dissertation for submission:

Signed: _____ Date: _____

Signed: _____ Date: _____

Abstract

The fundamental coordination chemistry of rhenium still has a pivotal role to play towards the development of functional rhenium radiopharmaceuticals with target-specific biodistribution patterns. One of the numerous design considerations to take into account is the use multidentate chelators that can potentially stabilize oxorhenium(V) complexes but also offer a manner of which to manipulate the hydrophobicity and lipophilicity of rhenium complexes through derivatization of their multidentate chelators. In contrast to these oxorhenium(V) complexes which are prone to oxidation to $[ReO_4]^-$ by water, rhenium(I) complexes containing the *facial* tricarbonyl rhenium(I) core, *fac*-$[Re^I(CO)_3]^+$ are typically stable in aqueous media. Furthermore, the chemical inertness and the small size of the *fac*-$[Re^I(CO)_3]^+$ core relative to the size of Re(V) core makes it ideal for the design of novel rhenium radiopharmaceuticals. In addition, the remaining coordination sites of the *fac*-$[Re^I(CO)_3]^+$ core could be utilized for coordination to scaffolds incorporating biological entities which can potentially manipulate the biodistribution patterns of formulated rhenium(I) radiopharmaceuticals. The integrated and bifunctional design approaches towards rhenium radiopharmaceutical design will need to be enforced which involves the inclusion of biologically relevant moieties in multidentate chelators or attachment of biological relevant moieties to bifunctional chelators.

In chapter 3, the coordination behaviours of multidentate diimines encompassing chromone moieties are considered. The formation of a novel rhenium (I) complex, *fac*-$[Re(CO)_3$(chrpychr)] (**1**) from the equimolar coordination reaction between [2-(4-oxo-4*H*-chromen-3-*yl*)-5*H*-chromeno[2,3-*d*]pyrimidin-5-one] (chrpychr) and $[Re(CO)_5Br]$. In addition, the formation and characterization of a novel dinuclear rhenium(I) compound, *fac*-$(Re(CO)_3Br)_2$(μ-chret) (**2**) [*chret* = *N, N'-bis*((2-amino-3-imino)methylenechromone-1,2-ethane] and a mononuclear metal complex, *fac*-$[Re(CO)_3$(bzch)Br] (**3**) [bzch = 2-benzimidazole-4*H*-chromen-4-one]. The metal

complexes were characterized by ^{1}H NMR-, IR-, UV-Vis, melting point and conductivity measurements. The solid-state structures for the metal complexes were confirmed *via* single crystal X-ray analysis. The simulated IR spectra for the respective metal complexes provided insight in the interpretation of their corresponding experimental spectra.

Chapter 4 entails the isolation of novel rhenium(I) and -(V) complexes with perimidine ligands incorporating fused N-donor heterocyclics. The equimolar coordination reactions of 2-(benzothiazole)-2,3-dihydro-1*H*-perimidine (bzpm) and 2,3-dihydro-2-(pyridine)-1*H*-perimidine (pypm) with [$Re(CO)_5Br$] afforded the rhenium(I) complexes: *fac*-[$Re(CO)_3$(bzpm)Br](**1**) and *fac*-[$Re(CO)_3$(pypm)Br](**2**), respectively. The oxo-free rhenium(V) complex, *cis*-[Re(pyrnp)$Br_2(PPh_3)$](**3**) {H_3pyrnp = 8-((1*H*-pyrrole)iminomethyl)naphthalene-1-amine} was isolated from the reaction of *trans*-[$ReOBr_3(PPh_3)_3$]with two-fold molar excess of 2,3-dihydro-2-(1*H*-pyrrole)-1*H*-perimidine (pyrpm). These metal complexes were characterized *via* ^{1}H NMR-, IR-, UV-Vis spectroscopy, melting point and conductivity measurements. Single crystal X-ray analysis provides a definitive confirmation of the structural elucidations of the metal complexes. The DNA binding interactions of the rhenium(I) metal complexes were evaluated through UV-Vis titrations with Calf-Thymus (CT)-DNA.

Keywords: Rhenium, Spectral Characterization, Crystal Structure, DFT studies, Perimidine, pyrrole, chromone, benzothiazole DNA binding.

Preface

All experimental works described in this research study were carried out in the School of Chemistry and Physics at the University of KwaZulu-Natal, Pietermaritzburg Campus from August 2013 to December 2015, under the supervision of Doctor Alex B. Xulu and Doctor Irvin N. Booysen.

This work is original and have been undertaken by the author and have not otherwise been submitted in any form for any degree to any tertiary institution. Where use has been made of the work of others, it is duly acknowledged in the text.

Declaration 1 – Plagiarism

I, Ifeoma Ebinumoliseh declare that

1 The research reported in this dissertation, except where otherwise indicated is my original research.
2 This dissertation has not been submitted for any degree or examination at any other university.
3 This dissertation does not contain other person's data, pictures, graphs or other information, unless specifically noted as being sourced from other persons.
4 This dissertation does not contain other person's writing unless specifically stated as being sourced from other researchers. Where other written sources have been quoted, then
    a. There words have been re-written but the general information attributed to them has been referenced.
    b. Where their exact words have been used, then their writing has been placed in italics and inside quotation marks, and referenced.
    c. This thesis does not contain text, graphics or tables copied and pasted from the internet, unless specifically acknowledged, and the source being detailed in the thesis and in the References sections.

Signed: _____

Declaration 2 - Publications:

Manuscript published:

1. Irvin Noel Booysen, Ifeoma Ebinumoliseh, Matthew Piers Akerman, Bheki Xulu, A *Rhenium(I) compound bearing a dimerized Chromone NO bidentate chelator,* Inorg. Chem. Comm. 62 (2015) 8-10.

Manuscripts in preparation:

1. Ifeoma Ebinumoliseh, Irvin Noel Booysen, Matthew Piers Akerman, Bheki Xulua, *Formation, characterization and computational studies of mono- and dinuclear Rhenium(I) Chromone compounds*.
2. Irvin Noel Booysen, Ifeoma Ebinumoliseh, Siphamandla Sithebe, Matthew Piers Akerman, Bheki Xulu, *Coordination behaviours of Perimidine ligands incorporating fused N-donor heterocyclics towards Rhenium(I) and –(V).*

The compounds involved in all the aforementioned manuscripts have been synthesized, characterized and analyzed by myself. Single crystal samples were run and solved by Dr M. Akerman.

Signed: _____ Signed: _____

Ifeoma Ebinumoliseh *Dr B.A. Xulu*

Signed: _____

Dr I.N. Booysen

Acknowledgement

I would like to express my sincere gratitude to God, without whom I would not have found enough strength to survive this research project.

Many thanks to Dr. Irvin N. Booysen for the supervision of this research project, his readiness to support with apt ideas and the innumerable hours and time he invested in this research project.

I appreciate Dr. Alex B. Xulu's relentless support and guidance all through this research project. There were many times when I felt like throwing in the towel but his comforting words were impactful at those times.

I thank Prof. Orde Q. Munro for his fatherly role, Dr. Matthew P. Akerman for his patience and expertise with the crystallographic analysis as well as Dr. S. Sithebe for his ingenious ideas with some synthetic procudures.

I am grateful to my research group members, including Muhammed Ismail Bilaal and Sumayya Chohan as well as other chemistry colleagues for their help and encouragement.

I am immensely grateful to the National Research Foundation (NRF) for funding and to the Chemistry Department at the University of KwaZulu-Natal for providing laboratory space and equipment.

I am eternally grateful to my mother, Mrs Beatrice Ebinum, my sisters; Danumego Mpamugo, Ihinosen Ebinum, Ebelechukwu Ebinum and my brothers; Kenneth

Ebinum and Anthony Ebinum for their love and support. There is no way I would have survived the rigors of this research project without their outstanding support.

Crystallographic Data

Supplementary data for all the crystal structures obtained during this study are stored on a compact disk that is attached to the inside back cover of this dissertation. The following are the data.

- Final coordinates and equivalent isotropic displacement parameters of the non-hydrogen atoms;
- Final crystal data and details of the structure determinations;
- Isotropic displacement parameters;
- Hydrogen atom positions;
- Contact distances;
- Torsion angles;
- Hydrogen-bonds.

Table of Contents

Abstract ii

Preface iv

Declaration 1 v

Declaration 2 vi

Acknowledgements vii

Chapter 1

Introduction

1.1 General Background 1

1.2 Aim and Motivation 2

1.3 Schiff Bases and their *d*-block Metal Complexes 6

1.4 Rhenium Radiopharmaceuticals 8

1.5 General Chemistry of Rhenium(I) and –(V) 12

1.6 Coordination Chemistry of Rhenium(I) and –(V) 14

1.7 References 18

Chapter 2

Materials and Methods

2.1 Handling Rhenium 21

2.2 Materials 21

2.3 Instrumentation 23

2.4 References 24

Chapter 3

Formation, Characterization and Computational Studies of Mono- and Dinuclear Rhenium (I) Chromone Compounds

3.1 Introduction 25

3.2 Experimental 27

3.3 Results and Discussion 32

3.4 Reference 53

Chapter 4

Coordination behaviours of Perimidine ligands incorporating fused N-donor heterocyclics towards Rhenium(I) and –(V)

4.1 Introduction 59

4.2 Experimental 61

4.3 DNA Binding Studies 68

4.4 Results and Discussion 69

4.5 Reference 84

Chapter 5

Conclusion and Future Work 89

Chapter 1

Introduction

1.1 General background:

The continued expansion on the coordination chemistry of rhenium reflects its diverse applications in radiopharmacy, catalysis and bioluminescence [**1**-**3**]. The main attribute owing to rhenium's various applications, it's the fact that metal complexes with oxidation states ranging from −1 to +7 have been reported, *e.g.* $NH_4Re^{VII}O_4$ [**4**-**5**]. This chemical versatility is emphasized in a number of robust chemical cores which can stabilize rhenium in high (*e.g.* $[ReN]^{3+}$, $[ReO]^{3+}$ and $[ReO_4]^{+}$) and low (*e.g. fac*-$[Re(CO)_3]^{+}$ and $[ReCl_3]^{3+}$) oxidation states [**4**]. Furthermore, the *in vivo* and *in vitro* bio-imaging capabilities of the low spin d^6 rhenium(I) complexes arises from its optimal photochemical properties [**6**]. Among the numerous catalytic rhenium compounds, methyltrioxorhenium (MTO) have been widely studied in the epoxidation of olefins and as catalytic oxidants [**7**].

In addition, the β-emitting 186/188-rhenium radionuclides have well-suited half-lives and β-max energies for the treatment of malignant growths in the body [**8**]. However, there are still challenges to design rhenium radiopharmaceuticals that can be synthesized *via* one-pot methods in high yields. In addition, other design criteria like charge, size, lipophilicity and hydrophobicity that influence the biodistribution of potential rhenium radiopharmaceuticals should also be taken into account [**9**]. Moreover, current design strategies for manipulating the biodistribution of a metallopharmaceuticals, is to incorporate a biologically active moiety in the coordination sphere of the metal complex or to make use of a bifunctional chelator which coordinates to the metal centre and covalently link to the biologically active moiety [**9**, **10**].

1.2 Aim and motivation:

The imperative of designing organorhenium compounds with biologically relevant moieties arises from the requirement that the next generation of rhenium radiopharmaceuticals must have target-specific biodistribution patterns [**9**]. Thus, we have investigated the design, syntheses, characterization and DNA binding studies of *facial* tricarbonylrhenium(I) and rhenium(V) complexes with multidentate chelates incorporating various biologically relevant moieties. These biologically relevant moieties includes chromone, benzothiazole, pyrrole and 1,3-dihydroperimidine, see **Figure 1.1.**

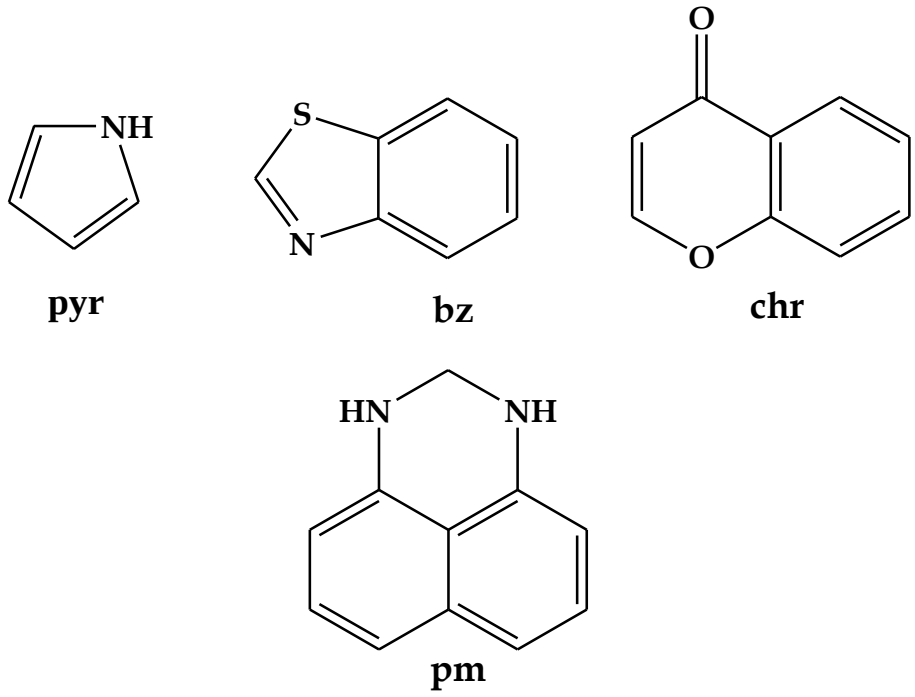

Figure 1.1: *Structures of the biologically active moieties (BAMs): pyrrole (pyr), benzothiazole (bz), chromone (chr) and 1,3-dihydroperimidine (pm).*

The chromone moiety is an important pharmacophore for a large number of pharmaceuticals with a variety of medicinal applications [**11**]. Typical examples include 3,7-substituted chromones (see, **Figure 1.2**) which have shown to be effective obesity suppressants and these molecules functions through binding to the melanin-concentrating hormone receptor 1 (MCH1R) [**12**]. Furthermore, the chromone moiety

is naturally occurring constituent found in the plant kingdom as secondary metabolites which allow chromone-derived drugs to be physiological biocompatible in cells while rendering diverse pharmacological activities in the treatment of several diseases. The aforementioned is illustrated by an alkaloid, Rohitukine extracted from the leaves and stems of Amoora Rohituka. This alkaloid exhibits antiinflammatory and immunomodulatory properties while showing moderate cytotoxicity against human HL-60 (*viz.* promyelocytic leukemia) and HCT-116 (*viz.* colon cancer cells) [**11**]. Furthermore, the isolation of rhenium(I) and –(V) compounds with chromone mono-imines have been successful and this provides an impetus for exploring the coordination behaviour of chromone diimines towards the $[Re^{V}O]^{3+}$ and *fac*-$[Re^{I}(CO)_3]^{+}$ cores [**13**, **14**].

Pyrroles can be found in various marine natural products, *e.g.* the Caribbean sponge *Agelas cerebrum* containing various bromopyrrole alkaloids (see **Figure 1.3**) which have showed optimal anticancer against various human tumour cells and antimalarial activities against various malaria strains [**15-19**].

Synthetic molecules containing the benzothiazole group have shown to exhibit unique structure-activity relationships. For example, the *bis*-benzothiazole derivatives showed superior herbicidal activities than their structural analogues containing one benzothiazole moiety each [**20].** In a survey of a series of benzothiazoles, it was been discovered that the benzothiazole derivative, ^{11}C-labelled 2-(4-methylaminophenyl)-6-hydroxybenzothiazole (known as Pittsburgh Compound B, see **Figure 1.4**) can provide diagnostics of amyloid deposits in the brain of patients suffering from Alzheimer's disease [**21**].

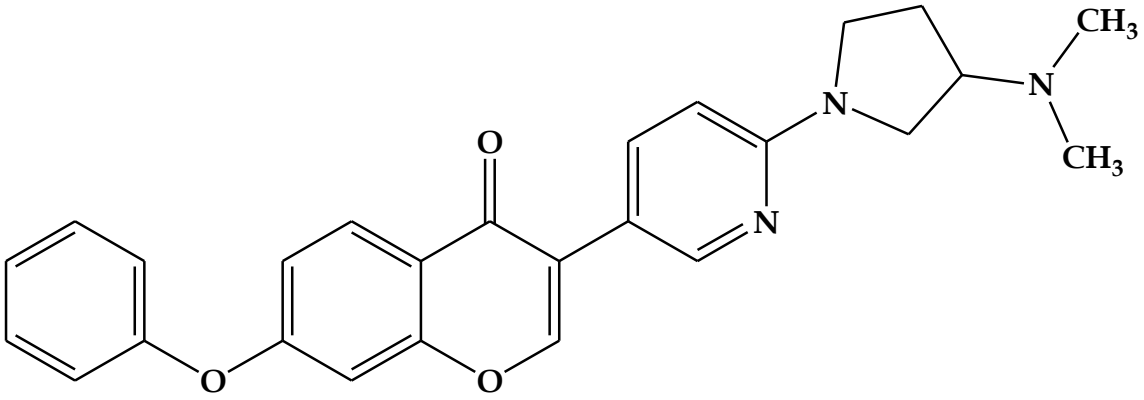

Figure 1.2: *Structure of 3-(N, N'-dimethyl-1-(pyridine)pyrrolidine-3-amine)-7-phenoxy-chromone which is a potential oral-administered obesity suppressor.*

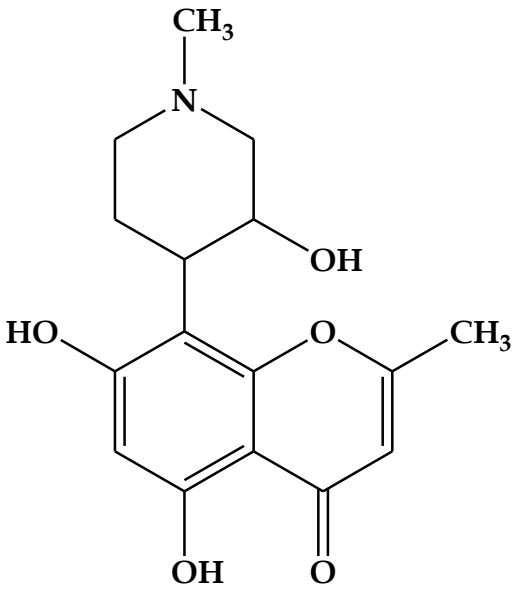

Figure 1.3: *Structure of Rohitukine (5, 7-dihydroxy-2-methyl-8-[4-(3-hydroxy-1-methyl)-piperininyl]-4-H-1-benzopyran-4-one).*

Besides the profoundly diverse biological activities of perimidines, this class of heterocyclic compounds and their metal complexes have been widely investigated as sensors and fluorescent switches due to their unique fused π-conjugated and non-conjugated systems [**22-25**]. For example, the perimidines: 4-(2,3-dihydro-1*H*-perimidin-2-*yl*)-2-methoxyphenol (see **Figure 1.5**) and 2-(quinoxalin-2-*yl*)-2, 3-

dihydro-1*H*-perimidine showed intense intra-ligand π-π^* relaxations in their respective emission spectra [**22**]. More interestingly, is that only 4-(2,3-dihydro-1*H*-perimidin-2-*yl*)-2-methoxyphenol exhibit solvatochromic effects ascribed to the variable degree of hydrogen-bonding between the methoxy group of the perimidine compound and the respective solvents used in the study. Hypothetically, combining the biological activities and luminescent properties of 1,3-dihydroperimidine (pm) chelators with the radiotherapeutic capabilities of rhenium radionuclides could lead to the development of dual diagnostic and therapeutic rhenium radiopharmaceuticals.

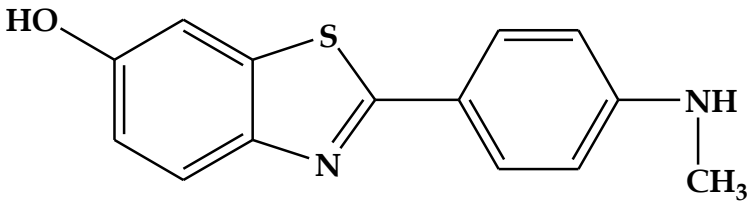

Figure 1.4: *Structure of the diagnostic radiopharmaceutical, ^{11}C-radiolabelled Pittsburgh compound.*

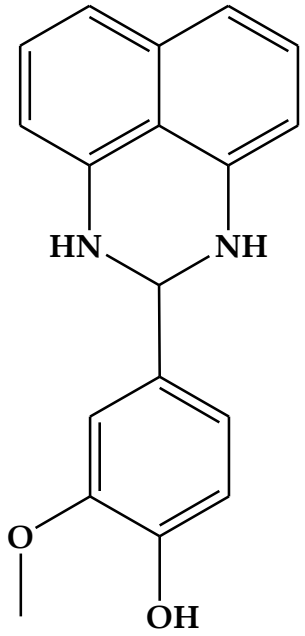

Figure 1.5: *Structure of a photoluminescent perimidine compound, 4-(2,3-dihydro-1H-perimidin-2-yl)-2-methoxyphenol.*

1.3 Schiff bases and their *d*-block metal complexes:

Tailoring the structural features of Schiff bases has become a simple but effective manner to manipulate the properties of the ligands and their transition metal complexes. For example, the appended groups connect to the imino bonds can be easily altered to influence the catalytic activities of Schiff bases of *d*-block metal complexes, *e.g.* upon increasing the number of chlorine substituents on the diimine, *N, N'-bis*(hydroxybenzylidene)-1,2-ethylenediamine framework for ruthenium(III) complex analogues, the efficiency of electrocatalytic epoxyoxidation of cyclooctene is evident from the increased turnover frequencies and current efficiencies of the diimine ruthenium(III)-based electrocatalysts [**26**]. Another advantage of Schiff bases as ligand is that biologically relevant moieties can be readily included in the framework of Schiff bases [**27**]. In **Figure 1.6**, the chromone moieties is integrated in the neutral bidentate azo-Schiff bases coordinated to selected first row transition metal complexes exhibiting octahedral geometries *via* the '2+2' coordination modes of the two azo-Schiff base chelates and the remaining coordination sites being occupied by *trans*-positioned chloro co-ligands. Significant to the aforementioned research study is that the highly *pi*-conjugated nature of the chromone-azo-Schiff bases allow the latter and its *3d* transition metal complexes to produce optimal high quantum yields and intense ligand-based fluorescence peaks.

Meticulous design of Schiff bases with the appropriate combinations of donor atoms can enforce preferential coordination of Schiff bases to specific metals in various oxidation states. In particular, oxovanadium(IV) and dioxovanadium(V) cores have been extensively shown to be stabilized by Schiff bases containing a combination of hard and soft donor atoms, see **Figure 1.7** [**28**]. Preferential coordination of a transition metal in different oxidation states is depicting by the variable coordination modes of the multidentate Schiff base, 2, 6-*bis*(2-hydroxyphenyliminomethyl)pyridine (H_2dhp) in [Re(dhp)(PPh_3)$_2$]I and *fac*-[Re(CO)$_3$(H_2dhp)Br] where the diimine chelator acts as dianionic N_3O_2 pentadentate and neutral $N_{pyridine}N_{Schiff\ base}$ ligands, respectively [**29**]. In rare cases, metal-carbene

bonds have been formed through imino carbons; as seen in the paramagnetic ruthenium(III) complex, *trans*-[RuCl(bzp)(PPh_3)$_2$] (Hbzp = *N*-(2-hydroxybenzylidene)-benzimidazole) [**30**]. Another factor that influence the stabilization of Schiff base metal complexes, is metal chelation, *i.e.* the position of functional groups, donor atoms, mono-imine or higher order imines which determines whether constrained or unconstrained bite-angles are formed as well as the number of chelate rings within the coordination spheres of the metal complexes.

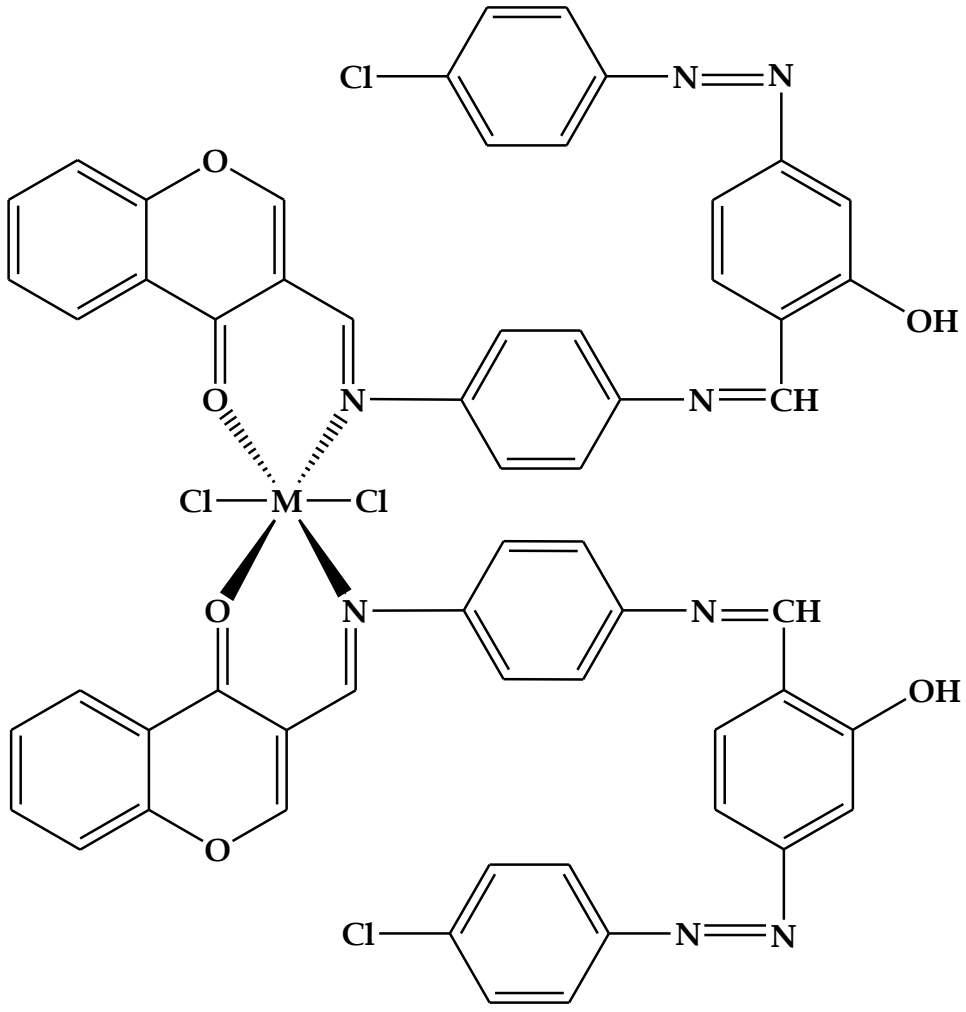

Figure 1.6: *The general octahedral geometry of the 3d transition metal complexes containing neutral chromone-azo-Schiff bases where M = Ni, Co, Zn or Cu.*

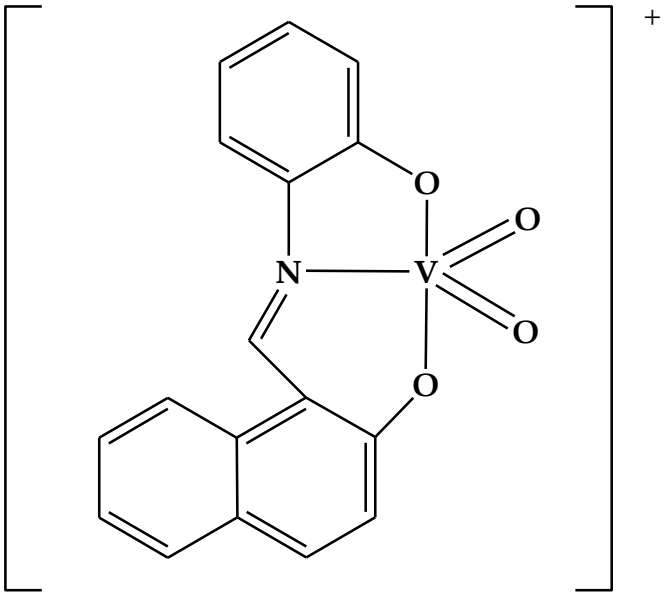

Figure 1.7: *A tridentate dianionic ONO Schiff base stabilizing the acidic $[VO_2]^+$ core.*

1.4 Rhenium radiopharmaceuticals:

1.4.1 Rhenium radionuclides

Rhenium has two β-emitting isotopes, ^{186}Re, with half-life of 3.77 days and ^{188}Re with a relatively stable half-life of 16.9 days. The 186-rhenium radionuclide can be produced by neutron irradiation of natural rhenium in a nuclear reactor. However, since natural rhenium consists of ^{185} Re (37.4%) and ^{187}Re (62.6%), this radiochemical process leads to considerable impurities. Alternatively, the radionuclide with the shorter half-life (*viz.* ^{188}Re) can be removed by allowing it to decay but this will result in considerable loss in activity of the desired isotope (*viz.* ^{186}Re) **[31, 32]**.

$$^{185}\text{Re} + n \rightarrow {}^{186}\text{Re}$$

The 188-rhenium radionuclide can be obtained as a solution of $^{188}ReO_4$ in high specific activity from an ^{188}W generator similar in design to the commonly used ^{99m}Tc generator [**31**]. Such a generator with 0.5 Ci of ^{188}W which has the potential to provide therapeutic treatments to several hundred patients over a 2-6 month lifetime. The major disadvantage of ^{188}Re for therapeutic applications is the relatively short half-life of 17 Hrs [**32**], **w**hich does not impede its applications in treatment of metastatic bone cancer, non-resectable liver cancer.

$$^{188}WO_4^{2-} \rightarrow {}^{188}ReO_4^{-} + \beta$$

1.4.2 Rhenium radiopharmaceuticals: design approaches and applications

Several approaches have been employed for the design and applications of rhenium radiopharmaceuticals namely the match pair, integrated and bifunctional approaches [**31**, **32**]. The match pair approach entails the design of rhenium radiopharmaceuticals analogously based on diagnostic 99m-technetium radiopharmaceuticals are already well-established. The motivation behind this design approach is the fact that rhenium and technetium are group congeners which have similar coordination chemistries due to the 'lanthanide contraction' which ensures that the complexes of the two elements have similar physical characteristics (size, lipophilicity, *etc*). Structurally, they are similar due to the presence of the $\{M^{I}(CO)_3\}^+$ (M = Tc, Re). Once such example, is a Tc^{V} complex of dimercaptosuccinic acid (DMSA) which is used widely as an agent for the imaging of a relatively rare medullary thyroid carcinoma. The comparable radiolabelled Re^{V} complex has the expected square pyramidal structure with an apical oxo-group and exists as a mixture of isomers, see **Figure 1.8**. Another class of radiopharmaceuticals based on ^{186}Re and ^{188}Re labelled bearing bisphosphonate hydroxyethylidenephosphonate (HEDP) ligands were developed as therapeutic analogues of the 99m-technetium

bisphosphonates. They are routinely used for SPECT imaging of bone metastases that arise from malignant cancers. The main design flaw in the match pair approach is that oxorhenium(V) complexes were notoriously unstable in aqueous media than their oxotechnetium(V) counterpart complexes as it undergoes disproportionation reaction to afford two rhenium species in oxidation states of +IV and +VII respectively.

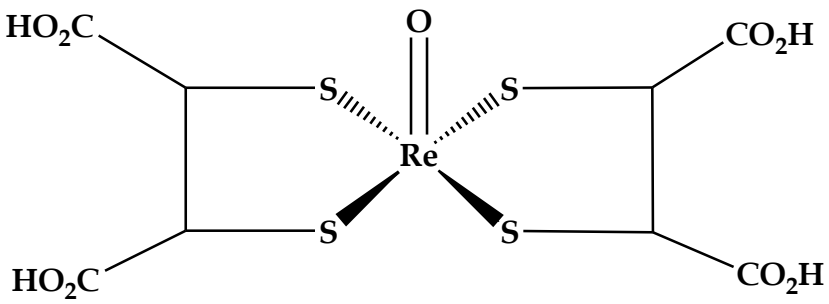

Figure 1.8: *An oxorhenium(V) complex of dimercaptosuccinic acid (DMSA).*

Integrated approach involves the manipulation of the metal complex structure to meet the topology of a biologically active molecule. An example is a rhenium complex which mimics the structure of progesterone, see **Figure: 1.9.** Alternatively, a biological activity moiety can be incorporated in the framework of the organic chelator.

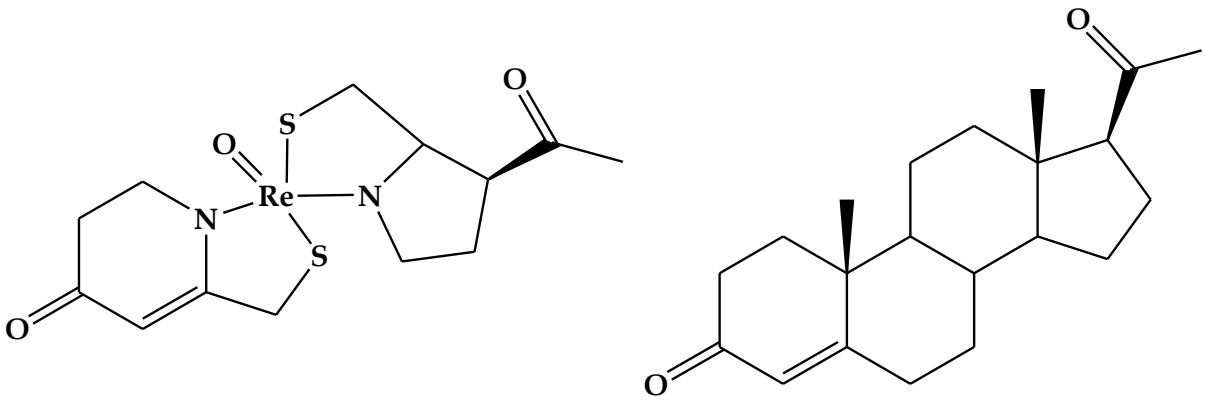

Figure 1.9: *A structure of oxorhenium(V) complex mimicking the structure of progesterone.*

The bifunctional approach as the name implies involves the use of a bifunctional chelator which can stabilize the metal centre in a specific oxidation state while the bifunctional chelator is either directly covalently bonded to a biologically active moiety or linked through an organic linker [**33**]. This design approach provides significant improvements in that the biological activity moiety remains unhindered electronic properties remain intact allowing it to facilitate biodistribution of the radiopharmaceutical. This provides interaction of the biological active moiety with targeted growths in the human body. Furthermore, depending on the oxidation state of the metal centre, the bifunctional chelator can be designed with the appropriate donor atoms. Recent designs based on the *fac*-$[Re(CO)_3]^+$ core have afforded targeting rhenium radiopharmaceuticals for the treatment of bone metastases. One of the complexes was tethered to a bifunctional ligand bearing a bisphosphonate functional group [**34**], although it has not undergone clinical trials. Another example includes the conjugation of glucosamines to monoanionic NNO-donor multidentate chelates coordinated to the *fac*-$[Re(CO)_3]^+$ core, see **Figure 1.10** [**35**].

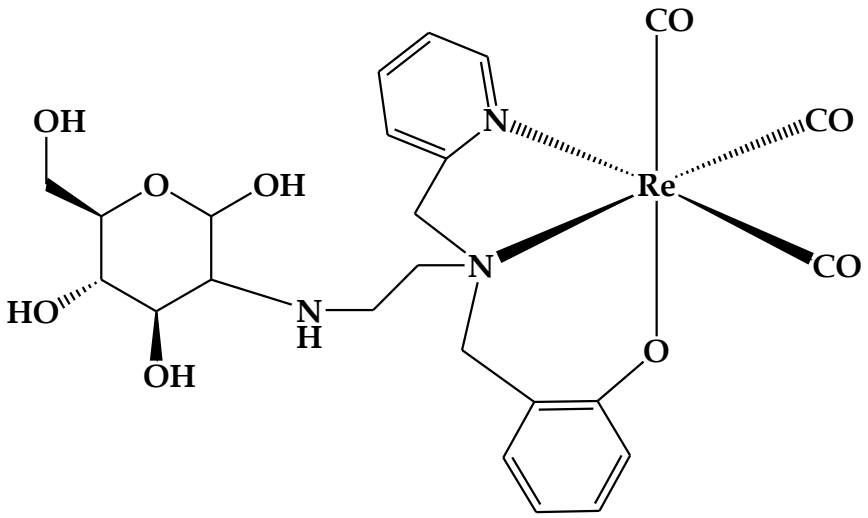

Figure 1.10: *A facial tricarbonyl rhenium(I) complex with a monoanionic NNO tridentate chelator with the bridging amine linker containing glucopyranose moiety.*

1.5 General chemistry of rhenium(I) and –(V):

1.5.1 The fac-$[Re^{I}(CO)_3]^+$ core

Alberto *et al*. were the first to report the synthesis of the rhenium(I) aqua complex, *fac*-$[Re(CO)_3(H_2O)_3]^+$ in a simple one step experimental procedure by the reduction Alberto *et al*. were the first to report the synthesis of the rhenium(I) aqua complex, *fac*-$[Re(CO)_3(H_2O)_3]^+$ in a simple one step experimental procedure by the reduction of perrhenate in an aqueous solution of sodium borohydride and in the presence of carbon monoxide [**8**]. Designing radiopharmaceuticals with the metal precursor, *fac*-$[Re(CO)_3(H_2O)_3]^+$ exploits the aqueous stability of the metal tricarbonyl core whilst manipulating the displacement of the relatively labile water ligands to attach pertinent biomolecules to the *fac*-$[Re^{I}(CO)_3]^+$ core. Moreover, a variety of multidentate ligand systems have been reacted with the aforementioned *facial* tricarbonyl rhenium(I) triaqua complex cation in all cases they substitute the labile aqua co-ligands [**36**, **37**].

The *fac*-$[M(CO)_3]^+${M = Tc or Re} core cations possess several favourable properties including:

- Chemical inertness of the *fac*-$[M(CO)_3]^+$ core due to the low spin d^6 configuration. This provides a convenient platform for *in vitro* and *in vivo* studies.
- The small size of the *fac*-$[M(CO)_3]^+$ core allows flexibility and accessibility for labelling with various biologically active molecules.
- The high stability in aqueous media compared to radiopharmaceuticals containing the oxorhenium(V) core. The latter is prone to oxidation to $[ReO_4]^-$ by water.

1.5 *Oxorhenium(V) core*

Rhenium(V) compounds are generally diamagnetic due to their spin-paired d^2 electronic configuration. These metal complexes have mostly octahedral coordination geometry and are stabilized by various metal cores such as the nitride

$\{Re^{V}N\}^{2+}$ [**38**], imido $\{Re^{V}NR\}^{3+}$, oxo $\{Re^{V}O\}^{3+}$ [**39**]. Among the numerous rhenium(V) metal cores, oxorhenium(V) complexes are the most predominant and can undergo various reactions:

- Oxorhenium(V) complexes are normally oxidized by strong oxidants which results in the formation of $[ReO_4]^-$, without forming any intermediates. For example, $[ReOCl_4(H_2O)]^-$ in 10 M HNO_3 is oxidized by NO_2^- to $[ReO_4]^-$ as shown in the following reaction [**40**, **41**]:

$$5[ReOCl_4\ (H_2O)]^- + 2NO_2^- \rightarrow\ 3[ReO_4]^- + 10HCl + 2[ReOCl_5(NO)]^-$$

- Oxorhenium(V) complexes can also undergo reduction as the common route to Re(III) complexes, *e.g.* the reduction of a mono oxorhenium(V) complex by triphenylphosphine *via* the removal of the terminal oxide [**42**]. In the reaction shown below, the terminal oxide is replaced by the solvent molecule CH_3CN and $OPPh_3$ is the only oxidation by-product.

trans-$[ReOCl_3(PPh_3)_2]$ + CH_3CN + PPh_3 → *trans*-$[ReCl_3(MeCN)(PPh_3)_2]$ + $OPPh_3$

- Oxorhenium(V) complexes have shown to readily disproportionate to Re(IV) and Re(VI) species, as shown in the chemical reaction below [**41**]:

$$3[ReOCl_5]^{2-}\ + H_2O \rightarrow 3[ReO_4] +\ \ 2[ReCl_6]^{2-}\ \ + Cl + 2HCl$$

- Ligand substitution is readily affected by conducting coordination reactions with stirring at room temperature or by gentle heating in a suitable solvent. An example is shown in the following reactions where tetrahydrofuran and ethanol produce different products [**43**]:

fac- $[ReOCl_3(OPPh_3)(SMe_2)]$ + Dppen $\xrightarrow{THF}$ *fac*- $[ReOCl_3(Dppen)]$ + $OPPh_3$ + SMe_2

fac- $[ReOCl_3(OPPh_3)(SMe_2)]$ + Dppen $\xrightarrow{EtOH}$ *fac*- $[ReOCl_2(OEt)(Dppen)]$ + $OPPh_3$ + SMe_2 + HCl

- Formation of rhenium(V) dimers most commonly occurs through the use of dioxorhenium(V) precursors but the use of multidentate ligands have also shown to be excellent bridging ligands both for the *fac*-$[Re(CO)_3]^+$ and $[ReO]^{3+}$ units in dinuclear compounds. For example, a multiply-bridged dimer (μ-Cl)(μ-O)(μ-moa)$_2$ $[Re^{III}Re^{IV}(PPh_3)]_2$(H_2moa =2-mercapto-orotic acid) was isolated when rhenium (V) was used as a precursor [**44**].

Coordination chemistry of rhenium (I) and (V):

1.6.1 Rhenium(I) compounds with bidentate N, X {X = O or N} ligands

Synergism between the rhenium(I) centre and its *facial* orientated carbonyl co-ligands (*i.e.* sigma metal-to-ligand and corresponding *pi*-back bonding) affords a rigid *fac*-tricarbonylrhenium(I) unit which implies that there is only three available coordination sites that can be manipulated. By far the most rhenium(I) compounds have bidentate chelating ligands accompanied with a halide occupying the last available coordination site. Furthermore, as rhenium in its oxidation state +I exhibits low acidic character balanced by a halide co-ligand, these bidentate ligands typically contains neutral donor atoms (*e.g.* pyridyl and imino nitrogens).

This coordination chemistry of *facial* tricarbonylrhenium(I) compounds is illustrated by its benzo pyrazolylamidino complex (a component obtained from coupling of 3, 5-dimethylpyrazole with benzonitrile) was successfully coordinated to the rhenium(I) core to obtain a bidentate $N_{Schiff\ base}N_{Benzonitrile}$ coordination mode, see **Figure 1.11** [**45**]. Examples of NO-donor bidentate chelates coordinated *fac*-$[Re(CO)_3]^+$, include the mononuclear, *fac*-$[Re(CO)_3(IPPO)(L)]$ (L = pyridine or dimethylaminopyridine) (IPPOH = 2-(imidazo[1,2-*a*]pyridin-2-yl)phenol) [see **Figure**

1.12] and the dinuclear, *fac*-[{$Re(CO)_3$}$_2$($IPPO)_2$] compounds. The influence of the nature of solvents is again emphasized through isolation of aforementioned metal compounds given by the fact that the dinuclear compound could only be formed in the non-coordinative solvent, toluene [**46**].

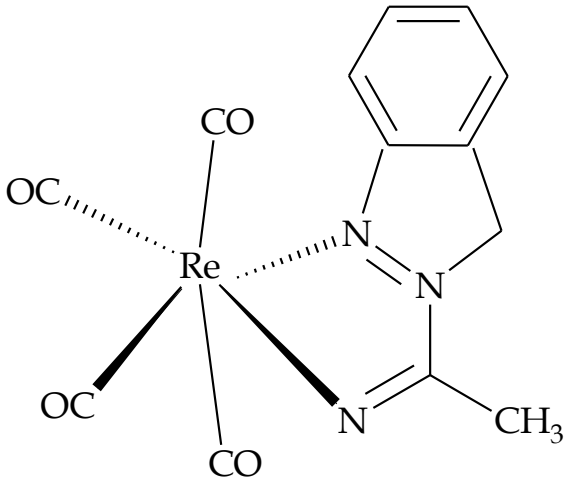

Figure 1.11: *Structure of the rhenium(I) complex [X = Br or Cl] with the neutral bidentate parazolamidino ligand.*

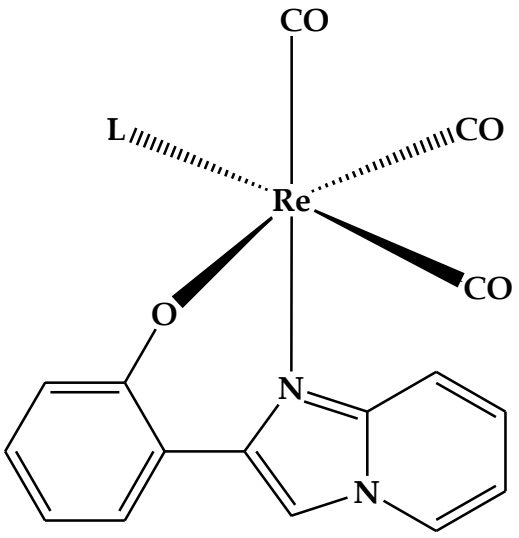

Figure 1.12: *General structure of the mononuclear metal complexes, fac-[Re(CO)$_3$(IPPO)(L)] where L is pyridine or dimethylaminopyridine.*

1.6.2 Rhenium(V) complexes with multidentate N-donor ligands

Displacement of the oxorhenium(V) core requires ligands containing donor atoms that can provide enough electron density to stabilize the highly charged rhenium(V) centre. For example, ligands containing the amino groups are known to substitute at the oxorhenium(V) through single deprotonation to afford Re-NH cores (*viz.* rhenium amido bonds), double deprotonation to form either the $[Re=N]^{3+}$ bent imido or the $[Re\equiv N]^{3+}$ linear phenylimido if the lone pair on the nitrogen also gets involved in bonding to the metal centre.

Several literature example of linear phenylimido rhenium(V) complexes with aniline and 1,2-diaminobenzene have been reported [**47-51**]. The uracil derivative, 5,6-diamino-1,3-dimethyluracil (H_2ddd) has successfully substituted the dioxo co-ligands of the metal precursor, *cis*-[$ReO_2I(PPh_3)_2$] to form the "2+1" oxofree rhenium(V) complex cation, *trans*-$[Re(ddd)(Hddd)I(PPh_3)_2]^+$ (see **Figure 1.13**) where the bidentate Hddd six-membered chelate ring is afforded by rhenium-amido and rhenium–amino bonds while the ddd monodentate moiety is afforded by the triply bonded rhenium imido bond [**52**]. Later on the condensation of 1, 2-diaminobenzene and 5, 6-diamino-1, 3-dimethyluracil with various respective 2-substituted aldehydes afforded the corresponding multidentate Schiff bases which readily allowed the formation of rhenium-bent imido bonds upon reacting them with oxorhenium(V) precursors [**53-56**]. More specifically, the oxo-free rhenium(V) compound was formed from the reaction between *cis*-$[Re^VO_2I(PPh_3)_2]$ and H_3duo (*N*-(2-hydroxybenzylidene)-5-amino-1,3-dimethyluracil) led to the formation of the oxofree, imido compound, *trans*-$[Re^V(ddd)(Hduo)(PPh_3)_2]I$ [**57**].

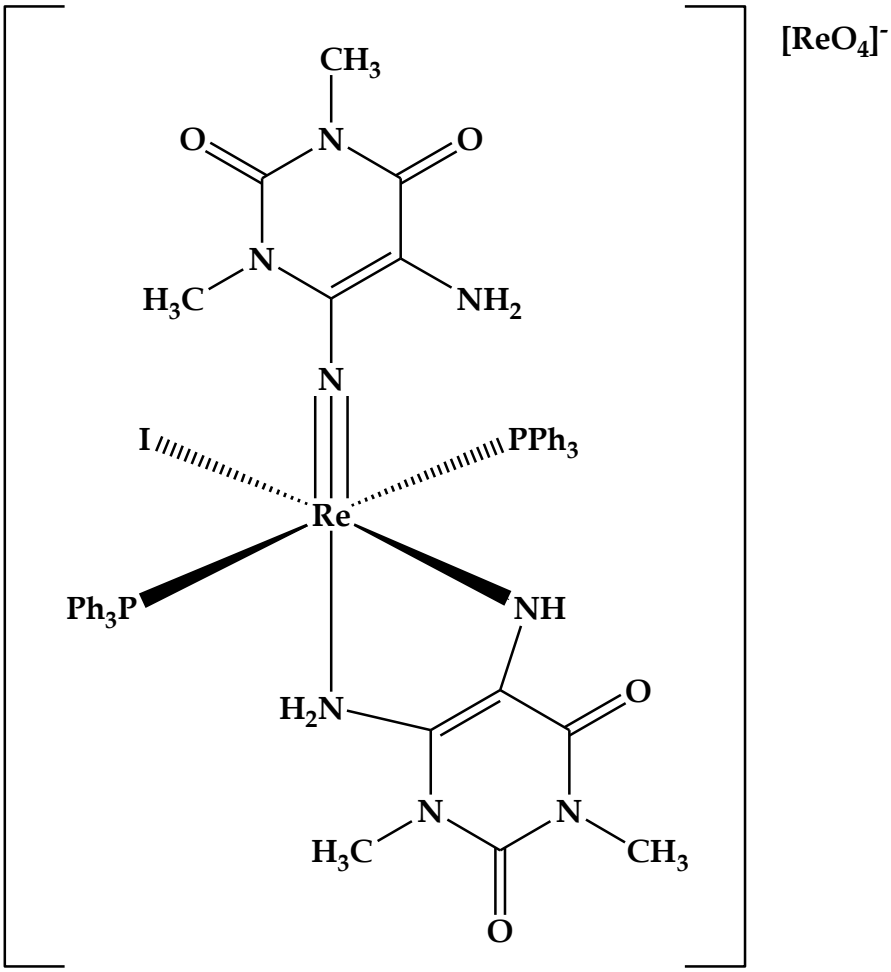

Figure 1.13: *Structure of a imido, amido, amino oxofree rhenium(V) compound.*

1.7 References

[1] J. Lecina, Pilar Cortés, M. Llagostera, C. Piera, J. Suades, *Bioorg. Med. Chem.* 22 (2014) 3262.

[2] J. Hawecker, J.M. Lehn, R. Ziessel, *J. Chem. Soc., Chem. Commun.* (1984) 328.

[3] K. Kowalski, Ł. Szczupak, T. Berna, R. Czerwieniec, *J. Organomet. Chem.* 782 (2015) 124.

[4] J. Mukiza, E.C. Hosten, T.I.A. Gerber, *Polyhedron* 110 (2016) 106.

[5] J.A. Casey, R.K. Murmann, *J. Am. Chem. Soc.* 92 (1970) 78.

[6] T.G. Fenton, M.E. Louis, G. Li, *J. Mol. Catal. A: Chem*. 411 (2016) 272.

[7] F.E. Kuhn, A. Scherbaum, W.A. Herrmann, *J. Organomet. Chem.* 689 (2004) 4149.

[8] R. Alberto, R. Schibi, R Wailbel, U. Abram, A.P Schubiger, *Coord. Chem. Rev.* 190-192 (1999) 901.

[9] M. Bartholoma, J. Valliant, K.P. Maresca, J.B. Zubieta, *Chem. Commun.* (2009) 493.

[10] J.R.J Sorenson,. Metal Ions in Biological Systems. *Marcel Dekker*: New York 14 (1976).

[11] S. Khadem, R. Marles, *Molecules* 17 (2012) 191.

[12] B. Dyck, L. Zhao, J. Tamiya, J. Pontillo, S. Hudson, B. Ching, C.E. Heise, J. Wen, C. Norton, A. Madan, D. Schwarz, W. Wade, V.S. Goodfellow, *Bioorg. Med. Chem. Lett.* 16 (2006) 4237.

[13] I.N. Booysen, M. B. Ismail, M.P. Akerman, *J. Coord. Chem.* 66 (2013) 4371.

[14] I.N. Booysen, M.B. Ismail, O. Q. Munro, *Inorg. Chem. Commun.* 30 (2013) 168.

[15] E.L. Regalado, A. Laguna, J. Mendiola, O.P. Thomas, C. Nogueiras, *Quím. Nova.* 34 (2011) 2.

[16] A.R. Carroll, P.J. Scheuer, *J. Org. Chem.* 55 (1990) 4426.

[17] A. Cipres, D.P.O Malley, K. Li, D. Finlay, P.S. Baran, K. Vuori, *ACS Chem. Biol.* 5 (2010) 195.

[18] D. Deidda, G. Lampis, R. Fioravanti, M. Biava, G. C. Porretta, S. Zanetti, R. Pompei, *Antimicrob. Agents Chemother.* 42 (1998) 3035.

[19] T. Huang, J. Sun, L. An, L. Zhang, C. Han, *Bioorg. Med .Chem. Lett.* 26 (2016) 1854.

[20] B.L. Handen, A.D. Cohen, U. Channamalappa, P. Bulova, S.A. Cannon, W.I. Cohen, C.A. Mathis, J.C. Price, W.E. Klunk, *Alzheimer's & Dementia* 8 (2012) 496.

[21] G. Varsha , V. Arun, P.P. Robinson, M. Sebastian, D. Varghese, P. Leeju, V.P. Jayachandran, K.K.M. Yusuff , *Tetrahedron Lett.* 51 (2010) 2174.

[22] T.S. Pandian, V. Srinivasadesikan, M.C. Lin, J. Kang, *Tetrahedron* 71 (2015) 7782.

[23] C.C. Chou, H. Liu, L.H. Chao, C.C Yang, *New. J. Chem.* 39 (2015) 1260.

[24] C.C. Chou, H. Liu, L.H. Chao, *Chem. Commun***.** (2009) 6382.

[25] A. Ouraria, M. Khelafia, D. Aggouna, A. Jutand, C. Amatore, *Electrochim. Acta* 75 (2012) 366.

[26] C. Anitha, C.D Sheela, P. Tharmaraj, S. Johnson Raja. *Spectrochim. Acta A* 98 (2012) 35.

[27] S.Y. Ebrahimipour, I. Sheikhshoaie, A.C. Kautz, M. Ameri,H. Pasban-Aliabadi, H.A. Rudbari, G. Bruno, C. Janiak, *Polyhedron* 93 (2015) 99.

[28] I.N.Booysen, A. Adebisi, O.Q. Munro, B. Xulu, *Polyhedron* 73 (2014) 1.

[29] K. Potgieter, P. Mayer, T.I.A. Gerber, I.N. Booysen, *Polyhedron* 28 (2009) 2808.

[30] J.R. Dilworth, S.J. Parrott, *Chem. Soc. Rev*., 27 (1998) 43.

[31] S. Jürgens, W.A. Herrmann, F.E. Kühn, *J. Organomet. Chem.* 751 (2014) 83.

[32] J.P. Dizio, R. Fiasschi, A. Davison, A.G. Jones, J.A. Katzenellenbogen, *Biocong. Chem.* 2 (1991) 353.

[33] U. Abram, R. Alberto *J. Braz. Chem. Soc.* 17 (2006) 1486.

[34] M.L. Bowen, N.C. Lim, C.B. Ewart, R. Misri, C.L. Ferreira, U. Hafeli, M.J. Adam, C. Orvig, *Dalton Trans.* (2009) 9216.

[35] C. Spagnul, R. Alberto, G. Gasser, S. Ferrari, V. Pierroz, A. Bergamo, *J. Inorg. Biochem.* 122 (2013) 57.

[36] D.J. Kramer, A. Davison, A.G. Jones, *Inorg. Chim. Acta* 312 (2001) 215.

[37] G. Rouchias, *Chem. Rev*. 74 (1974) 531.

[38] P.S. Donnely, *Dalton Trans.* 40 (2011) 999.

[39] D. Freni, D. Gusto, P. Romiti, G. Minghetti, *Gazz. Chim. Ital.* 99 (1969) 286.

[40] F.A. Cotton, S.J. Lippard, *Inorg. Chem*. 4 (1965) 1621.

[41] J.C. Vites, M.M. Lynam, *Coord. Chem. Rev.* 172 (1998) 357.

[42] Q. Sigouin, A.L. Beauchamp, *Inorg. Chim. Acta* 358 (2005) 4489.

[43] J. Mukiza, T.I.A. Gerber, E. Hosten, Inorg. *Inorg. Chem. Commun.* (2016), accepted, doi: 10.1016/j.inoche.2016.03.008.

[44] P. Gómez-Iglesias, F. Guyon, A. Khatyr, G. Ulrich, M. Knorr, J.M. Martín-Alvarez, D. Miguel, F. Villafañe. *Dalton Trans,* 44 (2015) 17516.

[45] P. Saxena, B. Shankar, M. Sathiyendiran, *J. Organomet. Chem.*, 799 (2015) 82.

[46] I. Booysen, Thomas I.A. Gerber, P. Mayer, H.J. Schalekamp, *J. Coord Chem*. 60 (2007) 1755.

[47] G. Bandoli, T.I.A. Gerber, J. Perils, J.G.H. du Preez, *lnorg. Chim. Acta* 278 (1998) 96.

[48] X. Schoultz, T.I.A. Gerber, E. Hosten, R. Betz, L. Rhyman, P. Ramasami, *Polyhedron* 96 (2015) 6.

[49] C.S. Masui, J.M. Mayer, *lnorg. Chim. Acta* 251 (1996) 325.

[50] B. Machura, I Gryca, *Polyhedron* 53 (2013) 8.

[51] T.I.A. Gerber, D.G. Luzipo, P. Mayer, *J. Coord Chem.* 2006 (59) 1515.

[52] P. Mayer, E. Hosten, T.I.A. Gerber, I. Booysen, *J. Iran. Chem. Soc.* 7 (2010) 775.

[53] M.T. Ahmet, B. Coutinho, J.R. Dilworth, J.R. Miller, S.J. Parrott, Y. Zheng, *Polyhedron* 15 (1996) 2041.

[54] T.I.A. Gerber, D. Luzipo, P. Mayer, *J. Coord. Chem.* 59 (2006) 1149.

[55] T.I.A. Gerber, D.G. Luzipo, P. Mayer, *J. Coord. Chem*. 59 (2006) 1801.

[56] I.N. Booysen, M. Ismail, T. I.A. Gerber, M. Akerman, Benjamin Van Brecht, *S. Afr. J. Chem.* 65 (2012) 174.

Chapter 2

Materials and Methods

2.1 Handling of Rhenium

Having used non-radioactive rhenium metal precursors in this project, special precautions on radioactivity safety were not taken into consideration. In addition, no other purification process was carried out on the metal precursors.

2.2 Materials

2.2.1 Metal precursors

(a) Ammonium perrhenate

Ammonium perrhenate $(NH_4)[ReO_4]$ was obtained from Sigma-Aldrich at +99% purity and used without any further purification.

(b) Rhenium(I) pentacarbonyl bromide

Rhenium(I) pentacarbonyl bromide, $[Re(CO)_5Br]$ was obtained from Sigma-Aldrich at 98% purity and used without any further purification.

(c) Rhenium(I) pentacarbonyl chloride

Rhenium(I) pentacarbonyl chloride, $[Re(CO)_5Cl]$, was obtained from Sigma-Aldrich at 98% purity and used without further purification.

(d) trans-$[ReOBr_3(PPh_3)_2]$[1]

To a solution of 1.0 g of $(NH_4)[ReO_4]$ in 3 cm^3 concentrated hydrobromic acid, 5.0 g of triphenylphosphine in 50 cm^3 glacial acetic acid was added. The resultant reaction

mixture was stirred for 1 hour at 20^{o}C. A mustard yellow precipitate formed which was filtered, washed with glacial acetic acid and diethyl ether and dried under vacuum

2.2.2 Solvents and specialized chemicals

Calf Thymus (CT)-DNA and Phosphate Buffered Saline (PBS) tablets were obtained from Sigma Aldrich and used as is. All solvents and common salts were obtained from Merck SA. Reagent grade toluene was dried over sodium wire and other solvents were used without further purification.

2.2.3 Organic precursors

All organic precursors and their corresponding percentage impurities are given in **Table 2.1.** These chemicals were obtained from Sigma-Aldrich.

Table 2.1: *Organic precursors attained from Sigma-Aldrich.*

Name	**Purity**
3, 5-Diamino-1,2,4-triazole	99%
2-Amino-3-formylchromone	97%
Ethylenediamine	98%
1,2-Diaminobenzene	99.5%
1,8-Diaminonaphthalene	99%
Pyrrole-2-carboxaldehyde	98%
2 Pyridine carboxaldehyde	99%
Benzothiazole-2-carboxaldehyde	97%

2.3 Instrumentation:

The infrared spectra were recorded on a Perkin-Elmer 100 spectrometer in the 4000 – 450 cm^{-1} range. The ^{1}H NMR spectra was obtained using Bruker Avance 400 MHz spectrometer. All NMR spectra were recorded in deuterated dimethylsulphoxide. UV-Vis spectra were recorded using Perkin Elmer Lambda 25. The extinction coefficients (ε) are given in $dm^{3}.mol^{-1}.cm^{-1}$. Melting points were determined using a Stuart SMP3 melting point apparatus. The conductivity measurements were determined at 295K on a Radiometer R21M127CDM 230 conductivity and pH meter. The standard solution of 1M KCl was employed for calibration of the electrode. The X-ray data for the metal complexes were recorded on a Bruker Apex Duo equipped with an Oxford Instruments Cryojet operating at 100(2) K and an Incoatec microsource operating at 30W power. Computational modelling was conducted using the Gaussian 09W [**2**]. The conductivity measurements were determined at 295K on a Radiometer R21M127CDM 230 conductivity and pH meter. DNA binding studies were conducted on a Shimadzu UV-1800 Spectrophotometer coupled with a Shimadzu CPS temperature controller.

2.4 References

[1] Johnson, N. P.; Lock, C. J. L.; Wilkinson, G. Inorg. Synth. 9 (1967) 145.

[2] M.J. Frisch, G.W. Trucks, H.B. Schlegel, G.E. Scuseria, M.A. Robb, J.R. Cheeseman, G. Scalmani, V. Barone, B. Mennucci, G.A. Petersson, H. Nakatsuji, M. Caricato, X. Li, H.P. Hratchian, A.F. Izmaylov, J. Bloino, G. Zheng, J.L. Sonnenberg, M. Hada, M. Ehara, K. Toyota, R. Fukuda, J. Hasegawa, M. Ishida, T. Nakajima, Y. Honda, O. Kitao, H. Nakai, T. Vreven, J.A. Montgomery Jr., J.E. Peralta, F. Ogliaro, M. Bearpark, J.J. Heyd, E. Brothers, K.N. Kudin, V.N. Staroverov, R. Kobayashi, J. Normand, K. Raghavachari, A. Rendell, J.C. Burant, S.S. Iyengar, J. Tomasi, M. Cossi, N. Rega, J.M. Millam, M. Klene, J.E. Knox, J.B. Cross, V. Bakken, C. Adamo, J. Jaramillo, R. Gomperts, R.E. Stratmann, O. Yazyev, A.J. Austin, R. Cammi, C. Pomelli, J.W. Ochterski, R.L. Martin, K. Morokuma, V.G. Zakrzewski, G.A. Voth, P. Salvador, J.J. Dannenberg, S. Dapprich, A.D. Daniels, O. Farkas, J.B. Foresman, J.V. Ortiz, J. Cioslowski, D.J. Fox, GAUSSIAN 09 (Revision A.01), *Gaussian Inc., Wallingford*, CT, 2009.

Chapter 3

Formation, Characterization and Computational Studies of Mono- and Dinuclear Rhenium(I) Chromone Compounds

3.1 Introduction

The considerable attention received by the coordination chemistry of rhenium stems from the ideal properties of its 186- and 188-radionuclides which are well suited for radiotherapy [**1-3**]. For example, the bone-targeting therapeutic radiopharmaceutical, rhenium-HEDP (HEDP = hydroxyethylidene disphosphonate) has several advantages over the commercially available alternatives in terms of efficacy, safety and the ability to be produced on site, allowing for rapid treatment of patients with painful bone metastases [**4**]. Furthermore, the *facial* tricarbonylrhenium(I) core has shown to serve as an ideal synthon for the formulation of new rhenium radiopharmaceuticals. This is illustrated by the *facial* tricarbonylrhenium(I) complexes stability under physiological conditions where the small size of the *fac*-$[Re(CO)_3]^+$ core allows binding to various biological entities [**5-6**]. However, the next generation of potential rhenium radiopharmaceuticals requires chelators which can stabilize the metal centre both in the low and high oxidation states [**7**]. Furthermore, these multidentate chelators should also cater for the inclusion of biologically active moieties which may aid in target specific biodistribution of the metallopharmaceuticals [**8**, **9**].

Hence, in this chapter, the coordination susceptibility of multidentate chromone ligands towards the *facial* tricarbonyl rhenium(I) core is described. The rhenium(I) complex, *fac*-$[Re(CO)_3$(chrpychr)Br] (**1**) was isolated from the equimolar reaction

between 2-(4-oxo-4*H*-chromen-3-yl)-5*H*-chromeno[2,3-*d*]pyrimidin-5-one (chrpychr) and [Re(CO)$_5$Br]. The coordination reactions of [Re(CO)$_5$Br] with the diimines: *N, N'-bis*((2-amino-3-imino)methylenechromone-1,2-ethane (chret) and *N,N'-bis*((3-chromone)methylene)benzene-1,2-diamine (chb) afforded a novel dinuclear rhenium(I) compound, *fac*-(Re(CO)$_3$Br)$_2$(μ-chret) (**2**) and a mononuclear compound *fac*-[Re(CO)$_3$(bzch)Br] (**3**) [bzch = 2-benzimidazole-4*H*-chromen-4-one].

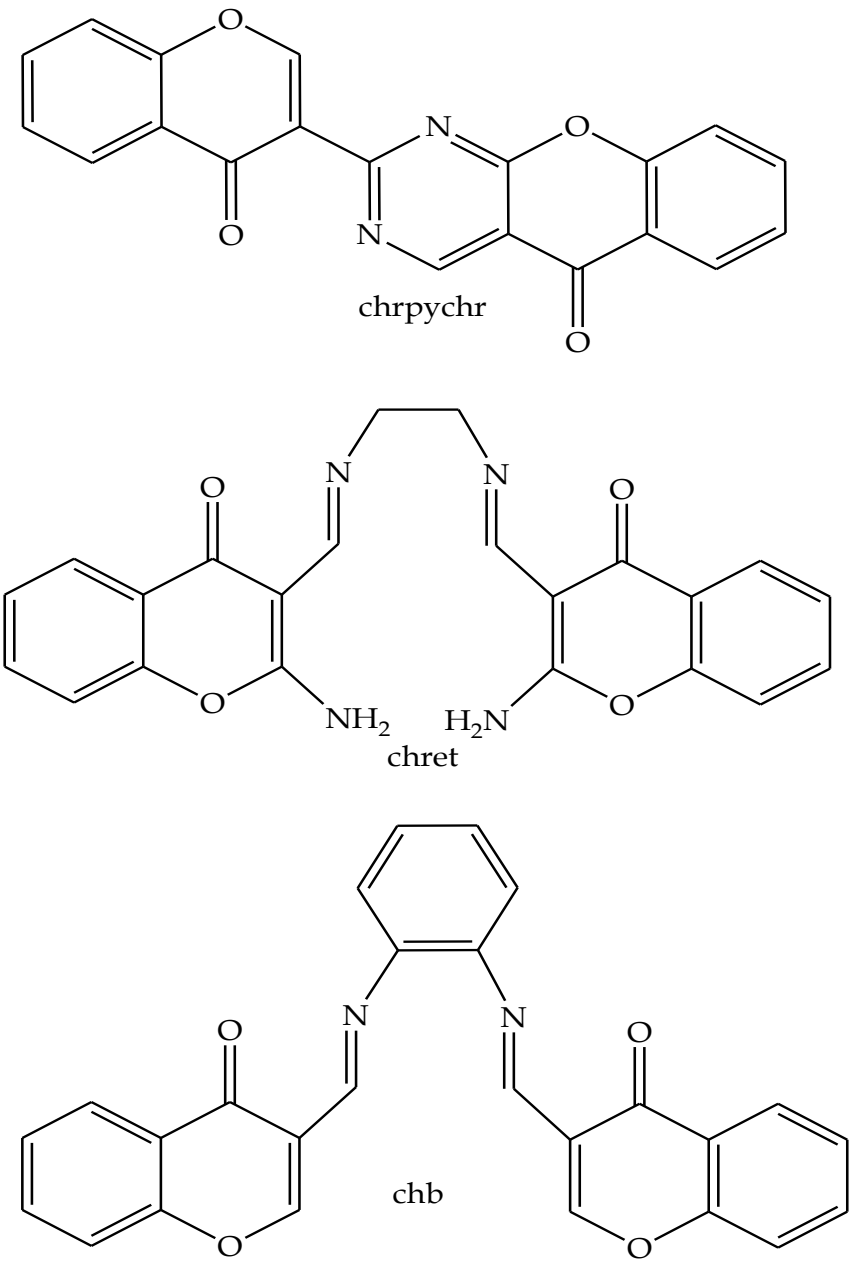

Fig. 3.1: *structure of ligands chb, chrpychr and chret .*

3.2 Experimental:

3.2 Syntheses of ligands

3.2.1 2-(4-oxo-4H-chromen-3-yl)-5H-chromeno[2,3-d]pyrimidin-5-one (chrpychr)

The title compound was prepared from the 2:1 molar condensation reaction between 2-amino-3-formylchromone (0.125 g, 0.660 mmol) and 3,5-diamino-1, 2, 4-triazole (0.0327 g, 0.330 mmol) in 15 cm^3 of methanol acidified with 3 drops of the trifluoroacetic acid. The resultant reaction mixture was heated at reflux temperature for 4 hrs. Thereafter, the volume of the reaction mixture was reduced to 10 cm^3 on a hotplate and placed in an ice-bath to induce the formation of a yellow precipitate which was filtered and washed with cold methanol as well as petroleum ether. M.P = 170 – 175 °C, yield = 32 %. IR (ν_{max}/cm^{-1}): ν(C=O) 1618, 1544 (vs); ν(C=N) 1505, 1465 (vs); ν(O-C-O) 1417, 1370(s). ^{1}H NMR (295 K/ppm, see **Fig. 3.1**): 10.08 (s, 1H, *H23*), 9.60 (br, s, 1H, *H11*), 8.03 (d, 2H, *H6*, *H19*), 7.74 (t, 2H, *H8*, *H17*), 7.49 – 7.40 (m, 4H, *H7*, *H9*, *H16*, *H18*).

3.2.2 N, N'-bis((2-amino-3-imino)methylenechromone-1,2-ethane (*chret*)

The titled diimine was prepared from a 2:1 molar condensation reaction between 2-amino-3-formylchromone (0.201 g, 1.064 mmol) and ethylene diamine (0.032 g, 0.532 mmol) in 20 cm^3 of absolute ethanol. The reaction mixture was heated until reflux for 3 hrs and stirred further overnight. Afterwards, the reaction mixture was concentrated and cooled in an ice bath to induce precipitation. A yellow precipitate was filtered, washed with cold ethanol and petroleum ether. M.P. = 135-140 ˚C, yield = 78%. IR (ν_{max}/cm^{-1}): ν(C=O) 1661 (vs); ν(C=N) 1602 (vs); ν(O-C-O) 1451 (s). ^{1}H NMR (295 K/ppm, see **Fig. 3.3**): 10.89 (br, s, 2H, NH_2); 8.81 (br, s, 2H, NH_2); 8.72 (s, 2H, *H16*, *H19*); 7.98 (dd, 2H, *H9, H23, H12*, *H26*); 7.67 (t, 2H, *H10*, *H26*); 7.37 (t, 2H, *H11*, *H25*); 3.83 (s, 4H, *H17, H17', H18, H18'*). UV-Vis (DMSO, λ_{max} (ε, $M^{-1}cm^{-1}$)): 327 nm (sh, 40340); 349 nm (sh, 50240); 363 nm (52080); 397 nm (sh, 24770); 484 (sh, 20130).

3.2.3 N, N′-bis((3-chromone)methylene)benzene-1,2-diamine (chb)

The diimine, chb was obtained from the condensation reaction of 1,2-diaminobenzene with a two-fold molar equivalent of 3-formylchromone [**10**].

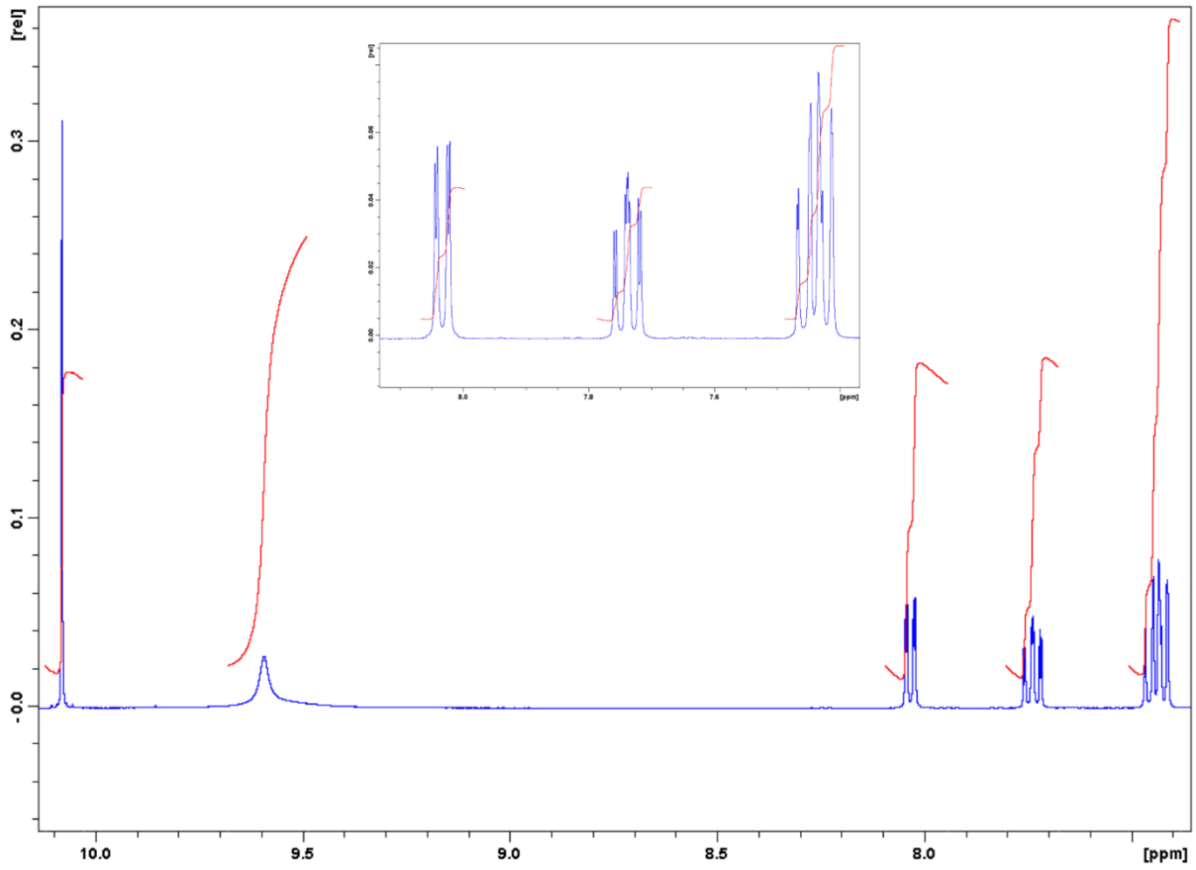

Fig. 3.2: *^{1}H NMR spectrum of chrpychr collected in deuterated dimethylsulphoxide.*

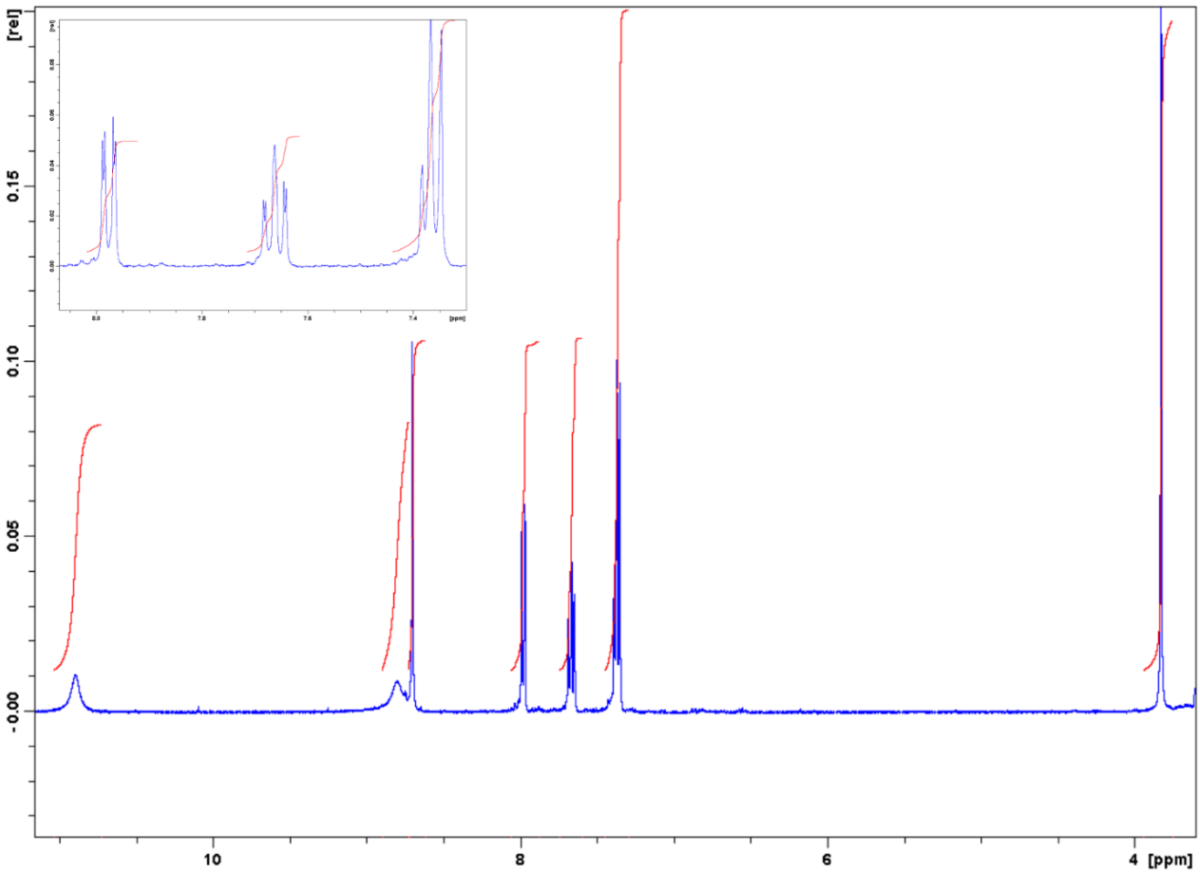

Fig. 3.3: *^{1}H NMR spectrum of chret. The inset shows the aromatic signals between 7.35 and 8.30 ppm.*

3.2.2 Syntheses of metal complexes

*3.2.2.1 fac-[Re(CO)$_3$(chrpychr)] (**1**)*

A mixture of $Re(CO)_5Br$ (0.050 g, 0.123 mmol) and 2-(4-oxo-4*H*-chromen-3-yl)-5*H*-chromeno[2,3-*d*]pyrimidin-5-one (chrpychr) (0.042 g, 0.123 mmol) in 25 cm^3 of anhydrous toluene was heated at reflux under nitrogen for 4 hrs. Afterwards, the resultant reaction mixture was cooled to room temperature and filtered. An orange mother liquor was then left to evaporate slowly at room temperature to afford pale orange crystals after 10 days. M.P = 196 – 197 ^{O}C; yield = 7.5 %; Conductivity (DMF, $10^{-3}M$) 14.32 ohm. cm^2 mol^{-1}; IR (ν_{max}/cm^{-1}): ν(C≡O) 2023, 1919 (sh) and 1894 cm^{-1}(vs); ν(C=O) 1608, 1564 (vs); ν(C=N) 1493, 1456 (vs); ν(O-C-O) 1411, 1379(s). ^{1}H NMR (295 K /ppm): 10.08 (s, 1H, *H23*), 9.58 (br, d, 1H, *H11*), 8.04 (d, 2H, *H6*, *H19*),

7.75 (t, 2H, *H8*, *H17*); 7.49 – 7.40 (m, 4H, *H7*, *H9*, *H16*, *H18*). UV-Vis (DMF, λ_{max}(ε, $M^{-1}cm^{-1}$)). 291 (29600), 309 (sh, 20100), 355 (57800), 464 (4900).

*3.2.2.2 fac-(Re(CO)$_3$Br)$_2$(μ-chret) (**2**)*

A 1:1 molar reaction of $Re(CO)_5Br$ (0.050 g, 0.123 mmol) and chret (0.049 g, 0.123 mmol) in 15 cm^3 of anhydrous toluene was heated until reflux under nitrogen for 4 hrs. The resultant reaction mixture was cooled to room temperature and filtered. The orange precipitate was dried under vacuum while pale orange X-ray quality crystalline parallelograms were obtained from layering the precipitate with 1:1 (*v:v*) THF/Hexane over a period of five days. M.P = 215 - 220 ^oC; yield = 87%; Conductivity (DMSO, 10^{-3}M) 16.93 ohm. cm^2 mol^{-1}; IR (ν_{max}/cm^{-1}): ν(N-H) 2920, 2850 (m); ν(C≡O) 2015, 1871 (vs); ν(C=O) 1655 (s); ν(C=N) 1615, 1613 (s); ν(O-C-O) 1504 and 1464 cm^{-1} (s) [**Figure 3.19**]. ^{1}H NMR (295 K /ppm): 10.91 (br, s, 4H, 2x NH_2), 8.95 – 8.65 (m, 6H, *H4*, *H8*, *H11*, *H14*, *H24*, *H27*), 8.12 – 7.11 (m, 4H, *H12*, *H13*, *H25*, *H26*), 3.87 (br, s, 4H, *H9*, *H9'*, *H10*, *H10'*). UV-Vis (DMSO, λ_{max}(ε, $M^{-1}cm^{-1}$)): 269 nm (24159); 296 (sh, 20140); 405 (sh, 2464).

*3.2.2.3 fac-[Re(CO)$_3$(bzch)Br] (**3**)*

The equimolar coordination reaction between $[Re(CO)_5Br]$ (0.050 g, 0.123 mmol) and chb (0.057 g, 0.123 mmol) in 15 cm^3 of anhydrous toluene was heated until reflux under nitrogen for 4 hrs. Afterwards, the resultant reaction mixture was cooled to room temperature, an orange precipitate was filtered and dried under vacuum. Pale orange cubic crystals suitable for X-ray analysis were obtained from dissolving the precipitate in tetrahydrofuran and layering with hexane. M.P = 210 – 211 ^oC; yield = 93%; Conductivity (DMSO, 10^{-3} M): 23.72 ohm.cm^2mol^{-1}; IR (ν_{max}/cm^{-1}): ν(N-H) 2915 (w), ν(C≡O) 2015, 1871 (vs); ν(C=O) 1628, 1607 (s); ν(C=N) 1567 (s); ν(O-C-O) 1482, 1461. ^{1}H NMR (295 K/ppm): 9.69 (s, 1H, *H1*); 9.39 (s, 1H, *NH*); 8.27-7.22 (m, 8H, *H3, H4, H5, H6, H12, H13, H14, H15*). UV-Vis (DMSO, λ_{max}(ε, M^{-1} cm^{-1})): 275 nm (sh, 26107); 282 nm (27295); 309 (sh, 22025); 394 (6614); 418 (sh, 4394).

3.2.2.4 X-Ray Crystallography.

The X-ray data for **1**.C_7H_8, **2**.3(C_4H_8O) and **3**.C_7H_8 were recorded on a Bruker Apex Duo equipped with an Oxford Instruments Cryojet operating at 100(2) K and an Incoatec microsource operating at 30W power. Crystal and structure refinement data are given in **Table 3.1**. Selected bond lengths and angles are given in **Tables 3.2 - 3.4**, respectively. In all three cases the data were collected with Mo Kα (λ = 0.71073 Å) radiation at a crystal-to-detector distance of 50 mm. The following conditions were used for data collection: omega and phi scans with exposures taken at 30 W X-ray power and 0.50º frame widths using APEX2 [**11**]. The data were reduced with the program SAINT [**11**] using outlier rejection, scan speed scaling, as well as standard Lorentz and polarization correction factors. A SADABS semi-empirical multi-scan absorption correction [**12**] was applied to the data. Direct methods, SHELX-2014 [**13**] and WinGX [**14**] were used to solve all three structures. All non-hydrogen atoms were located in the difference density map and refined anisotropically with SHELX-2014 [**13**]. All hydrogen atoms were included as idealised contributors in the least squares process. Their positions were calculated using a standard riding model with C-$H_{aromatic}$ distances of 0.93 Å and U_{iso} = 1.2 U_{eq}, C-$H_{methylene}$ distances of 0.99 Å and U_{iso} = 1.2 U_{eq} and C–H_{methyl} distances of 0.98 Å and U_{iso} = 1.5 U_{eq}.

3.2.2.5 Computational details:

Computational calculations were conducted with GAUSSIAN 09W [**15**]. Geometry optimizations of the metal complexes were achieved through DFT calculations using the B3LYP functionals. The 6-311G^{++} (*d, p*) basis set was applied to all the C, H, N, O and Br and the LANL2DZ basis set, which makes use of effective core potentials was applied to the metal centre [**16**]. Prior to the calculations, the solvent molecules of recrystallization for the respective metal complexes were omitted from their crystal structures and the resultant structures were used as the starting conformers. Good

agreement was found between the optimized and the crystal structures (see **Tables 3.2 - 3.4**). Minor deviations are attributed to the fact that gas was optimized-structure do not account for non-classical hydrogen bonding interactions nor any short distance contacts. Using the optimized structure of the metal complex, did not yield values for the frequency calculations. This confirmed that the calculated structures are at global minima on their individual potential energy surfaces [**17**].

3.3 Results and Discussions

*3.3.1 Synthesis, spectral characterization and computational studies of fac-[Re(CO)$_3$(chrpychr)] (**1**)*

In an attempt to isolate the diimine, 3, 5-*bis*-(3-methylimino-chromone)-1*H*-1, 2, 4-triazole (prchr) in the presence of trifluoro acetic acid; the free-ligand, chrpychr was inadvertently isolated, see proposed mechanism for the formation of chrpychr in **Scheme 3.1**. The 1:1 molar reaction between chrpychr and [Re(CO)$_5$Br] under inert conditions led to the formation of the rhenium(I) complex, *fac*-[Re(CO)$_3$(chrpychr)Br] (**1**) in low yield of 80%. The molar conductivity measurement [14.32 ohm. cm^2 mol^{-1}] of **1** affirms that it is a non-electrolyte in *N, N'*-dimethylformamide [**18**].

Trifluoroacetic acid has been utilized in numerous molecular transformations reactions [**19**]. In the proposed synthetic route of chrpychr, it is envisaged trifluoroacetic acid promotes the deamination of one mole of 2-amino-3-formylchromone. Subsequently, 3, 5-diamino-1, 2, 4-triazole neutralizes the carbocationic form of 3-formylchromone (see **Scheme 3.1**). Finally, the resultant 3-formylchromone condenses with the by-product amide ion and the remaining 2-amino-3-formylchromone to afford 2-(4-oxo-4*H*-chromen-3-yl)-5*H*-chromeno[2,3-*d*]pyrimidin-5-one (chrpychr). The free-ligand, chrpychr could not be isolated from conducting similar reactions without trifluoroacetic acid or 3, 5-diamino-1, 2, 4-triazole.

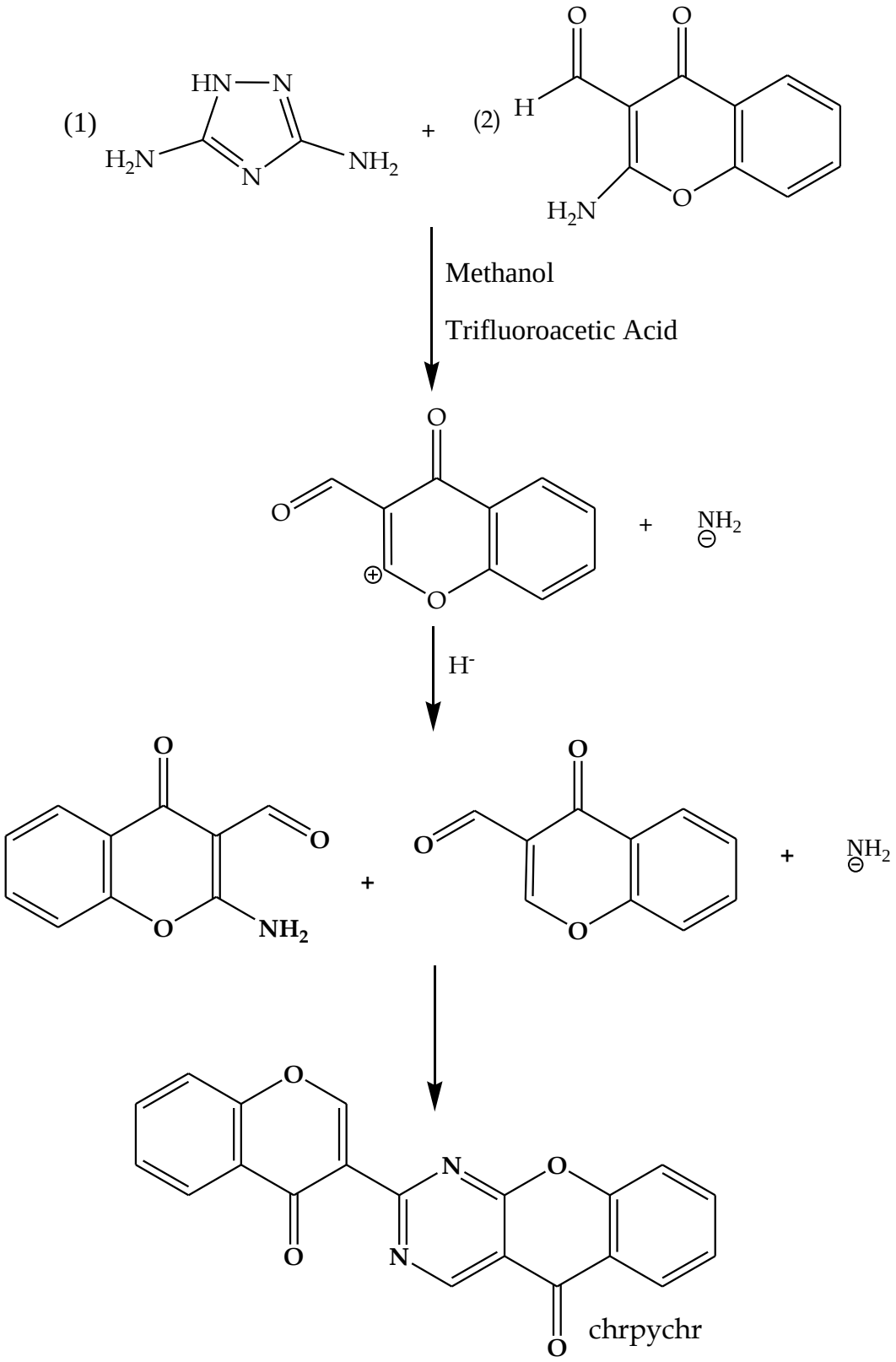

Scheme 3.1: *A proposed synthetic route for chrpychr.*

The IR spectrum of **1** is dominated by the intense vibrational bands of the tricarbonyl co-ligands at 2023, 1919 and 1894 cm^{-1}, see **Fig. 3.4**. The vibrations associated with the chrpychr free-ligand and its chelated form in **1** could not be readily assigned due to poorly resolved vibrational bands below 1800 cm^{-1} within the overlay IR spectra of **1** and its free-ligand, chrpychr. Hence, computational calculations of **1** at the DFT level aided in the identification of the vibrational bands associated with the chrpychr chelator [**20**].

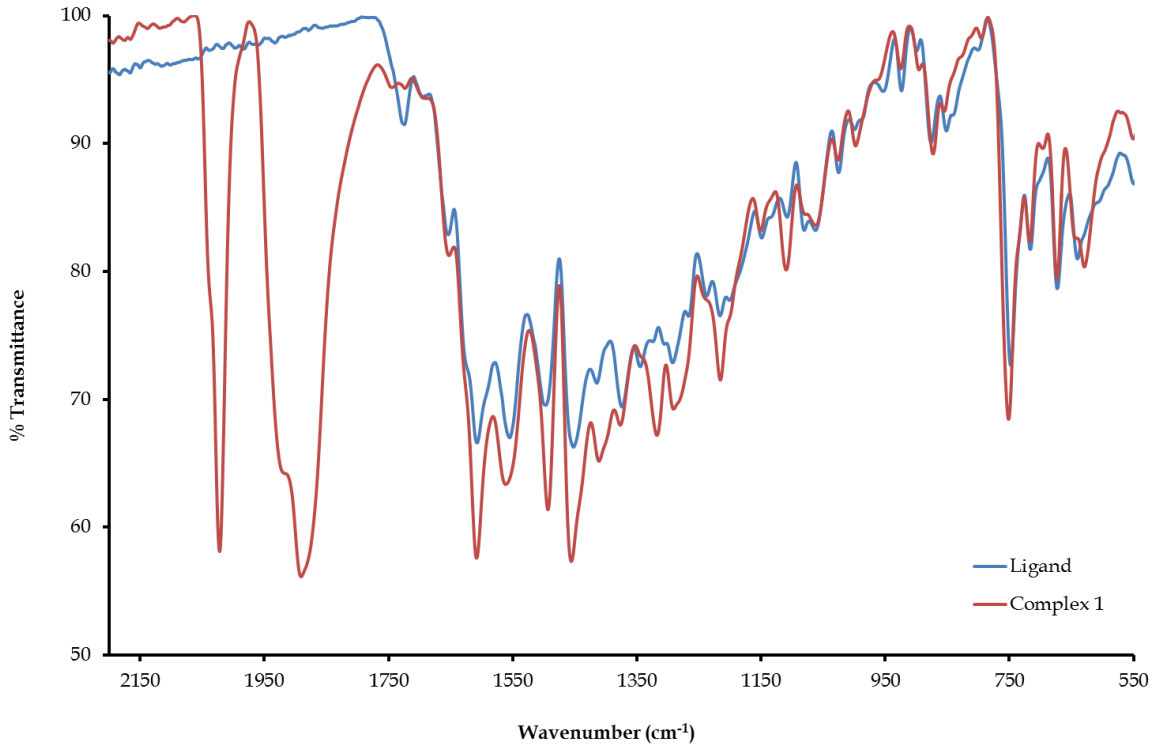

Fig 3.4: *Overlay IR spectra of complex **1** and its free-ligand, chrpychr.*

Notably, the vibration bonds of **1** below 1800 $cm^{-1}$are found at similar frequencies when compared to those of the *chrpychr* free-ligand below 1800cm^{-1} which suggests that the chrpychr coordinates to rhenium as a neutral chelator, see **Fig. 3.5.** In the calculated IR spectrum of **1**, the tri-carbonyl bonds vibrate at 2101, 2023 and 1999 cm^{-1}. Furthermore, two stretches for each of ν(C=O) [1608, 1564 cm^{-1} for **1** and 1618, 1544

cm^{-1} for free-ligand], ν(C=N) [1493, 1456 cm^{-1} for **1** and 1505, 1465 cm^{-1} for free-ligand] and ν(O-C-O) [1411, 1379 cm^{-1} for **1** and 1417, 1370 cm^{-1} for free-ligand] are observed in the experimental IR spectra of **1** and its free-ligand, chrpychr respectively. The latter assignments are based on the fact that the IR simulations of **1** shows that the ketonic [1652 and 1637 cm^{-1}], pyrimidyl C=N [1442 and 1405 cm^{-1}] and ether [1318 and 1347 cm^{-1}] bonds predominately vibrate at frequencies similar to the corresponding bonds in the experimental spectra.

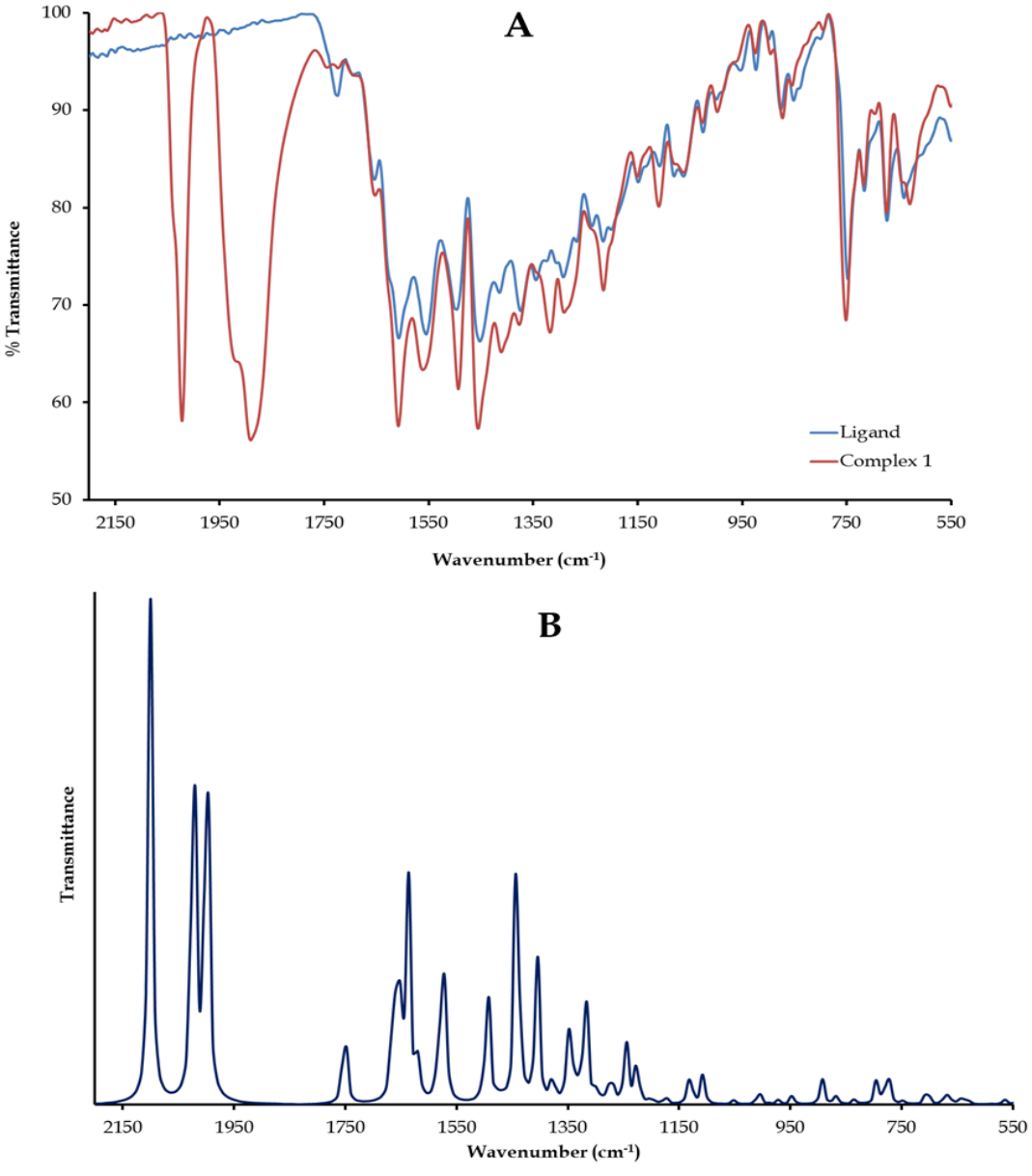

Fig 3.5: *(**A**) Overlay IR spectra of complex **1** and its free-ligand, chrpychr; (**B**) calculated IR spectrum of complex **1**.*

As indicated in terms of similarities between the IR spectrum of **1** and the free ligand, the proton NMR spectrum affirms that the chrpychr ligand coordinates as a neutral chelator due to the close similarities between its proton signals of those of **1**, see **Figs. 3.2** and **3.6**. For example, the chromone *H23* protons resonate at 10.08 ppm in the complex as well as the ligand. The same applies to the phenyl aromatic protons. Interestingly, the broad pyrimidyl singlet in the NMR spectrum of chrpychr splits into a broad doublet in **1**, this is ascribed to long range coupling. Due to, the highly delocalized and functionalized nature of the chrpychr numerous intraligand π-π^* electronic transitions are observed in the UV-Visible spectrum (See **Fig. 3.7**) below 400 nm.

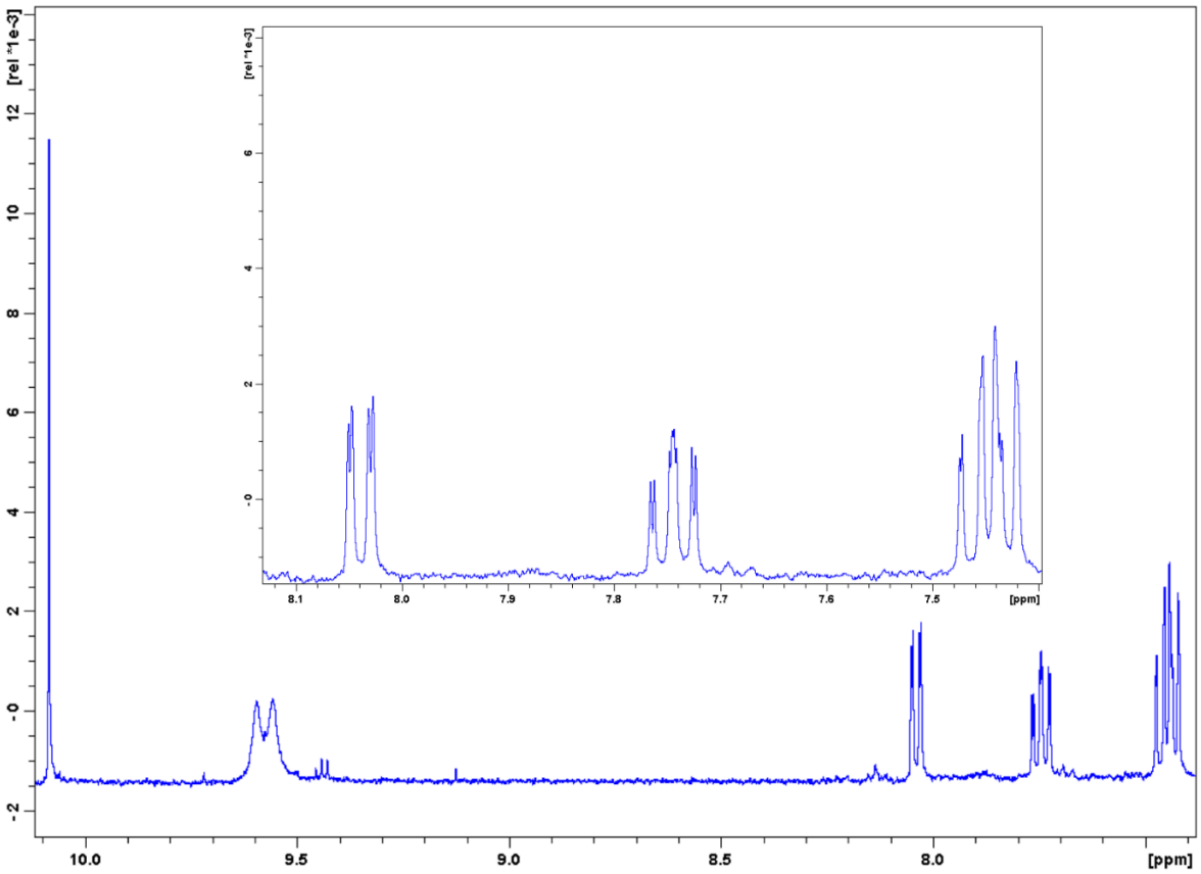

Fig. 3.6: *^{1}H NMR spectrum of complex **1** collected in deuterated dimethylsulphoxide.*

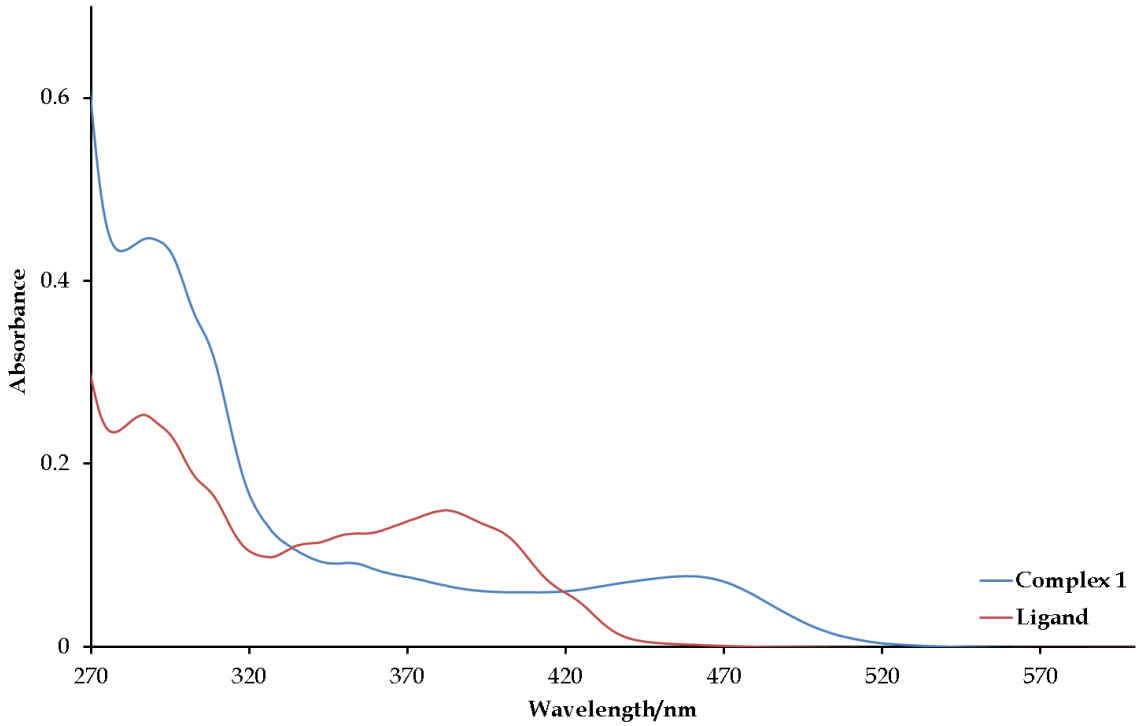

Fig 3.7: *Overlay UV/Vis spectra for the free-ligand, chrpychr and complex* ***1****.*

3.3.2 Synthesis, spectral characterization and computational studies of ***1,2 and 3:***

The compounds: *fac*-$(Re(CO)_3Br)_2(\mu$-chret) (**2**) and *fac*-[$Re(CO)_3$(bzch)Br] (**3**) [bzch = 2-benzimidazole-4*H*-chromen-4-one] were synthesized under anaerobic conditions from the equimolar reaction of [$Re(CO)_5Br$] with the diimines chret and chb, respectively. In **2**, the chret ligand bridges two *fac*-[$Re(CO)_3Br$] units while coordinating as a bidentate moiety to each metal centre *via* its $N_{imino}O_{keto}$ donor sets. X-ray structure of **3** (see **Fig.3.21**) revealed that the chb diimine underwent intraligand cyclization followed by the hydrolysis of one of its imine bonds. This was despite the anaerobic conditions of the reaction. In fact, the chloro rhenium(I) analogue, *fac*-[$Re(CO)_3$(bzch)Cl] were similarly formed from the reaction of [$Re(CO)_5Cl$] with the Schiff base ligand 2-(2- aminophenyliminomethyl)-4*H*-chromen-4-one (H_2pch) which led to the transformation of the latter to a bzch moiety [**18**]. However, no transformation of the diimine chb occured in the dinuclear ruthenium(III) compound, (μ-chb)[*mer*-$RuCl_3(PPh_3)]_2$ where the neutral chb moiety

bridges the two *cis*-[$Ru^{III}Cl_3$] cores *via* its ketonic oxygen and imino nitrogen atoms [**10**]. Furthermore, compounds **1** and **2** exhibit good solubility in high boiling point polar solvents including dimethylsulfoxide and dimethylformamide while showing a relatively modest solubility in tetrahydrofuran and poor solubility in chlorinated solvents such as chloroform. The low molar conductivities [Λ_M = 16.93 and 23.72 ohm.cm^{2}mol^{-1}] of the metallic compounds indicates their neutrality in DMSO.

The close correlation between the optimized and geometrical parameters of the respective complexes and the crystal structures is further emphasized by the low calculated root-mean-square deviation (RMSD), see **Fig. 3.8**. However, the somehow larger RMSD (0.720A°) of **2** is mainly ascribed to the high degree of largely freedom of rotation of the C-C single bonds within the chret chelator. Using the optimized structure of the metal complex, the lack of any negative Eigen values in the calculated frequencies confirmed that the structures are at global minima on their individual potential energy surfaces [**17**].

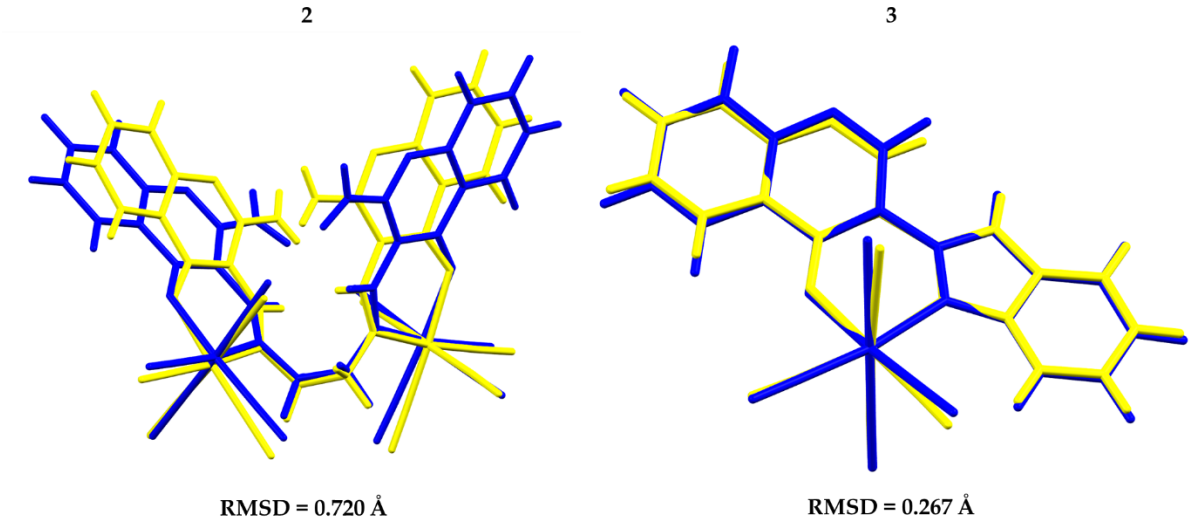

Fig. 3.8: *Overlay structures of the optimized and crystal structures for* **2** *and* **3** *with their corresponding RMSD values. The crystal structures are shown in yellow while the optimized structures are given in blue.*

Broad vibrational bands are observed below 1700 cm^{-1} in the experimental IR spectra of the metal complexes which could not be clearly assigned without the aid of the simulated IR spectra of **2** and **3**, see **Figs. 3.9 – 3.12**. Both the experimental [2015, 1871

cm^{-1} for **2** and **3**] and simulated [2105, 2018, 2016 cm^{-1} for **2** and 2097, 2017, 1993 cm^{-1} for **3**] IR spectra are dominated by the intense stretches of the carbonyl co-ligands. Similarly, the ν(N-H) vibrations of **2** and **3** appear as weak intensity vibrational bands in their respective simulated [3644 cm^{-1} for **2** and 3654, 3289 cm^{-1} for **3**] and experimental [2920, 2850 cm^{-1} for **2** and 2915 cm^{-1} for **3**] IR spectra. The simulated IR spectrum of **2** indicates distinctive vibrational bands associated with the ketonic (at 1687 cm^{-1}), imine (at 1567 cm^{-1}) and ether (at 1469 cm-^{1}) bonds whereas the corresponding IR stretching frequencies can be found at 1655 cm^{-1} [for ν(C=O)], 1464 cm^{-1} [for ν(O-C-O)], 1615 and 1613 cm^{-1} [for ν(C=N)] in the experimental IR spectrum of **2**. Correlating the simulated IR spectrum of **3** with its experimental IR spectrum, revealed that the experimental vibrations for ν(C=O) are found at 1628 and 1607 cm^{-1} while the ν(C=N) and ν(O-C-O) appears at 1567 cm^{-1} and 1461 cm^{-1}, respectively in the simulated spectra.

In the proton NMR spectrum of **2**, the aliphatic protons of the bridging ethane moiety resonates as a singlet at 3.87 ppm, see **Fig. 3.13**. A broad singlet at 10.91 ppm corresponds to the protons of the amino nitrogens of **1** but the analogous protons were observed as two broad signals in the proton NMR spectrum of the free-ligand, chret, see **Fig. 3.1** For **2**, the aromatic protons of the chromone moieties and the imino signal coalesce into two multiplets (*viz.* 8.95 – 8.65 ppm and 8.12 – 7.11 ppm) in comparison to the corresponding well-resolved signals at 8.72 ppm (for the imino protons) and 7.98, 7.67, 7.37 ppm (for the aromatic protons of the chromone moieties) of the free-ligand, chret. The most intense signal in the ^{1}H NMR spectrum of **3** is due to the *H1* proton positioned on the chromone moiety which appears as a sharp singlet (at 9.69 ppm).

The benzimidazole proton resonates as an intense signal at 9.39 ppm which integrates to one while the multiplet between 8.27 and 7.22 ppm are due to the remaining aromatic peaks. The presence of the *pi*-conjugated neutral chelators in **2** and **3** results in the occurrence of only intra-ligand π-π* transitions in their UV-Vis spectra, see **Figs. 3.13** and **3.14**. As expected, no metal-based *d-d* transitions are

observed at more red-shifted regions due to the low-spin d^6 electron configurations of **2** and **3**.

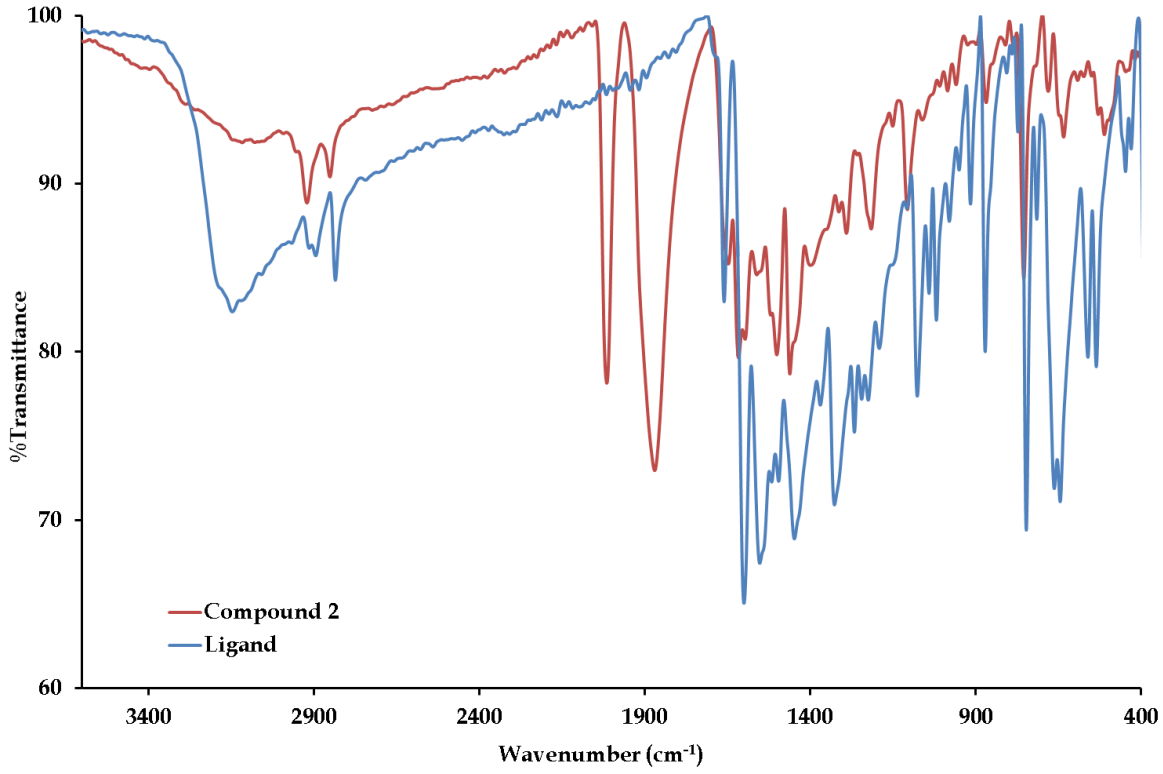

Fig 3.9: *Overlay IR Spectra of compound* **2** *and its free-ligand, chret between 400 and 4000 cm^{-1}.*

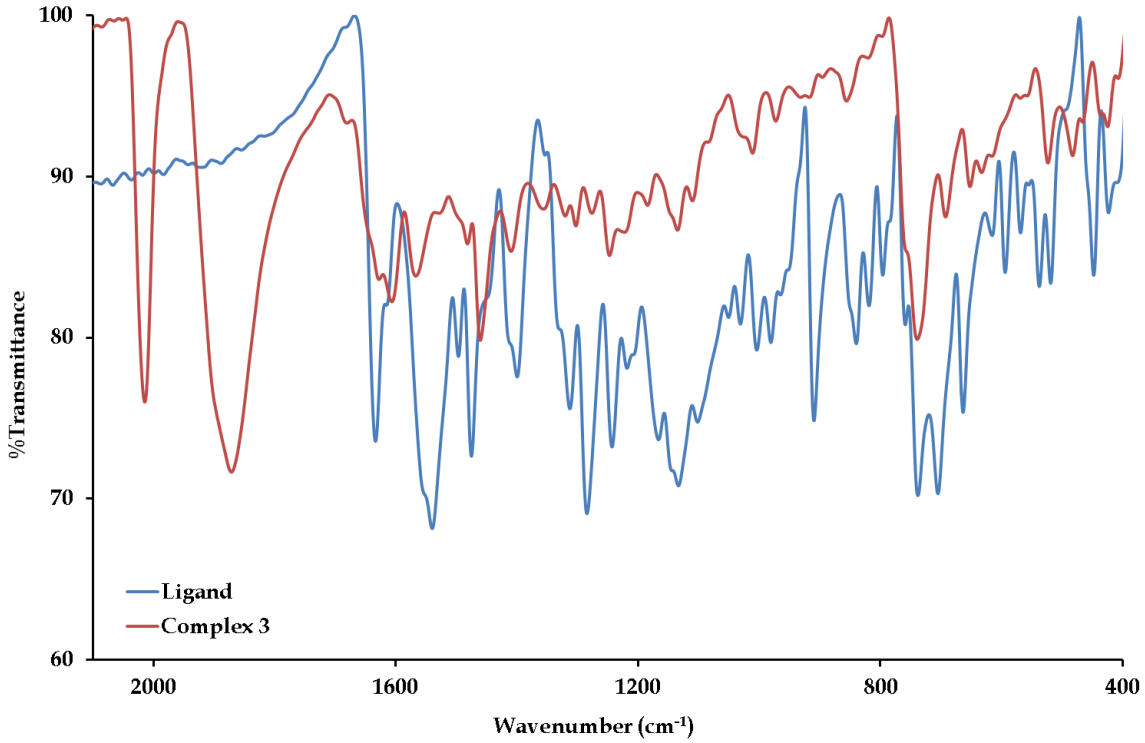

Fig 3.10: *Overlay IR Spectra of complex* ***3*** *and its free-ligand, chb between 400 and 2000 cm-1*.

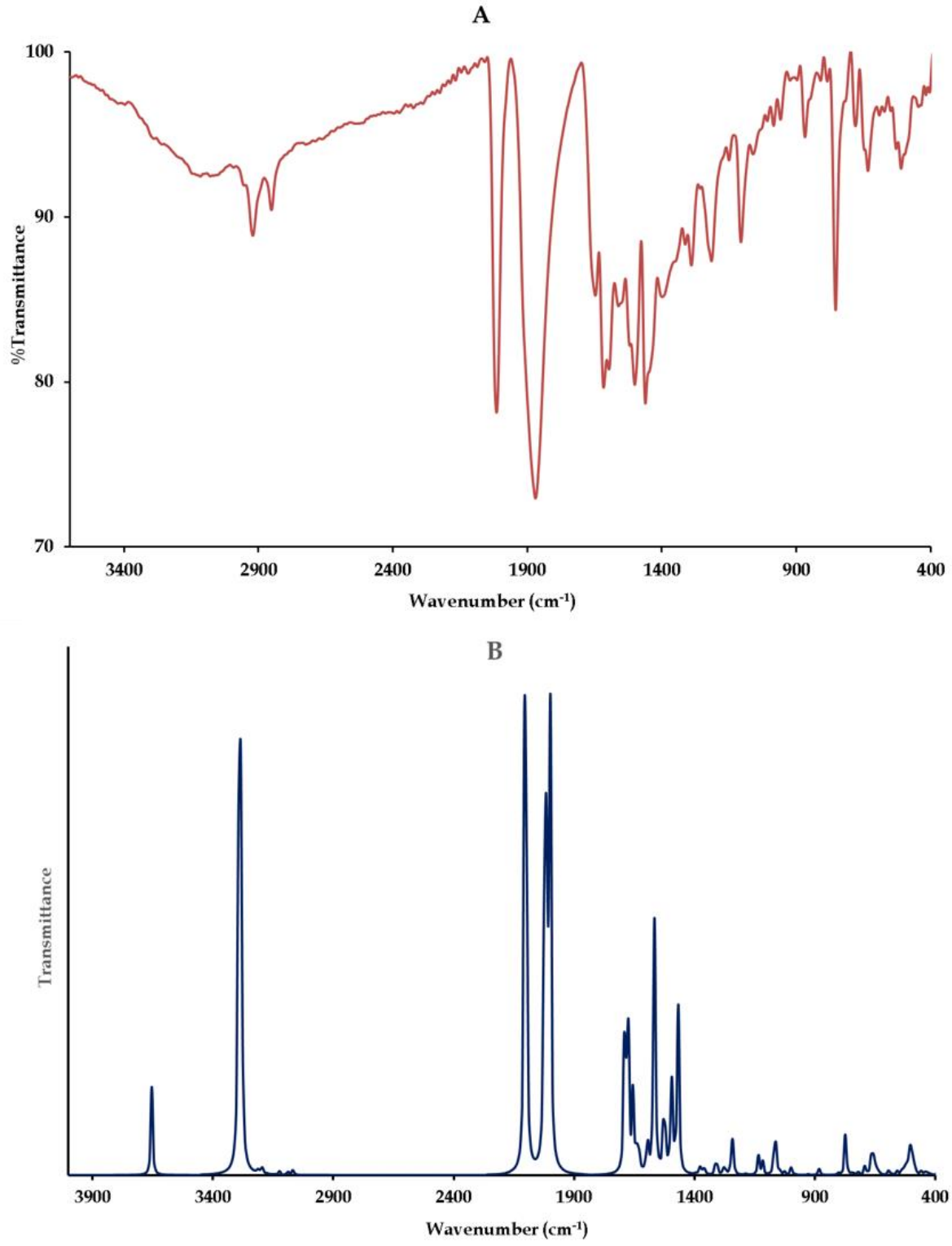

Fig. 3.11: *Comparison between experimental- (**A**) and simulated (**B**) spectrum of* **2**.

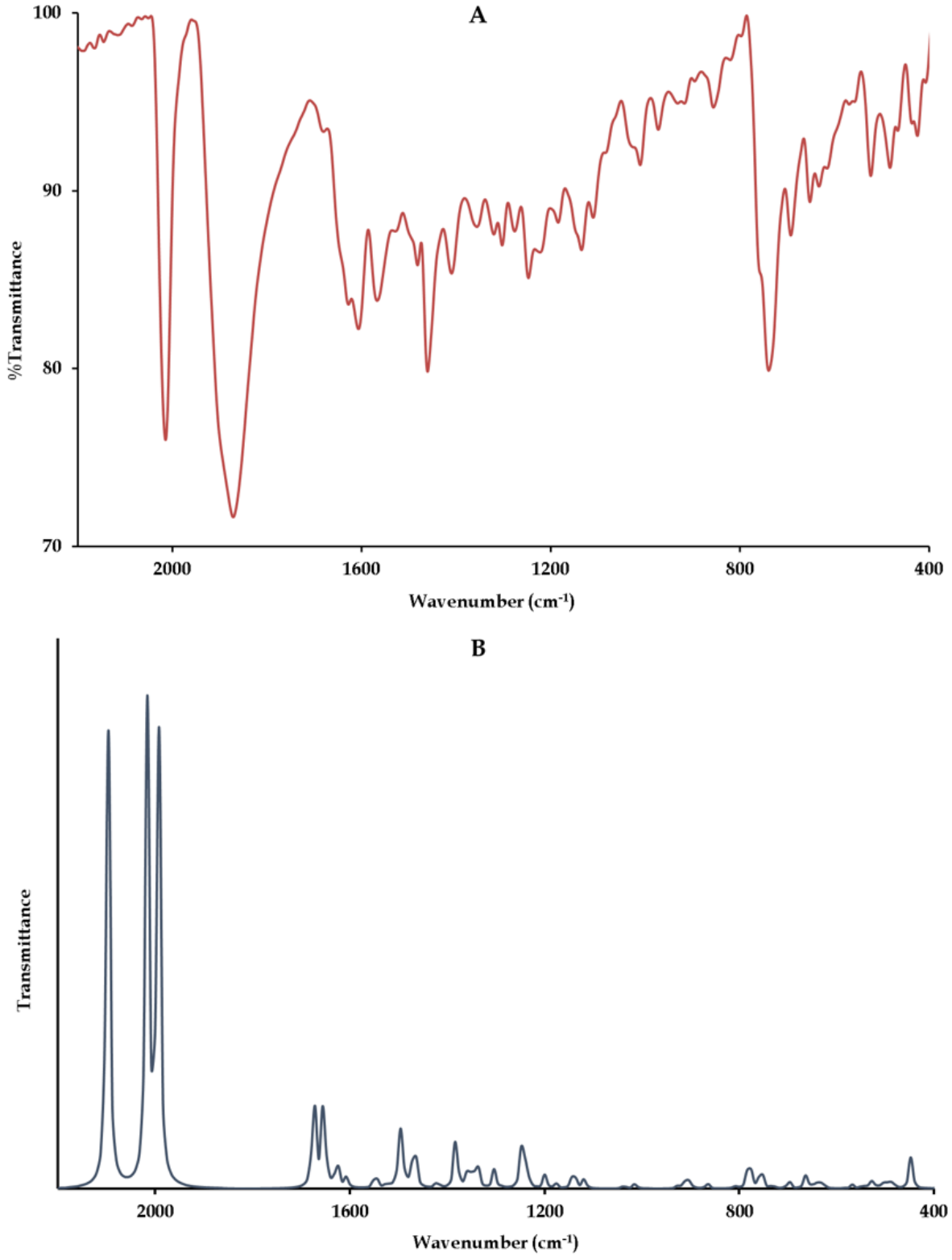

Fig. 3.12: *Comparison between experimental- (**A**) and simulated (**B**) spectrum of **3**.*

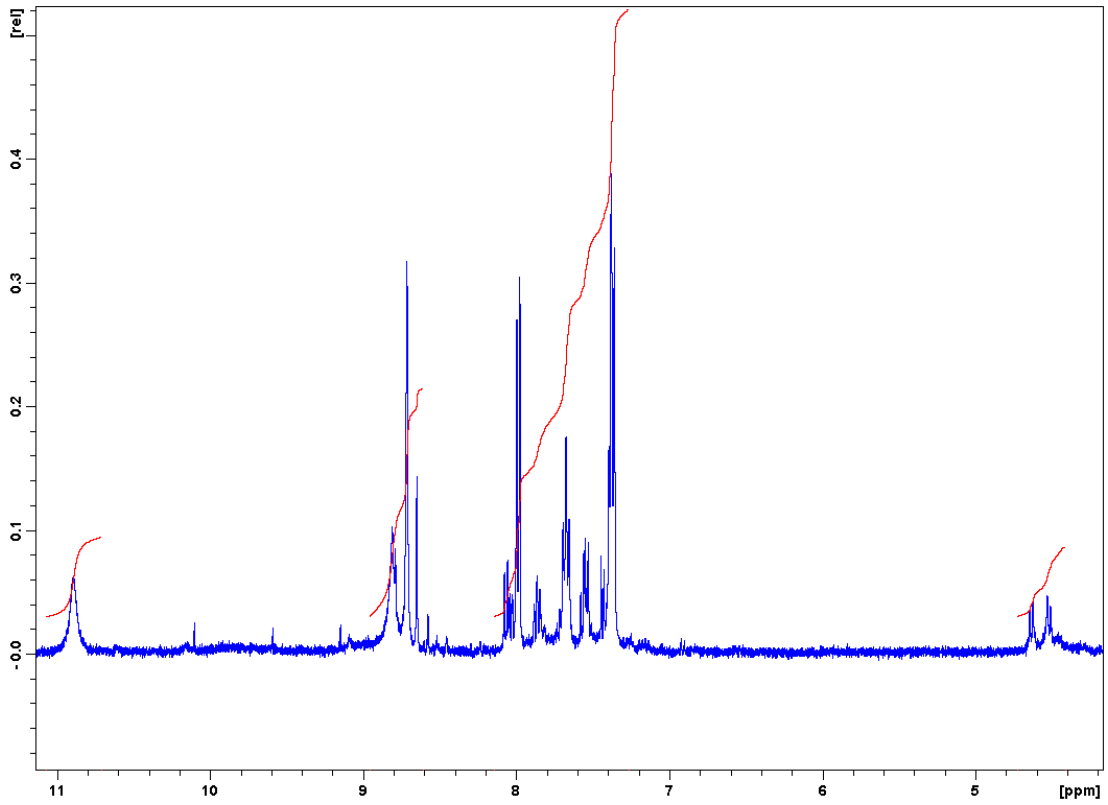

Fig. 3.13: *^{1}H NMR spectrum of compound* **2**.

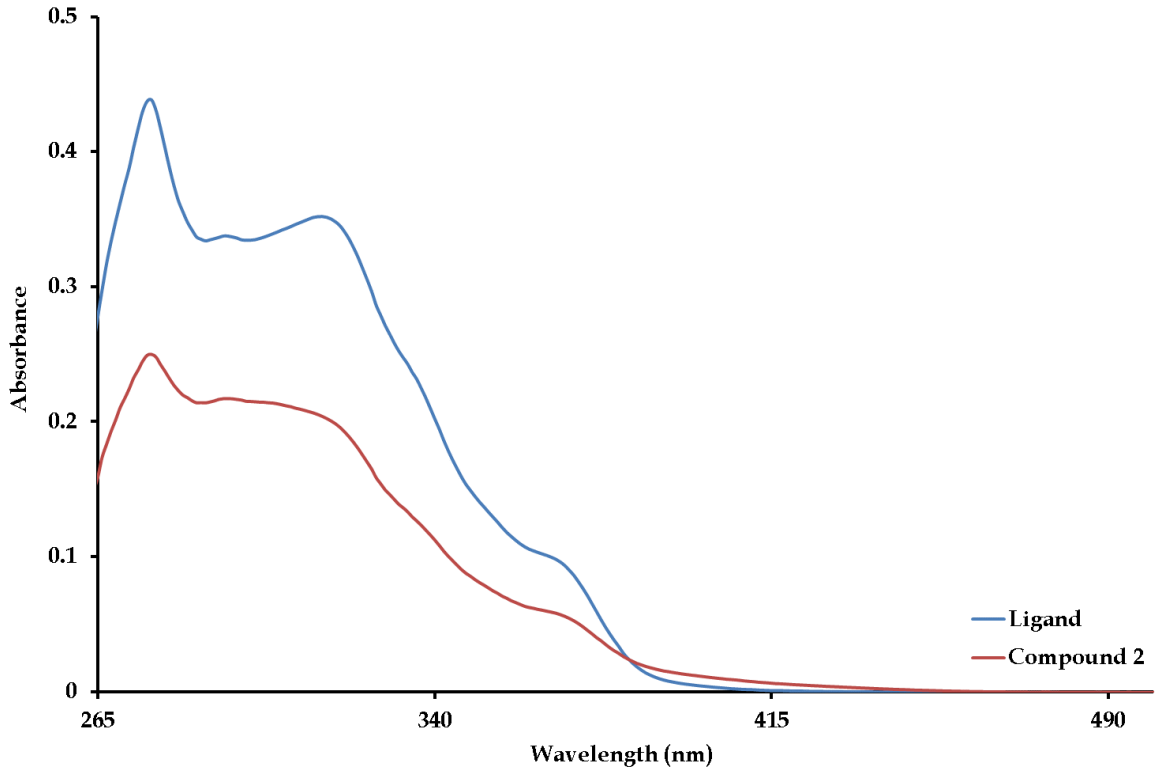

Fig 3.14: *Overlay UV/Vis spectra for the free-ligand, chret and compound* **2**.

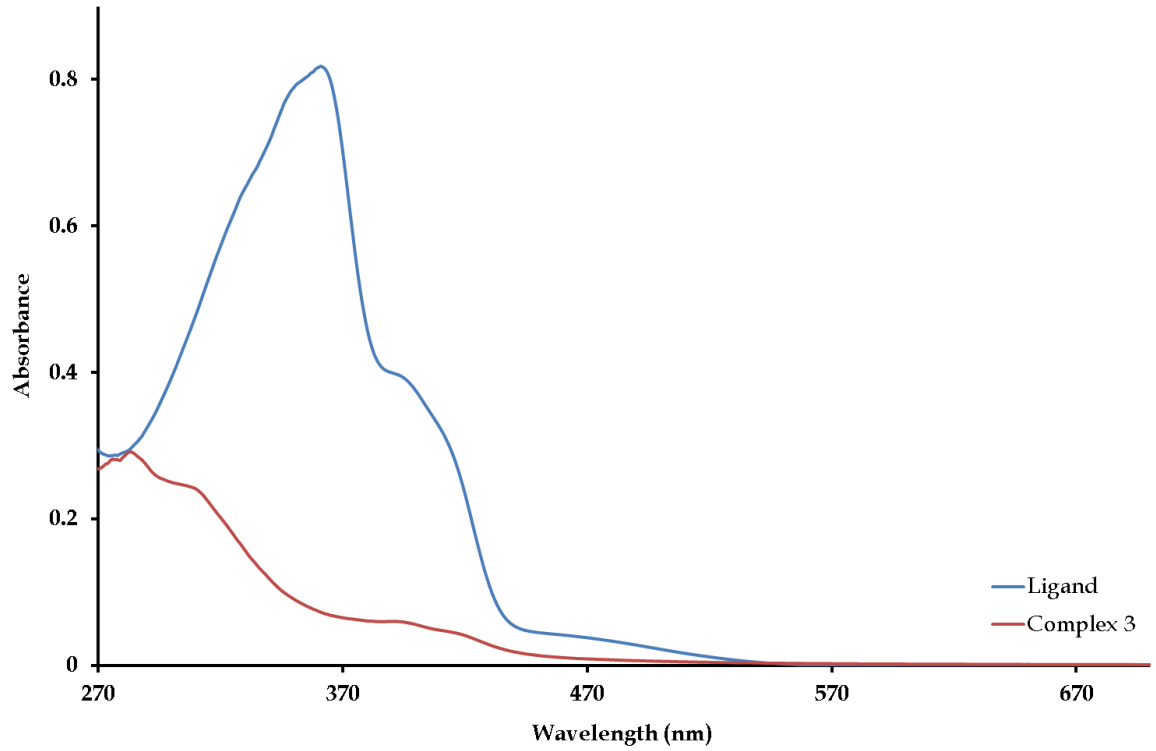

Fig 3.15: *Overlay UV/Vis spectra for the free-ligand, chb and complex* ***3****.*

3.3.3 Crystallographic studies

*3.3.3.1 Crystal structure of fac-[Re(CO)$_3$(chrpychr)(Br)] (**1**)*

X-ray structure analysis revealed that **1** co-crystallized with a toluene molecule in a *P2$_1$/n* space group see **Fig. 3.17.** The crystal lattice is stabilized by a series of intramolecular interactions [at 4.034 Å] between the co-planar conventional chromone moieties while similar interactions [at 3.674 Å] are found between co-planar chromone moieties modified with respective annealed pyrimidine rings. The intramolecular interactions between the modified chromone moieties are re-enforced by *pi*-stacking interactions [at 3.483 Å] between toluene molecules and the modified chromone moieties, see **Fig. 3.16**. Ultimately, these intermolecular interactions allows complex **1** and its solvent molecule of recrystallization to pack in columns aligned with the [*c*]-axis.

Complex **1** exhibits a distorted octahedral geometry imposed on by the constrained bite angles [O1-Re-N1 = 84.34(6)^{o}] (see **Fig. 3.17**). Consequently, the angles C1-Re-N1 [175.01(9)^{o}] and C3-Re-O1 [176.52(9)^{o}] equatorial as well as the axial plane [C2-Re-Br = 176.40(8)^{o}] deviate from linearity. The similarity in the bond length of C12-C13 bond [1.475(4) Å] confirms a bond order of one in the former. Single bond between C4-C12 [1.477(4) Å]. The degree of freedom about the C12-C13 allows the chromone and pyrimidine annealed chromone moieties to afford a dihedral angle of 12.24^{o}. Furthermore, the aforementioned moieties are also found out of the equatorial plane ReC1C3O1N1 equatorial plane by 21.78^{o} (*wrt* the chromone moiety) and 19.81^{o} (*wrt* the annealed pyrimidine annealed chromone moiety).

The difference in the cyclic C-O ether [*e.g.* C11-O2 = 1.326(3) Å] and C4-O1 [C4-O1 = 1.257(3) Å] bond lengths affirms that the latter is in the keto-form which is further supported by the fact that the Re-O1 [2.137(2) Å] bond distance is identical to an analogous bond found in *fac*-[Re(CO)$_3$(bzch)Cl] [2.137(2) Å] [**18**]. Evaluation of the rhenium to carbonyl bond distances revealed a shorter bond distance for the Re-C3 bond [1.898(2) Å] when compared to Re-C2 [1.921(5) Å] and Re-C1 [1.918(7) Å] bonds. This phenomenon is ascribed to the weaker *trans*-influence of the ketonic O1 opposite to the N1 atom and Br co-ligand. The C-N [C23-N1 = 1.347(3) Å, C13-N1 = 1.366(3) Å C13-N2 = 1.336(3) Å and C14-N2 = 1.317(3) Å] and C-C [C23-C22 = 1.383(4) Å and C14-C22 = 1.394(3) Å] bond lengths that constitutes the pyrimidine ring suggest that the latter is a delocalized π-system and implies that the pyrimidine N1 atom acts as a neutral donor to the metal centre.

The rhenium(I) to pyrimidine nitrogen bond length [2.232(2) Å] of **1** is significantly higher than the range [2.15(2) – 2.217(9) Å] for analogous bond lengths in other *facial* tricarbonyl rhenium(I) compounds [**21-25**]. However, in the nitrogen heterocyclic carbene rhenium(I) complex, *fac*-[Re(CO)$_3$(qpim)] (Hqpim = 1-(2-quinoxyl)-3-phenylimidazolium) [2.621(4) Å] the Re-Br bond distance is comparable to that of **1** [Re-Br = 2.6298(2) Å] [**25**].

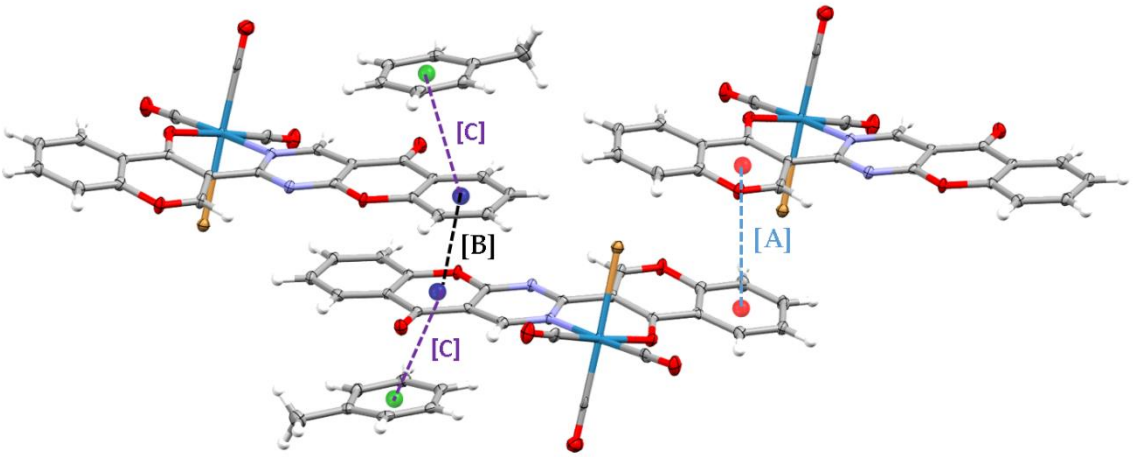

Fig. 3.16: *A perspective view illustrating the intermolecular interactions between adjacent molecules of* ***1****;* ***[A]*** *depicts the intermolecular interactions [at 4.034 Å] between the co-planar conventional chromone moieties,* ***[B]*** *depicts the intermolecular [at 3.674 Å] are found between co-planar chromone moieties modified with respective annealed pyrimidine rings and* ***[C]*** *depicts the pi-stacking interactions [at 3.483 Å] between toluene molecules and the modified chromone moieties.*

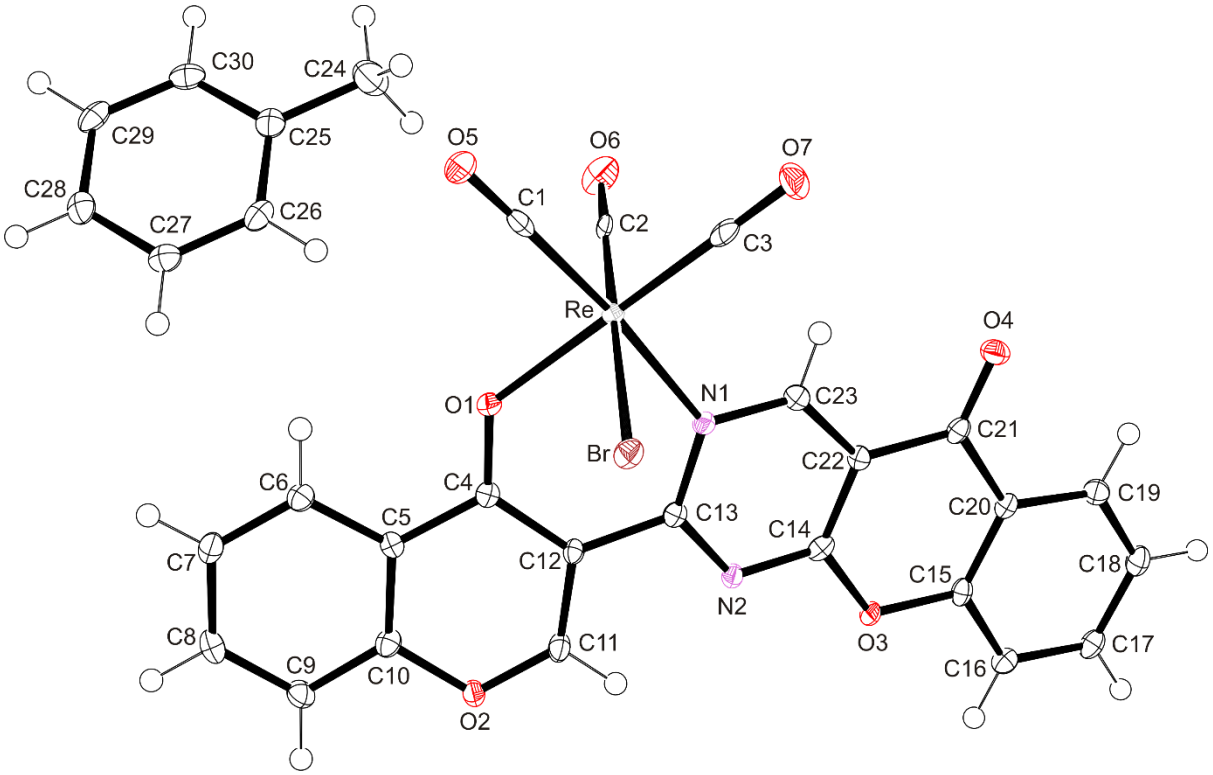

Fig. 3.17: *Thermal ellipsoid view of compound* ***1*** *showing 50 % probability displacement ellipsoids and the atom labelling.*

*3.3.3.2 Crystal structure of fac-$(Re(CO)_3Br)_2$(μ-chret) (**2**)*

Compound **2** co-crystallized with three tetrahydrofuran molecules of recrystallization in its triclinic unit cell. The crystal lattice of **2** is stabilized by a network of classical intramolecular [Br1···H4a-N4 = 2.73(4) Å and Br2···H2a-N2 = 2.60(4) Å] and intermolecular hydrogen bonding [O11A···H2b-N2 = 1.95(4) Å and O11B···H4b-N4 = 1.91(5) Å], see **Fig. 3.18**. Collectively these hydrogen bonding interactions allows molecules of **2** to pack in columns parallel to the [*a*]- and [*b*]-axes.

The geometry at each Re(I) metal centres of **2** are distorted octahedron which is largely imposed on by their constrained bite angles [O1-Re1-N1 = 84.48(8)^o and N3-Re2-O6 = 83.91(8)^o], see **Fig. 3.19**. Consequently, the C2-Re1-Br1 [176.84(8)^o], O1-Re1-C3 [177.41(9)^o], C1-Re1-N1 [176.2(1)^o], Br2-Re2-C6 [177.02(8)^o], C4-Re2-O6 [176.4(1)^o] and N3-Re2-O6 [174.2(1)^o] deviate from linearity. The flexibility of the bridging ethane moiety affords narrower C=N-C [C18-N3-C19 = 114.7(2)^o and C16-N1-C17 = 114.4(2)^o] bond angles than the expected 120^o for a bond angle containing a central sp^2 hybridized nitrogen. Despite the influence of the bridging ethane moiety, the imino bond of **2** are in the same range [1.284(3) - 1.301(5) Å] as similar bonds found in other Schiff bases [**26-29**]. Across the respective octahedrons, only the Re1-C2 [1.897(3) Å] and Re2-C6 [1.897(3) Å] bonds are nearly equidistant which reflects similar *trans*-influence induced on by the Br1 and Br2 atoms, respectively. Hence the comparable *cis*-orientated organometallic bonds [Re1-C1 = 1.941(3) Å, Re1-C3 = 1.894(3) Å, Re2-C4 = 1.908(3) Å and Re2-C5 = 1.931(5) Å] across the octahedrons in **2** differs.

The rhenium to ketonic [Re1-O1 = 2.138(2) Å and Re2-O6 = 2.139(2) Å] and imino nitrogen [Re1-N1 = 2.170(2) Å and Re2-N3 = 2.168(2) Å] bonds are similar to analogous bonds found within *fac*-[$Re(CO)_3$(chrpychr)Br] [chrpychr = 2-(4-oxo-4*H*-chromen-3-yl)-5*H*-chromeno[2,3-*d*]pyrimidin-5-one and [(*μ*-O){ReOCl(amp)}$_2$] [amp = 6-amino-3-methyl-1-phenyl-4-azahept-2-ene-1-one] [**18**, **10**]. Bond orders with the chret chelator is established based on the ketone bonds [C14-O1 = 1.259(4) Å and C28-O1 = 1.261(4) Å] being shorter than the carbonyl bonds [*e.g.* C1-O3 = 1.145(3) Å]

but yet longer than the ether bonds [*e.g.* C8-O2 = 1.383(3) Å and C21-O7 = 1.346(4) Å]. Also, the localized C=C bonds in the chromone moeities remain intact after the coordination of the chret chelators as these C=C bonds [C7-C15 = 1.413(4) Å and C17-C18 = 1.414(4) Å] are shorter than the C-C single bond [C17-C18 = 1.536(3) Å] that constitutes the bridging ethane moeity.

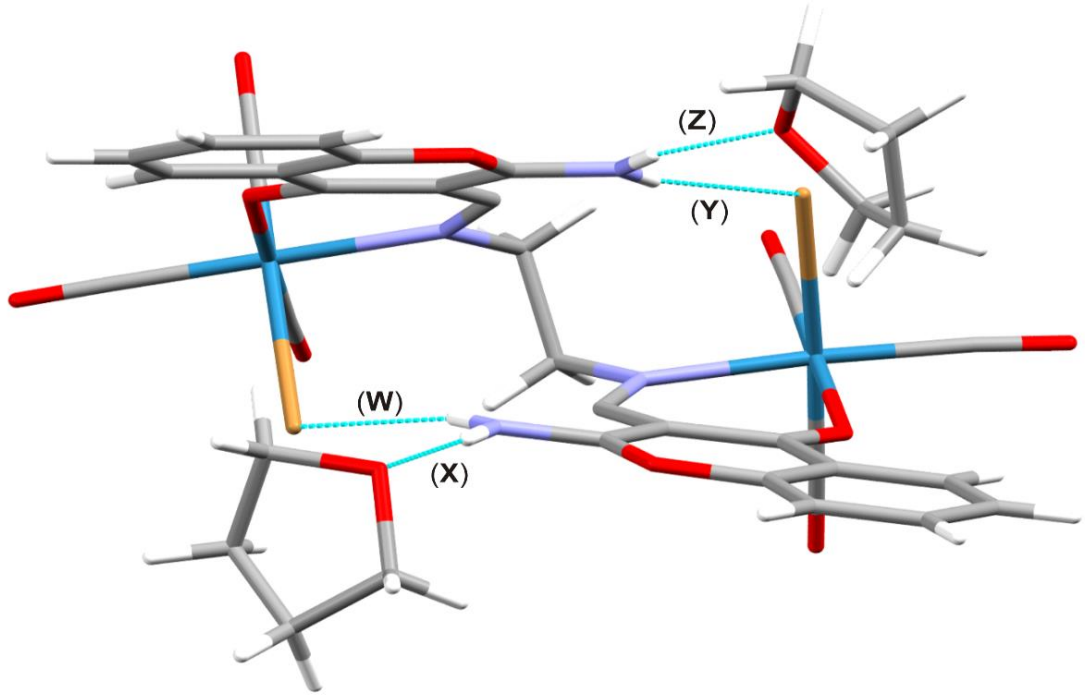

Fig. 3.18: *A perspective view of* **2** *illustrating the intramolecular [Br1···H4a-N4 = 2.73(4) Å (**W**) and Br2···H2a-N2 = 2.60(4) Å (**Y**)] and intermolecular hydrogen bonding [O11A···H2b-N2 = 1.95(4) Å (**X**) and O11B···H4b-N4 (**Z**)].*

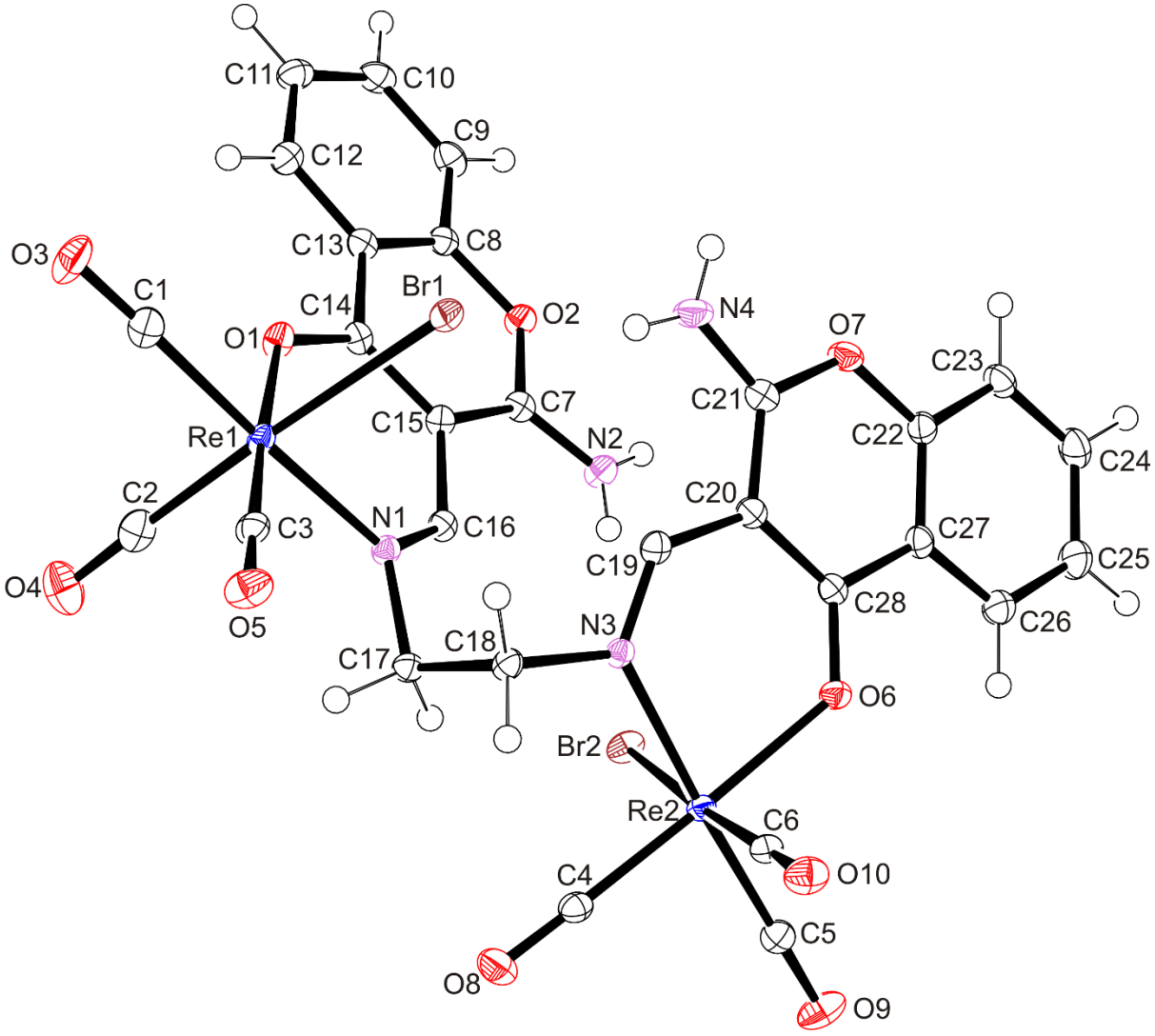

Fig. 3.19: *Thermal ellipsoid view of compound* **2** *showing 50 % probability displacement ellipsoids and the atom labelling. The tetrahydrofuran molecules of crystallization were omitted for clarity.*

*3.3.3.3 Crystal structure of fac-[Re(CO)$_3$(bzch)Cl] (**3**)*

Four molecules of **3** occupies the monoclinic unit cell and each of these molecules form dimers with molecules of **3** in adjacent unit cells *via* classical hydrogen-bonding interactions [Br1···N2A-H2A/Br1A···N2-H = 2.57(3) Å], see **Fig. 3.20.** Consequently, molecules of **3** are self-assembled in columns aligned with the [*b*]-axis. Indicative to 3, the constrained bite angle [O1-Re-N1 = 81.99(7)°] of **3** result in deviation of orthogonality in the opposing C1-Re-C3 [86.90(1)°] bond angle, see **Fig. 3.21**.

The rhenium to halide bond of **3** [Re-Br = 2.6322(8) Å] is comparable to those found in other *facial* tricarbonyl rhenium complexes [**30**, **31**, **32**]. All the remaining coordination bonds of **3** [Re-N1 = 2.186(2) Å, Re-O1 = 2.141(1) Å, Re-C1 = 1.931(2) Å, Re-C2 = 1.901(2) Å and Re-C3 = 1.901(2) Å] are similar to its chloro-analogue, *fac*-[$Re(CO)_3$(bzch)Cl], *viz.* Re-O_{ketone} = 2.137(2) Å, Re-$N_{benzimidazole}$ = 2.179(2) Å and Re-$C_{carbonyl}$ = 1.929(2) Å, 1.904(2) Å, 1.898(2) Å [**26**]. Furthermore, the double bond character of C10-N1 bonds [1.336(3) Å] are clearly established when compared to the C-N bond lengths [C10-N2 = 1.358(3) Å, C16-N1 = 1.401(3) Å and C11-N2 = 1.374(3) Å]. In addition, the bridging C9-C10 [1.466(3) Å] bond is single, based on the more shorter localized C=C [1.365(3) Å] chromone bond. In turn, the degree of freedom around the C9-10 single bond allows the chromone and benzimidazole plane to form a dihedral angle of 6.01°. Also, the benzimidazole and chromone moeities lies out of the plane of the O1N1C3C1 mean equotorial plane by 17.83° and 18.37°, respectively. The toluene molecule of recrystallization from an adjacent unit cell is nearly co-planar with the bzch chelator of **3** indicating π-π interactions between this toluene molecule and the bzch chelator.

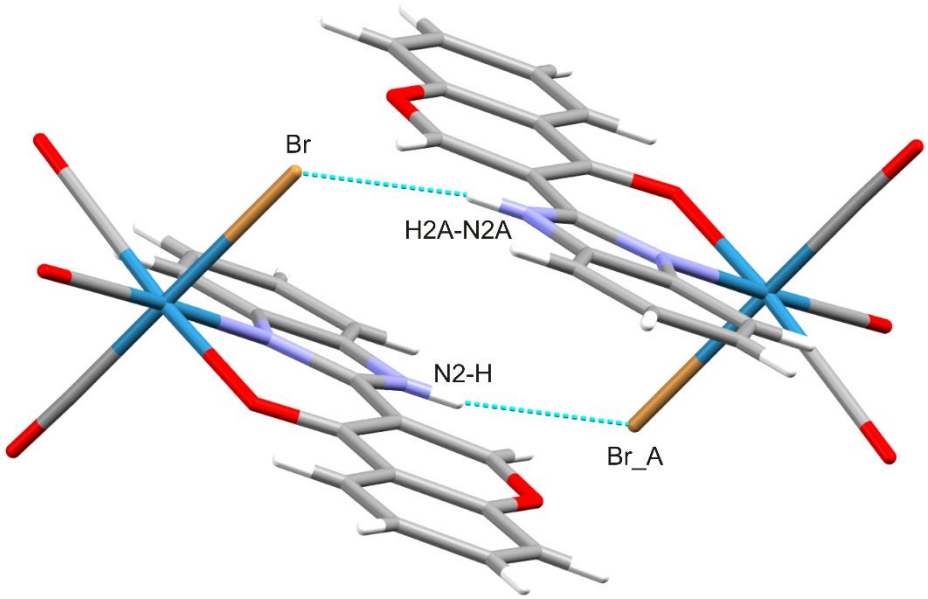

Fig. 3.20: *A perspective view of the dimer of* ***3*** *formed by hydrogen bonding interactions: Br1···N2A-H2A/Br_A···N2-H2 = 2.57(3) Å.*

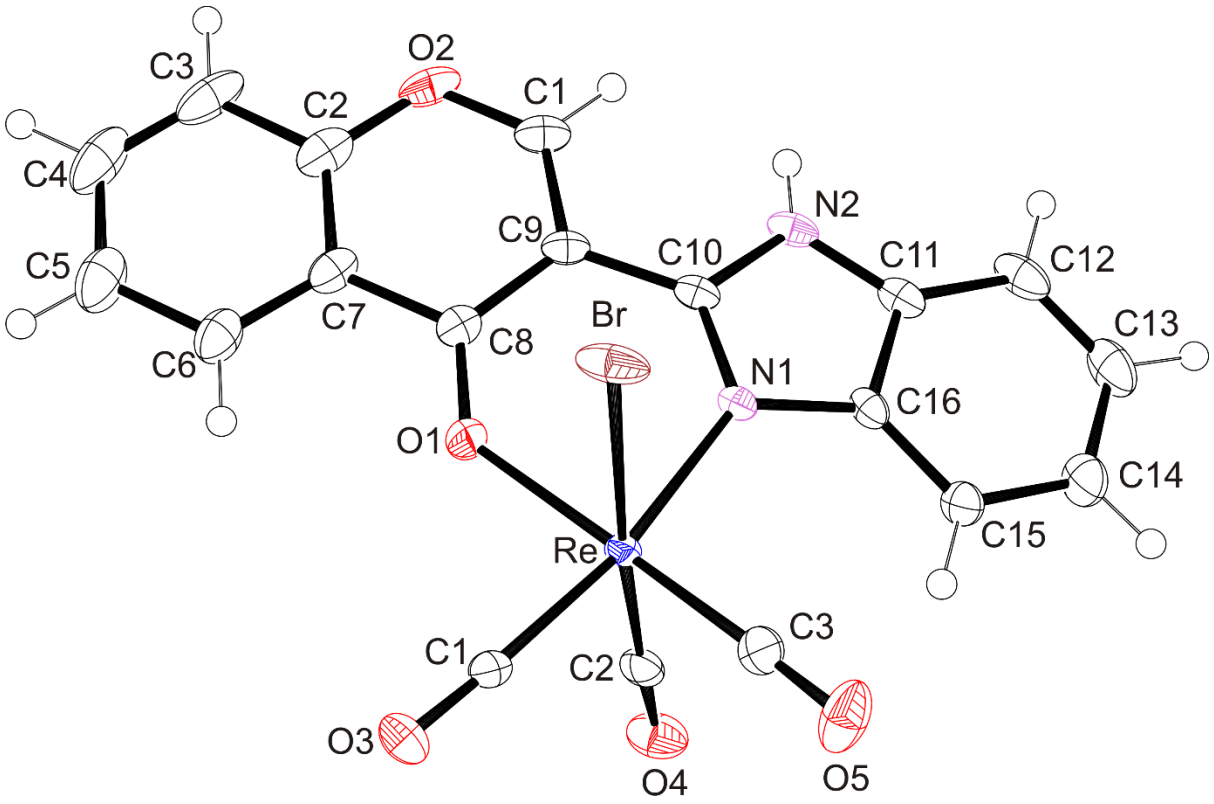

Fig. 3.21: *Thermal ellipsoid view of complex* ***3*** *showing 50 % probability displacement ellipsoids and the atom labelling. The toluene molecule of crystallization were omitted for clarity.*

3.4 References

[1] J.R. Dilworth, S.J. Parrott, *Chem. Soc. Rev.* 27 (1998) 43.

[2] S. Jurisson, D. Berning, J. Wei, M. Dangshe, *Chem. Rev*. 93 (1993) 1137.

[3] S. Jürgens, W.A. Herrmann, F.E. Kühn, *J. Organomet. Chem.* 751 (2014) 83.

[4] U. Abram, R. Alberto, *Braz. Chem. Soc.* 17 (2006) 1486.

[5] S.L. Binkley, T.C. Leeper, R.S. Rowlett, R.S. Herrick, C.J. Ziegler, *Metallomics* 3 (2011) 909.

[6] R.S. Herrick, T.J. Brunker, C. Maus, K. Crandall, A. Cetin, C.J. Ziegler, *Chem. Commun.* (2006) 4330.

[7] K. Potgieter, P. Mayer, T.I.A. Gerber, I.N. Booysen, *Polyhedron* 28 (2009) 2808.

[8] C.L. Ferreira, C.B. Ewart, S.R. Bayly, B. O. Patrick, J. Steele, M.J. Adam, C. Orvig, *Inorg. Chem*. 45 (2006) 6979.

[9] Q. Nadeem, D. Can, Y. Shen, M. Felber, Z. Mahmooda, R. Alberto, *Org. Biomol. Chem.* 12 (2014) 1966.

[10] I.N. Booysen, A. Adebisi, M.P. Akerman, O.Q. Munro, B. Xulu, *J. Coord. Chem.* DOI: 10.1080/00958972.2016.1177177.

[11] Bruker APEX2, SAINT and SADABS. *Bruker AXS Inc.* (2010) Madison, Wisconsin, USA.

[12] R.H. Blessing, *Acta Cryst.* A51 *(*1995) 33.

[13] G.M. Sheldrick, *Acta Cryst*. A64 (2008) 112.

[14] L.J. Farrugia, *J. Appl. Cryst.* 45 (2012) 849

[15] M.J. Frisch, G.W. Trucks, H.B. Schlegel, G.E. Scuseria, M.A. Robb, J.R. Cheeseman, G. Scalmani, V. Barone, B. Mennucci, G.A. Petersson, H. Nakatsuji, M. Caricato, X. Li, H.P. Hratchian, A.F. Izmaylov, J. Bloino, G. Zheng, J.L. Sonnenberg, M. Hada, M. Ehara, K. Toyota, R. Fukuda, J. Hasegawa, M. Ishida, T. Nakajima, Y. Honda, O. Kitao, H. Nakai, T. Vreven, J.A. Montgomery Jr., J.E. Peralta, F. Ogliaro, M. Bearpark, J.J. Heyd, E. Brothers, K.N. Kudin, V.N. Staroverov, R. Kobayashi, J. Normand, K. Raghavachari, A. Rendell, J.C. Burant, S.S. Iyengar, J. Tomasi, M. Cossi, N. Rega, J.M. Millam, M. Klene, J.E. Knox, J.B. Cross, V. Bakken, C. Adamo, J. Jaramillo, R. Gomperts, R.E. Stratmann, O. Yazyev, A.J. Austin, R. Cammi,

C. Pomelli, J.W. Ochterski, R.L. Martin, K. Morokuma, V.G. Zakrzewski, G.A. Voth, P. Salvador, J.J. Dannenberg, S. Dapprich, A.D. Daniels, O. Farkas, J.B. Foresman, J.V. Ortiz, J. Cioslowski, D.J. Fox, GAUSSIAN 09 (Revision A.01), *Gaussian Inc*., Wallingford, CT (2009).

[16] I.N. Booysen, M.B. Ismail, M.P. Akerman, *J. Coord. Chem.* 66 (2013) 4371.

[17] A. Brink, H.G. Visser, A. Roodt, *Polyhedron* 52 (2013) 416.

[18] I.N. Booysen, M.B. Ismail, O.Q. Munro, *Inorg. Chem. Comm.* 30 (2013) 168.

[19] E. Simon, J.S. Lopez, *J. Fluorine Chem.*,156 (2013) 73.

[20] I.N. Booysen, I. Ebinumoliseh, M. P. Akerman, B. Xulu, *Inorg. Chem. Comm.* 62 (2015) 8.

[21] K.D. Benkstein, J.T. Hupp, C.L. Stern, *J. Am. Chem. Soc.* 120 (1998) 12982.

[22] S.E. Kabir, J. Alam, S. Gash, K. Kundu, G. Hogarth, D.A. Tocher, G.M.G. Hossain, H.W. Roesky, *Daltons Trans*. (4458) 2009.

[23] R.J. Shaver, M.W. Perkovici, D.P. Rillema, G. Woods, *Inorg. Chem.* 34 (1999) 5446.

[24] G. Wang, Y. Liu, X. Chen, Y. Zheng, Z. Xue, *Inorg. Chim. Acta.* 394 (2013) 488.

[25] J.G. Vaughan, B.L. Reid, P.J. Wright, S. Ramanchandani, B.W. Skeleton, P. Raiteri, S. Muzzioli, D.H. Brown, S. Stagni, M. Massi, *Inorg. Chem.* 53 (2014) 3629.

[26] T. Jurca, O. Ramadan, I. Korobkov, D. S. Richeson. *J. Organomet. Chem.* 802 (2016) 27-31.

[27] J. Mukiza, T.I.A. Gerber, E.C. Hosten. *Inorg. Chem. Comm.* 57 (2015) 54.

[28] K. Potgieter, P. Mayer, T. Gerber , N. Yumata, E. Hosten , I. Booysen , R. Betz, M. Ismail, B. van Brecht, *Polyhedron* 49 (2013) 67.

[29] K. Potgieter, P. Mayer, T.I.A. Gerber, I.N. Booysen, *Polyhedron* 28 (2009) 2808.

[30] P. Mayer, T.I.A. Gerber, B. Buyambo, A. Abrahams, *Polyhedron* 28 (2009) 1174.

[31] P. Mayer, K.C. Potgieter, T.I.A. Gerber, *Polyhedron* 29 (2010) 1423.

[32] J. Ho, W.Y. Lee, K. J. Tai Koh, P.P. Foo Lee, Y.K. Yan. *J. Inorg. Biochem*. 119 (2013) 10.

Table 3.1: *Crystal data and structure refinement data.*

	1.C_7H_8	**2**.3(C_4H_8O)	**3**.C_7H_8
Empirical Formula	$C_{23}H_{10}BrN_2O_7Re.C_7H_8$	$C_{28}H_{18}Br_2N_4O_{10}Re_2.3(C_4H_8O)$	$C_{19}H_{10}BrN_2O_5Re.C_7H_8$
Formula weight	783.98	1318.99	704.53
Temperature/K	100(2)	100(2)	100(2)
Crystal system	Monoclinic	Triclinic	Monoclinic
Space group	$P2_1/n$	P-1	$P2_1/n$
Unit cell dimensions (Å, °)	a = 12.1814(5)	a = 1.28859(6)	a = 12.400(5)
	b = 13.3633(6)	b = 13.1199(6)	b = 11.778(5)
	c = 16.5656(7) Å	c = 14.9558(7)	c = 16.316(5)
	α = 90.000(5)	α= 114.601(2)	α = 90.000(5)
	β = 106.087(2)°	β = 98.138(2)	β = 92.469(5)
	γ = 90.000(5)	γ = 102.350(2)	γ = 90.000(5)
Crystal size (mm)	0.28 x 0.09 x 0.03	0.13 x 0.06 x 0.05	0.09 x 0.06 x 0.05
V(Å^3)	2591.02(19)	2168.73 (18)	2380.07(16)
Z	4	2	4
Density (calc.) (Mg/m^3)	2.011	2.020	1.966
Absorption coefficient (mm^{-1})	6.29	7.49	6.82
F(000)	1512	1268	1352
θ range for data collection (deg)	1.9; 26.1	1.6; 29.1	2.0; 29.0
Reflections measured	47342	41497	23824
Observed reflections [I>2σ(I)]	5015	10414	6310
Independent reflections	4526	11421	5621
Data/Restraints/parameters	4526/0/371	11421/0/566	5621/0/321
Goodness of fit on F^2	1.048	1.03	1.03
Observed R, wR^2	0.016; 0.033	0.018; 0.043	0.020; 0.042
R_{int}	0.033	0.018	0.027

Table 3.2: *Comparison between the experimental and calculated bond lengths (Å) and angles (°) for* ***1****.*

	Experimental	**Calculated**
Re-Br	2.6298(2)	2.65898
Re-O1	2.137(2)	2.17665
Re-N1	2.232(2)	2.27053
Re-C1	1.919(3)	1.92163
Re-C2	1.922(2)	1.91026
Re-C3	1.898(2)	1.91700
C12-C13	1.477(4)	1.48402
C11-O2	1.326(3)	1.32891
C4-O1	1.257(3)	1.24257
C23-N1	1.347(3)	1.34122
C13-N1	1.366(3)	1.36268
C13-N2	1.336(3)	1.33356
C14-N2	1.317(3)	1.31771
C23-C22	1.383(4)	1.38653
C14-C22	1.394(3)	1.39898
O1-Re-N1	84.34(6)	81.970
C1-Re-N1	175.01(9)	173.596
C3-Re-O1	176.52(9)	175.589
C2-Re-Br	176.40(8)	175.042

Table 3.3: *Selected bond lengths [Å] and bond angles [°] for* **2**.

	Experimental	**Optimized**
Re1-Br1	2.6455(3)	2.72064
Re2-Br2	2.6377(3)	2.72059
Re1-O1	2.137(2)	2.1765
Re2-O6	2.139(2)	2.1764
Re1-N1	2.169(2)	2.2224
Re2-N3	2.171(2)	2.2224
Re1-C1	1.942(3)	1.9344
Re1-C2	1.894(3)	1.9091
Re1-C3	1.897(3)	1.9071
Re2-C4	1.908(3)	1.9071
Re2-C5	1.932(3)	1.9091
Re2-C6	1.893(2)	1.9343
C16-N1	1.286(4)	1.2919
C19-N3	1.291(4)	1.2919
C14-O1	1.259(4)	1.2502
C28-O6	1.261(3)	1.2503
C1-O3	1.144(3)	1.1492
C8-O2	1.383(3)	1.3796
C21-O7	1.347(4)	1.3440
C7-C15	1.414(4)	1.4102
C20-C21	1.411(4)	1.4103
C17-C18	1.537(3)	1.5374
O1-Re1-N1	84.52(7)	83.027
O6-Re2-O6	83.93(7)	83.023
C2-Re1-Br1	176.85(8)	177.228
O1-Re1-C3	177.41(9)	176.550
C1-Re1-N1	176.2(1)	174.310
Br2-Re2-C6	176.99(8)	177.236
C4-Re2-O6	176.41(9)	176.545
N3-Re2-C5	174.2(1)	174.309
C16-N1-C11	115.0(2)	114.920
C18-N3-C19	114.8(2)	114.920

Table 3.4: *Selected bond lengths [Å] and bond angles [°] for* ***3****.*

	Experimental	**Optimized**
Re-Br	2.6322(8)	2.66556
Re-N1	2.186(2)	2.3072
Re-O1	2.141(2)	2.2226
Re-C1	1.931(2)	1.9263
Re-C2	1.901(2)	1.9150
Re-C3	1.901(2)	1.9034
C9-C10	1.466(3)	1.4608
C1-C9	1.365(3)	1.3601
O1-Re-N1	81.99(7)	80.800
C1-Re-C3	86.90(1)	88.380
Br-Re-C2	175.82(7)	176.266

Chapter 4

Coordination behaviours of Perimidine ligands incorporating fused N-donor heterocyclics towards Rhenium(I) and –(V)

4.1 Introduction:

Effective treatment of cancer and neurodegenerative diseases like Alzheimer's disease by radio-therapeutics requires non-invasive treatment of tumours and amyloidal plaques, respectively [**1-2**]. Rhenium radiopharmaceuticals might be a plausible alternative to physical removal of tumours or amyloidal plaques since the 186- and 188-rhenium radionuclides have optimal half-lives and beta-max energies suitable for the treatment of large (17 hrs and 2.10 MeV for the ^{188}Re radionuclide) and small (90 hrs and 1.07 MeV for ^{186}Re radionuclide) growths in the body [**3**]. Furthermore, rhenium exhibits stability in various oxidation states accompanied with rich coordination chemistry to several ligand systems containing combinations of numerous donor atoms [**4**]. In addition, the applied radiochemistry of rhenium is well developed for the production of the rhenium radionuclides and their subsequent utilization in radio-labelling to ligands [**5**].

However, the fundamental coordination chemistry of rhenium still has a pivotal role to play in designing functional rhenium radiopharmaceuticals as current trends involve exploring the coordination susceptibility of biologically relevant ligands towards the $[Re^{V}O]^{3+}$ and *fac*-$[Re^{I}(CO)_3]^{+}$ cores [**6-7**]. The biological entities within these classes of ligands can potentially facilitate the metal complex in exhibiting a target-specific biodistribution. Examples of this design strategy include rhenium complexes which are analogues of the Pittsburgh Compound B (2-(4-methylaminophenyl)-6-hydroxybenzothiazole)). The coordinated benzothiazole chelators induce the rhenium complexes to selectively target amyloidal plaques in

the brain [**8**]. Furthermore, the chelation of design ligands stabilizes the metalo complexes when compared to metal complexes with monodentate ligands under *in vivo* conditions [**9**]. In addition, interactions of the rhenium complex with DNA of cancerous tumours are also essential for a defined biodistribution patterns of the metallo drug and this factor is influenced mainly by electronic properties of the chelator [**10**].

We conducted the coordination reactions of the perimidine ligands incorporating fused N-donor heterocyclics: 2-(benzothiazole)-2,3-dihydro-1*H*-perimidine (bzpm) and 2,3-dihydro-2-(pyridine)-1*H*-perimidine (pypm) with $[Re(CO)_5Br]$ as well as 2,3-dihydro-2-(1*H*-pyrrole)-1*H*-perimidine (pyrpm) with *trans*-$[ReOBr_3(PPh_3)_3]$ to afford *fac*-$[Re(CO)_3(bzpm)Br]$ (**1**), *fac*-$[Re(CO)_3(pypm)Br]$ (**2**) and *cis*-$[Re(pyrnp)Br_2(PPh_3)]$ (**3**) {H_3pyrnp = 8-((1*H*-pyrrole)iminomethyl)naphthalene-1-amine}, respectively. The interest in these ligands stems from the various biological activities of the respective fused heterocyclic moeities and the perimidine core. More specifically, derivatives of the benzothiazole, pyridine or pyrrole moeities have shown to exhibit anticancer activities against various cancer cell lines while perimidine-derived compounds have been the leading candidates anti-(microbial/antifungal/cancer) agents, *e.g.* the Pd(II) complex of the perimidine ligand, 2-(2-thienyl)-2,3-dihydro-1*H*-perimidine and its free-ligand have shown antimicrobial activities against a series of microbes [**11-16**]. Furthermore, the Pd metal complexes were validated by the X-ray diffraction analysis structures of the metal complexes. The DNA binding capabilities of the metal complexes were evaluated by UV-Vis titrations with Calf Thymus (CT)-DNA.

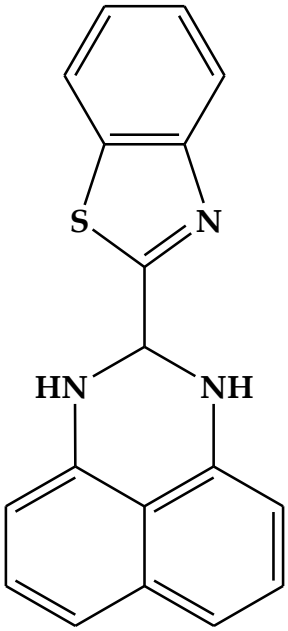

bzpm

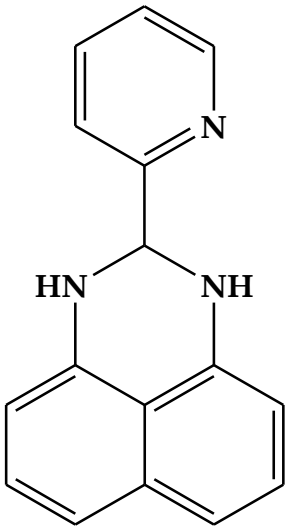

pypm

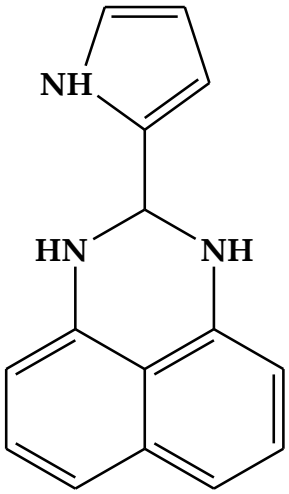

pyrpm

4.2 Experimental

4.2.1 Syntheses of ligands

4.2.1.1 2-(benzothiazole)-2,3-dihydro-1H-perimidine (bzpm)

The titled compound was prepared from a 1:1 molar condensation reaction between benzothiazole-2-carboxaldehyde (0.1928 g, 1.182 mmol) and 1, 8-diaminonaphthalene (0.187 g, 1.182 mmol) in 20 cm^3 of absolute ethanol. The catalyst employed was $AlCl_3.6H_2O$ (0.028 g, 0.118 mmol). The resultant reaction mixture was heated until reflux for 24 hrs. Afterwards, the volume of a dark brown solution was reduced using a rotary-evaporator and a dark brown precipitate was filtered off. This precipitate was purified *via* column chromatography using a 6:4 (*v:v*) ethyl acetate:hexane solvent system to produce a brown precipitate. M.P. = 205 – 206.5 ˚C, yield = 70%. IR (ν_{max}/cm^{-1}): ν(N-H) 3442, 3307 (m); ν(C=N) 1595 (s). ^{1}H NMR (295K/ ppm, see **Fig. 4.1**): 8.03 – 7.92 (m, 2H, *H5*, *H8*); 7.49 (t, 2H, *H6*, *H7*); 7.45 – 7.33 (m, 2H,

H14, *H18*); 7.06 (d, 2H, *H13, H19*); 6.61 (d, 2H, *N2H, N3H*); 5.93 (s, 1H, *H11*). UV-vis (DCM, (λ_{max} (ε, $M^{-1}cm^{-1}$))): 316 nm (7874); 338 nm (sh, 7548); 393 nm (sh, 2461).

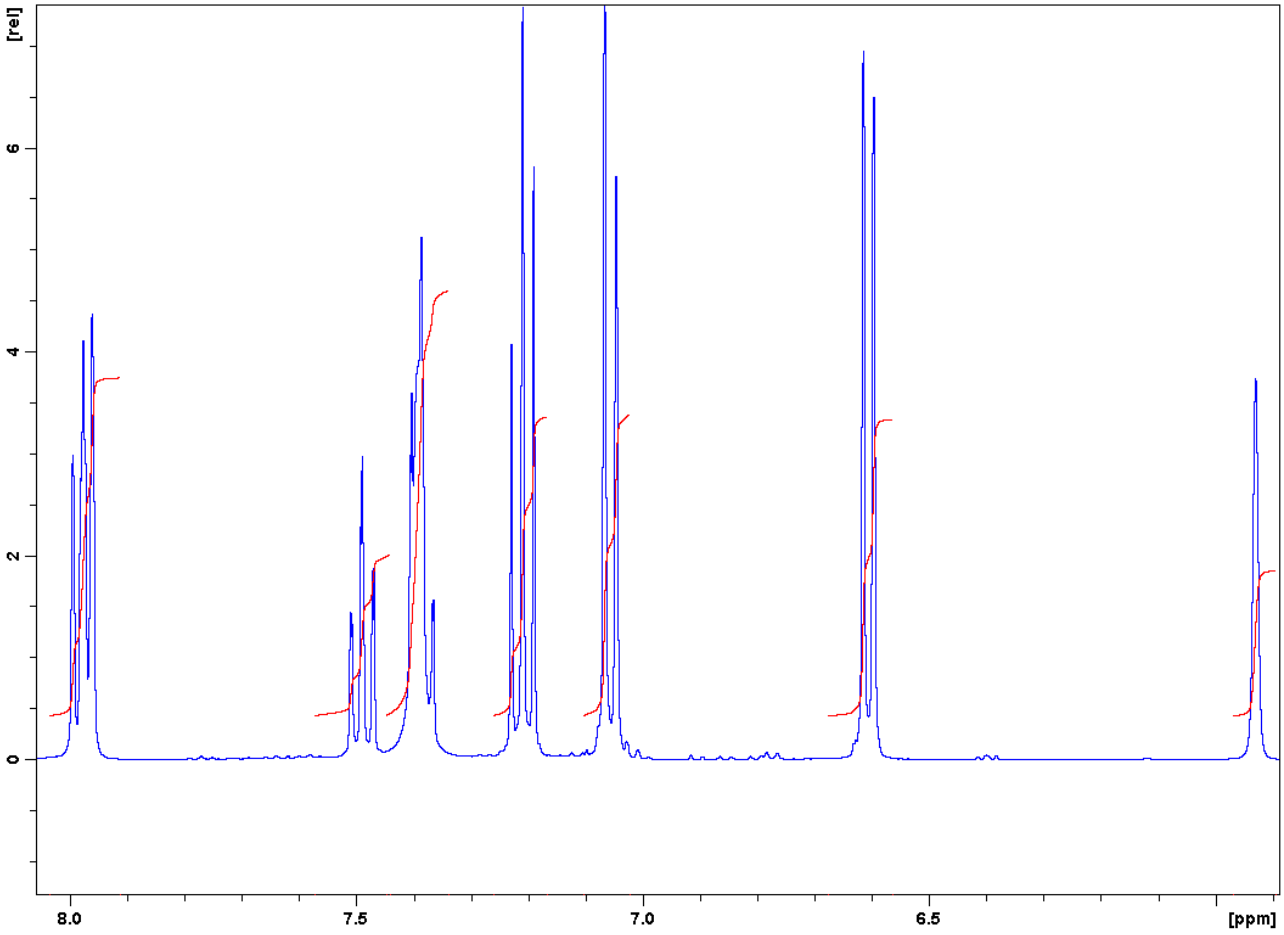

Fig. 4.1: *^{1}H NMR spectrum of the free-ligand, bzpm.*

4.2.1.2 2,3-dihydro-2-(pyridine)-1H-perimidine (pypm)

A 1:1 molar condensation reaction between 2-pyridinecarboxaldehyde (0.404 g, 3.774 mmol) and 1, 8-diaminonaphthalene (0.597 g, 3.774 mmol) was conducted in 20 cm^3 of absolute ethanol. A catalytic amount of $AlCl_3.6H_2O$ (0.091 g, 0.377 mmol) of the molarity was added to the reaction vessel. Then the reaction mixture was heated until reflux for 24 hrs. Afterwards, the volume of the reaction mixture was reduced using a rotary-evaporator to afford a brick-red precipitate. This precipitate was purified *via* column chromatography using a 6:4 (*v:v*) ethyl acetate:hexane solvent system to produce a brown precipitate. M.P. = 155-156.4 ˚C, yield = 67.5%. IR

(ν_{max}/cm^{-1}): ν(N-H) 3173, 3047 (m), ν(C=N) 1596 (vs). ^{1}H NMR (295 K/ppm, see **Fig. 4.2**): 8.60 (d, 1H, *H16*); 7.83 (t, 2H, *H17, H18*); 7.59 (d, 1H, *H19*); 7.41 – 7.34 (t, 2H, *H7, H11*); 6.99 (d, 2H, *H8, H10*); 6.92 (br, s, 2H, *N1H, N2H*); 5.48 (s, 1H, *H14*). UV-vis (DCM, (λ_{max} (ε, M^{-1}cm^{-1}))): 338 nm (sh, 17274), 353 nm (19362).

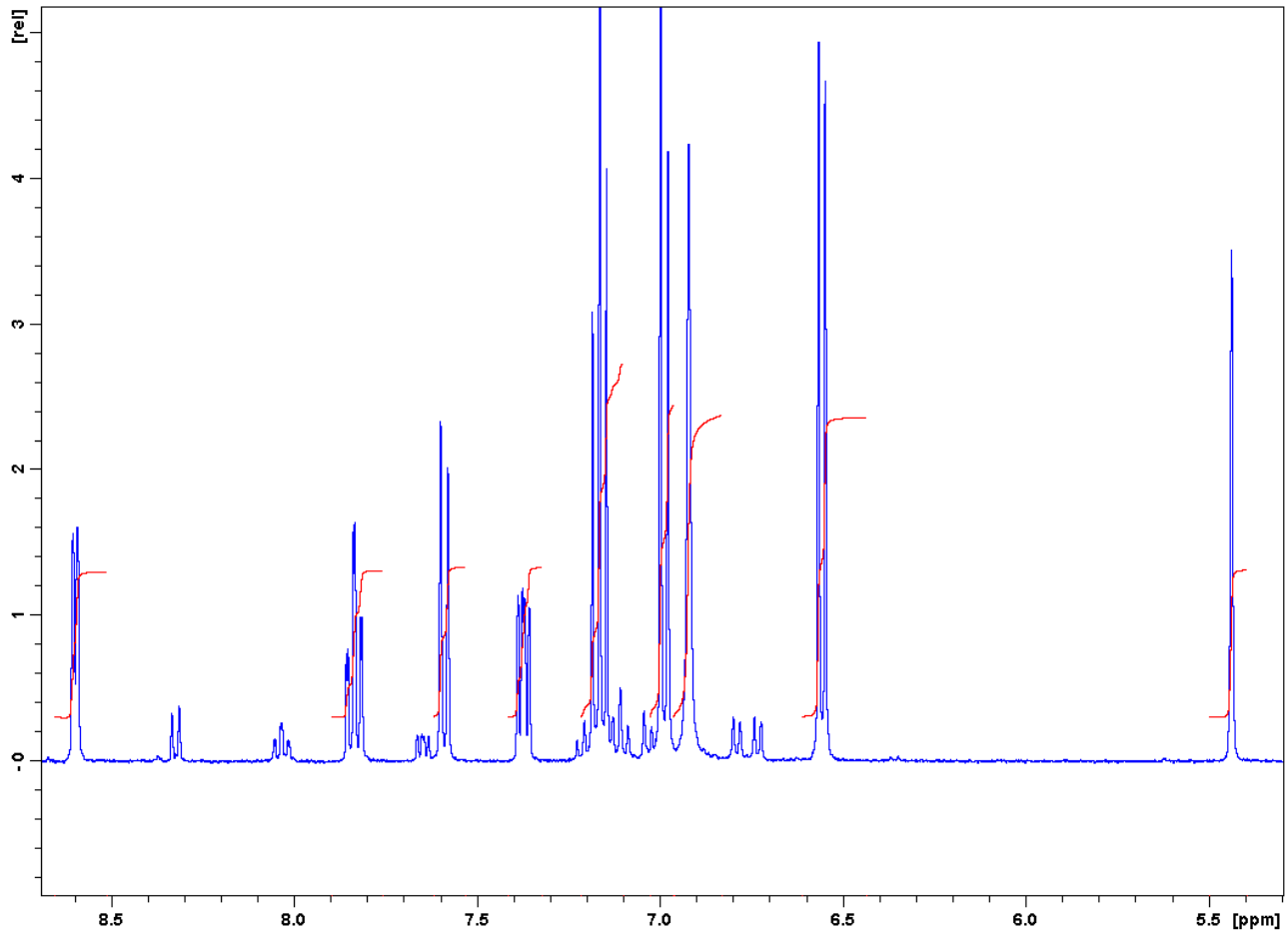

Fig. 4.2: *^{1}H NMR spectrum of the free-ligand, pypm.*

4.2.1.3 2,3-dihydro-2-(1H-pyrrole)-1H-perimidine (pyrpm)

Equimolar amounts of pyrrole-2-carboxaldehyde (0.100 g, 1.490 mmol), and 1, 8-diaminonaphthalene (0.235 g, 1.490 mmol) was dissolved in 20 cm^3 of absolute ethanol. The catalyst employed was $AlCl_3.6H_2O$ (0.035 g, 0.149 mmol). The resultant reaction mixture was heated until reflux for 24 hrs. Afterwards, the reaction mixture was reduced using rotary-evaporator and a dark brown precipitate was filtered-off. This precipitate was purified *via* column chromatography using silica as the

stationary phase and a 6:4 (*v:v*) ethyl acetate :hexane solvent system to produce a brown compound. M.P. = 150.2-152.6 ˚C, yield = 77%. IR (ν_{max}/cm^{-1}): ν(N-H)$_{pyrrole}$ 3331 (br, s); ν(N-H)$_{perimidine}$ 3130, 3041 (m). ^{1}H NMR (295 K /ppm): 7.29-7.24 (m, 1H, *H1*); 7.15 (t, 2H, *H8*, *H12*); 6.98 (d, 2H, *H9*, *H11*); 6.79-6.73 (m, 1H, *H2*); 6.50 (s, br, 2H, *N2H*, *N3H*); 6.03-5.98 (s, 1H, *H5*). UV-vis (DCM, (λ_{max} (ε, M^{-1}cm^{-1}))): 342 nm (sh, 17812), 353 nm (18504).

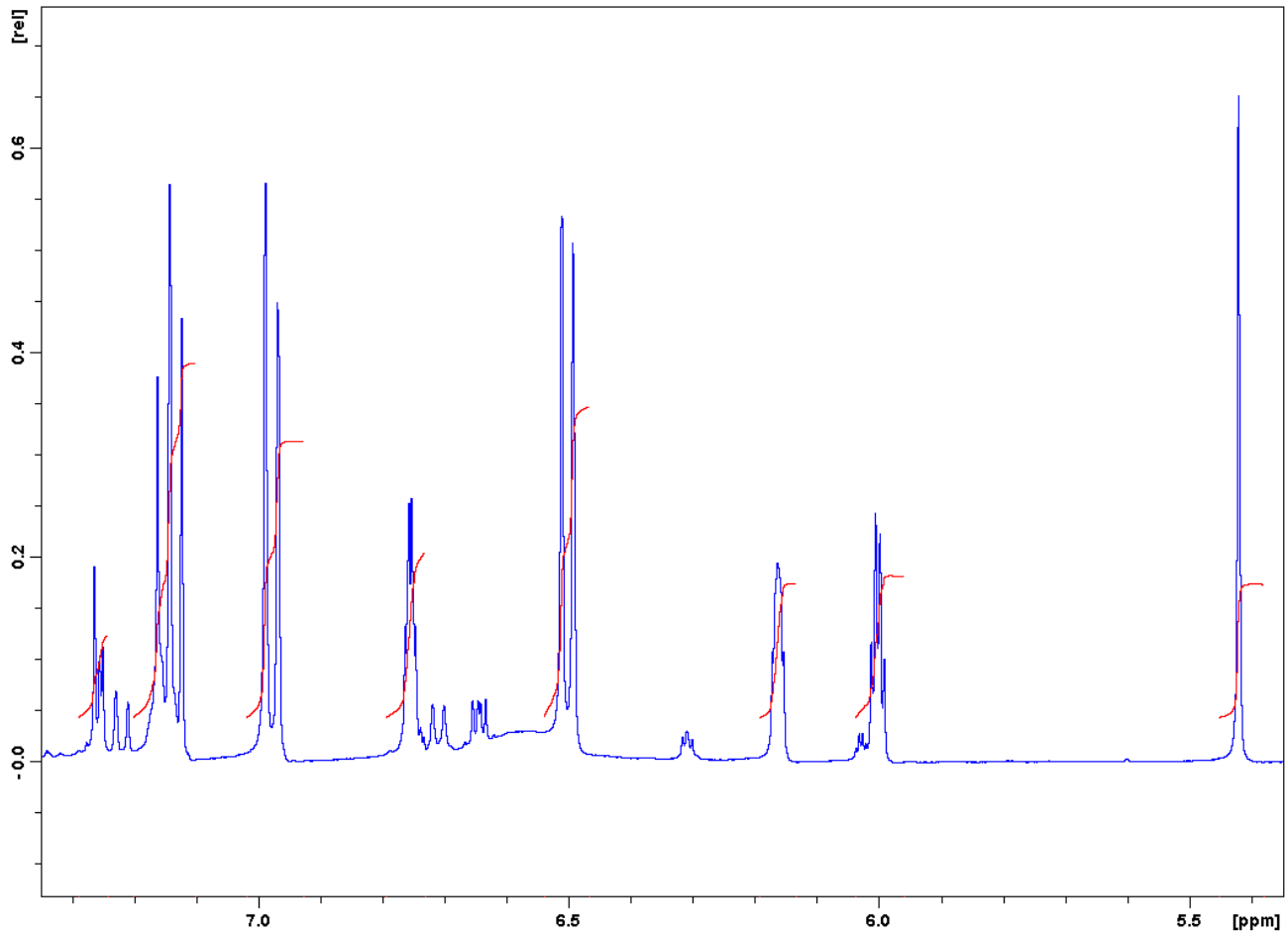

Fig. 4.3: *^{1}H NMR spectrum of pyrpm.*

4.2.2 Syntheses of metal complexes

*4.2.2.1 fac-[Re(CO)$_3$(bzpm)Br] (**1**)*

A 1:1 molar reaction mixture between [Re(CO)$_5$Br] (0.016 g, 0.038 mmol) and bzpm (0.013 g, 0.038 mmol) in 15 cm^3 of anhydrous toluene was heated until reflux under nitrogen for 4 hrs. The resultant reaction mixture was cooled to room temperature

and filtered. A dark brown precipitate was collected and dried under vacuum. Dark brown cubic crystals were obtained from layering the precipitate with 1:1 (*v:v*) THF/Hexane over a period of five days. M.P = 220-221 °C; yield = 89.9%; Conductivity (DMSO, 10^{-3}M) 23.72 ohm. $cm^2\ mol^{-1}$; IR (ν_{max}/cm^{-1}): ν(N-H) 3312, 3146 cm^{-1} (m); ν(C≡O) 2020, 1895 (vs); ν(C=N) 1604 (s). ^{1}H NMR (295 K/ppm, see **Fig. 4.4**): 8.63 (br, s, 1H, *N2H*); 8.43 (d, 1H, *H8*); 8.18 (d, 1H, *H5*); 8.04-6.71 (m, 7H, *H6, H7, H13, H14, H15, H17, H18*); 6.56 (d, 1H, *H19*); 6.33 (d, 1H, *N3H*); 5.90 (d, 1H, *H11*). UV-Vis (DMSO, λ_{max} (ε, $M^{-1}cm^{-1}$) 319 nm (9336); 339 nm (sh, 8676).

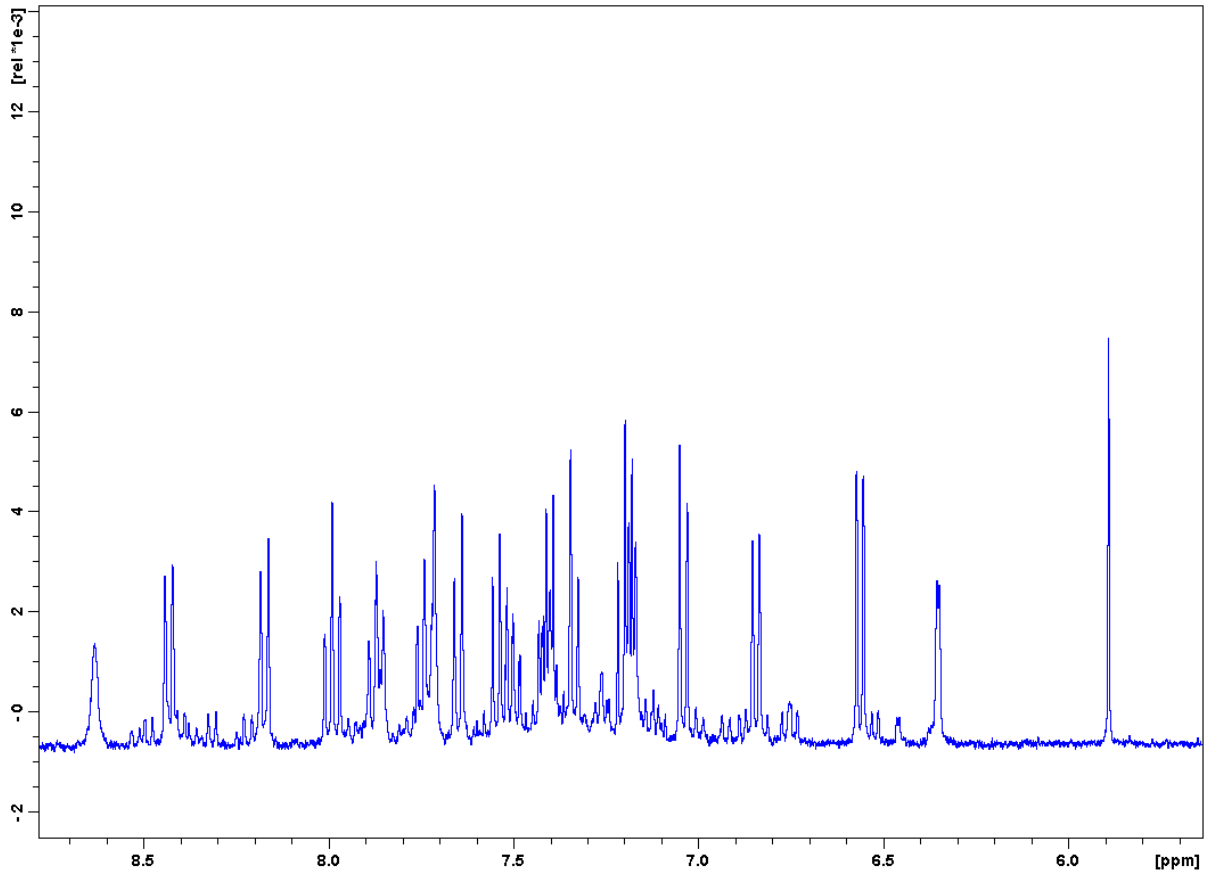

Fig. 4.4: *^{1}H NMR spectrum of complex **1**.*

*4.2.2.2 fac-[Re(CO)$_3$(pypm)Br] (**2**)*

The titled metal complex was isolated from the coordination reaction of [$Re(CO)_5Br$] (0.029 g, 0.073 mmol) with pypm (0.018 g, 0.073 mmol) in 15 cm^3 of anhydrous toluene was heated until reflux under nitrogen for 4 hrs. The resultant reaction

mixture was cooled to room temperature and filtered. A brick-red precipitate was collected and dried under vacuum. X-ray quality brick-red crystals were obtained from layering the precipitate with 1:1 (*v:v*) THF/Hexane over a period of five days. M.P = 190-200 ^{O}C; yield = 87%; Conductivity (DMSO, 10^{-3}M) 24.38 ohm.cm^{2}mol^{-1}; IR (ν_{max}/cm^{-1}): ν(N-H) 3295, 3210 cm^{-1} (m); ν(C≡O) 2019, 1888 (vs); ν(C=N) 1605 (s). 1H NMR (295 K/ppm, see **Fig. 4.5**): 11.84 (br, s, *N1H*); 9.15 (d, 1H, *H16*); 8.89 (d, 1H, *H19*); 8.69 (d, 1H, *H12*); 8.47 (t, 1H, *H17*); 8.13 (br, s, 1H, *H10*); 8.08 (d, 1H, *H8*); 7.91 (t, 1H, *H11*); 7.74 (t, 1H, *H7*); 7.61 (d, 1H, *H6*). UV-Vis (DMSO, λ_{max} (ε, M^{-1}cm^{-1})) 336 nm (37667); 393 nm (sh, 20963); 534 (sh, 3937).

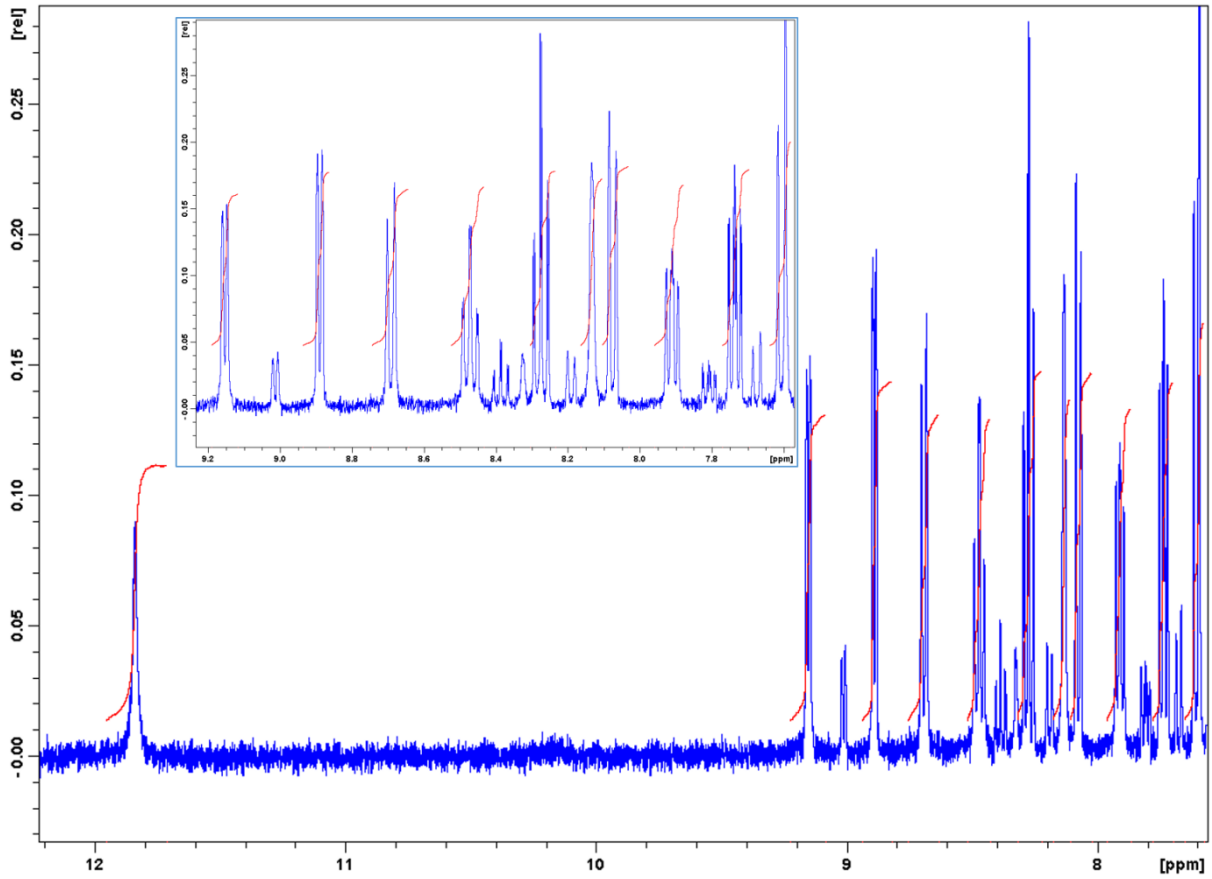

Fig. 4.5: *^{1}H NMR spectrum of complex* **2**.

4.2.2.3 cis-[Re(pyrnp)Br$_2$(PPh$_3$)] (***3***)

The equimolar reaction mixture of *trans*-[ReOBr$_3$(PPh$_3$)$_2$] (0.050 g, 0.052 mmol) and pyrpm (0.012 g, 0.052 mmol) in 15 cm^3 of anhydrous toluene was heated until reflux

for 4 hrs. The resultant reaction mixture was cooled to room temperature and filtered. The mother liquor was allowed to undergo slow evaporation and dark brown parallelogram XRD quality crystals were obtained after 10 days. M.P = 200-205 ^{O}C; yield = 80%; Conductivity (DMSO, 10^{-3}M) 24.95 ohm.cm^{2}mol^{-1}; IR (ν_{max}/cm^{-1}): ν(C=N)$_{Schiff\ base}$ 1576 (s); ν(C=N)$_{pyrrole}$ 1480 (m); ν(Re-N) 1116 (vs). ^{1}H NMR (295 K /ppm, see **Fig. 4.6**): 8.30 (d, 1H, *H1*); 8.16 (s, 1H, *H5*); 8.08 (d, 1H, *H3*); 7.80 (t, 1H, *H2*); 7.70-7.53 (m, 15H, *PPh$_3$*); 7.46-7.12 (m, 6H, *H7, H8, H9, H11, H12, H13*). UV-Vis (DMSO, λ_{max} (ε, M^{-1}cm^{-1})) 279 nm (17941); 285 nm (18490); 311 nm (sh, 15280); 397 nm (sh, 3734); 420 nm (sh, 2637).

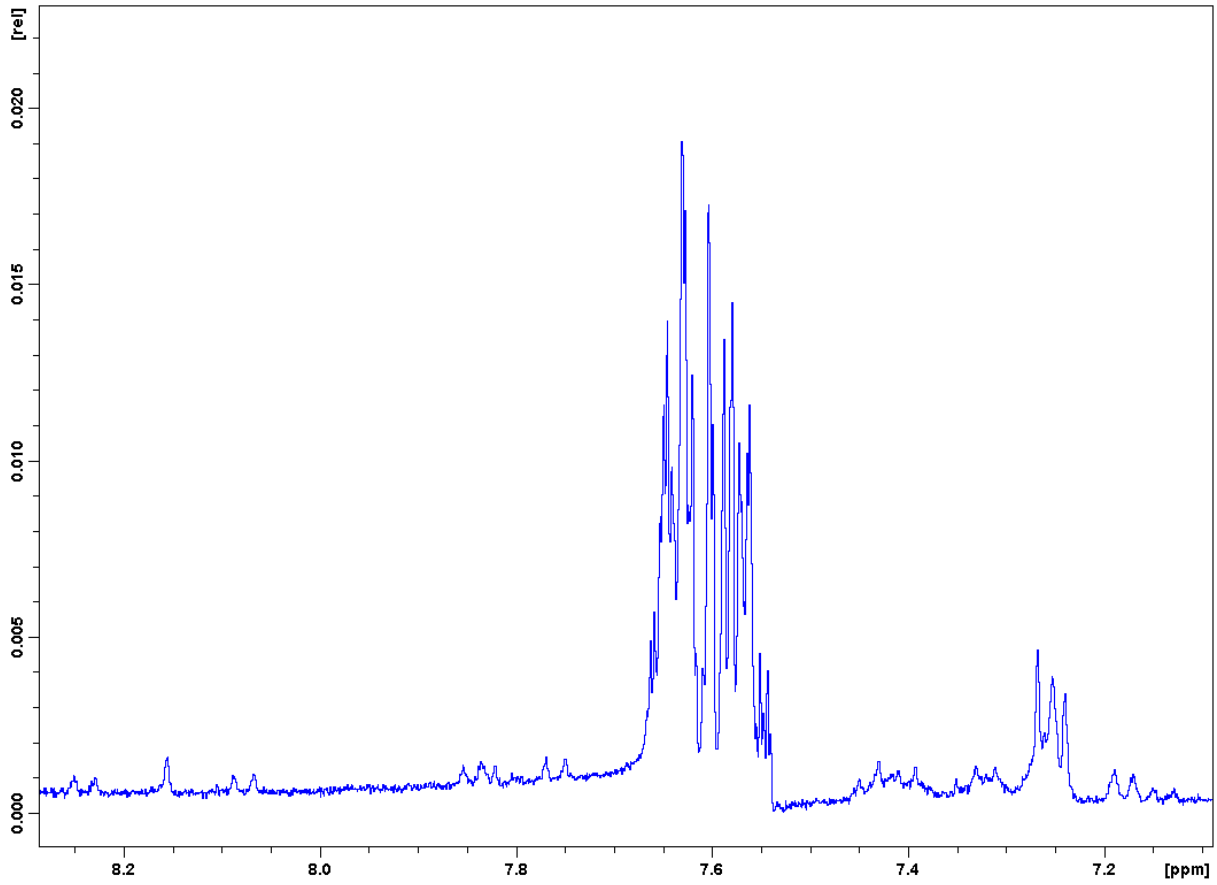

Fig. 4.6: *^{1}H NMR spectrum of complex* ***3***.

4.2.3 X-ray diffraction

The X-ray data for the metal complexes were recorded on a Bruker Apex Duo equipped with an Oxford Instruments Cryojet operating at 100(2) K and an Incoatec

microsource operating at 30 W power. Selected bond lengths and angles are given in Tables **2**, **3** and **4**, respectively. In all three cases the data were collected with MoKα (λ = 0.71073 Å) radiation at a crystal-to-detector distance of 50 mm. The following conditions were used for data collection: omega and phi scans with exposures taken at 30 W X-ray power and 0.50° frame widths using APEX2 [**17**]. The data were reduced with the program SAINT [**17**] using outlier rejection, scan speed scaling, as well as standard Lorentz and polarization correction factors. A SADABS semi-empirical multi-scan absorption correction [**18**] was applied to the data. Direct methods, SHELX-2014 [**19**] and WinGX [**20**] were used to solve all three structures. All non-hydrogen atoms were located in the difference density map and refined anisotropically with SHELX-2014 [**19**]. All hydrogen atoms were included as idealised contributors in the least squares process. Their positions were calculated using a standard riding model with C-$H_{aromatic}$ distances of 0.93 Å and U_{iso} = 1.2 U_{eq}, C-$H_{methylene}$ distances of 0.99 Å and U_{iso} = 1.2 U_{eq} and C–H_{methyl} distances of 0.98 Å and U_{iso} = 1.5 U_{eq}.

4.3 DNA Binding Studies

UV-Vis spectroscopic titrations were conducted using metal complex **1** or **2** and CT-DNA. The concentration of the metal complexes was 1 mM prepared in DMSO while the CT-DNA stock solution was prepared in a pH 7.4 PBS buffer solution prepared in ultrapure water. The DNA concentration per nucleotide base pair of the CT-DNA stock solution was determined using the absorption coefficient of the CT-DNA (ε_{260} = 6600 M^{-1} cm^{-1}). The CT-DNA stock solution was incubated at 25 °C over a period of 24 hrs.

The DNA titrations were conducting by adding (0 – 100 µl) incremental amount of CT-DNA (in pH 7.4 PBS buffer) to the sample cell containing 1 mM solutions of the respective metal complexes. The same volume of CT-DNA (in pH 7.4 PBS buffer)

was added stepwise in the reference cell to cancel out any absorptions associated with the CT-DNA. Prior to any UV-Vis measurements and each CT-DNA aliquot addition, a 3 minute incubation period was allowed during which the metallic compound and CT-DNA was homogeneously mixed.

4.4 Results and Discussion

4.4.1 Synthesis and spectral characterization

The rhenium compounds: *fac*-[Re(CO)$_3$(bzpm)Br](**1**), *fac*-[Re(CO)$_3$(pypm)Br](**2**) and *cis*-[Re(pyrnp)Br$_2$(PPh$_3$)](**3**) were synthesized under anaerobic conditions in good yields from the coordination reactions of [Re(CO)$_5$Br] with bzpm, pypm and pyrpm, respectively. These metal complexes exhibit good solubility in high boiling point polar solvents including dimethylsulfoxide and dimethylformamide but they are moderately soluble in tetrahydrofuran and toluene. In addition, poor solubility was observed in chlorinated solvents such as chloroform.

For **1** and **2**, bzpm and pypm moieties act respectively as neutral bidentate chelators *via* their N$_{perimidine}$N$_{benzothiazole}$ and N$_{perimidine}$N$_{pyridine}$ donor sets. For the formation of the oxo-free rhenium(V) complex **3**, the more acidic character of the rhenium(V) centre induced ring-opening of the central pyrimidine ring of pyrpm free-ligand which resulted in the coordination of the tridentate trianionic pyrpn Schiff base chelator. The low molar conductivity values of the metal complexes **1 - 3** are comparable to other neutral rhenium compounds in dimethylsulphoxide [**21**].

The IR spectra of **1** (at 2020 and 1895 cm^{-1}) and **2** (at 2019 and 1888 cm^{-1}) show intense vibrational bands indicative of rhenium(I) compounds that contain carbonyl co-ligands in *facial* orientations, see **Fig. 4.7** and **4.8**. Complex **3** is an oxo-free rhenium(V) complex based on the absence of Re=O stretch which is theoretically expected between 950 and 1000 cm^{-1} [**22-25**] contrasted by presence of a strong

bending frequency of rhenium(V)-imido bond, ν(Re=N) between 1050 and 1100 cm^{-1} [**26-29**]. Furthermore, for **3**, the disappearance of the three ν(N-H) vibrations originally found in the IR spectrum of the free-ligand, pyrpm (at 3331, 3130 and 3041 cm^{-1}) suggest that perimidine and pyrrole N-H protons of the pyrpn chelator (of **3**) have been deprotonated, see **Fig. 4.9**. In addition, the occurrence of the distinguishable C=N imine and pyrrole stretches in the IR spectrum of **3** suggests the ring-opening transformation of the free-ligand, pyrpm to the Schiff base chelator, pyrpn. In the case of **1** and **2** where their respective chelators are neutral; similar free-ligand [ν(N-H) at 3442, 3307 cm^{-1}; ν(C=N) at 1695 cm^{-1} for bzpm and ν(N-H) 3173, 3047 cm^{-1}; ν(C=N) 1596 cm^{-1} for pypm] and chelator [ν(N-H) at 3312, 3146 cm^{-1}; ν(C=N) at 1604 cm^{-1} for **1** and ν(N-H) at 3295, 3210 cm^{-1}; ν(C=N) at 1605 cm^{-1} for **2**] vibrations are found within the IR spectra of the free-ligands (for bzpm and pypm) and their respective metal complexes **1** and **2**.

The coordination of the chelator, bzpm to rhenium in **1** is confirmed by the coalescence of the aromatic signals for the chelator in the complex in contrast to its well-resolved signals observed in the free-ligand form. Further confirmation is comes from the splitting of the doublet of perimidine N-H signals (found in the NMR spectrum of the free-ligand) into two singlets at 8.63 (for *N2H*) and 6.33 (for *N3H*) ppm found in the IR spectrum of the **1**. Notably, in the proton NMR spectrum of **2** is the disappearance of one of the perimidyl nitrogen protons while the remaining N-H signal (for *N1H*) resonating at a significantly downfield position in comparison to the broad singlet observed at 6.92 ppm (for *N1H and N2H*) in the proton spectrum for the free-ligand, pypm. In fact, the X-ray crystal structure of **2** corroborates the missing perimidyl nitrogen proton as well as the *H14* atom (see Section 4.4.3) . In **Fig. 4.5** aromatic signals of **2** are in the form *d:d:d:t:s:d:t:t:d* where each signal integrates to one. The proton NMR spectrum of **3** (**Fig. 4.6**) is dominated by the intense multiplet (between 7.70 and 7.53 ppm) of the triphenylphosphine co-ligand. In comparison to the NMR spectrum of the free-ligand, pyrpm, no pyrrole and pyrimidyl N-H signals are observed in the NMR spectrum of **3.** The H5 signal is

shifted significantly downfield to 8.16 ppm. These observations emphasize the distinctive structural differences between the free-ligand, pyrpm and its chelator form, pyrpn.

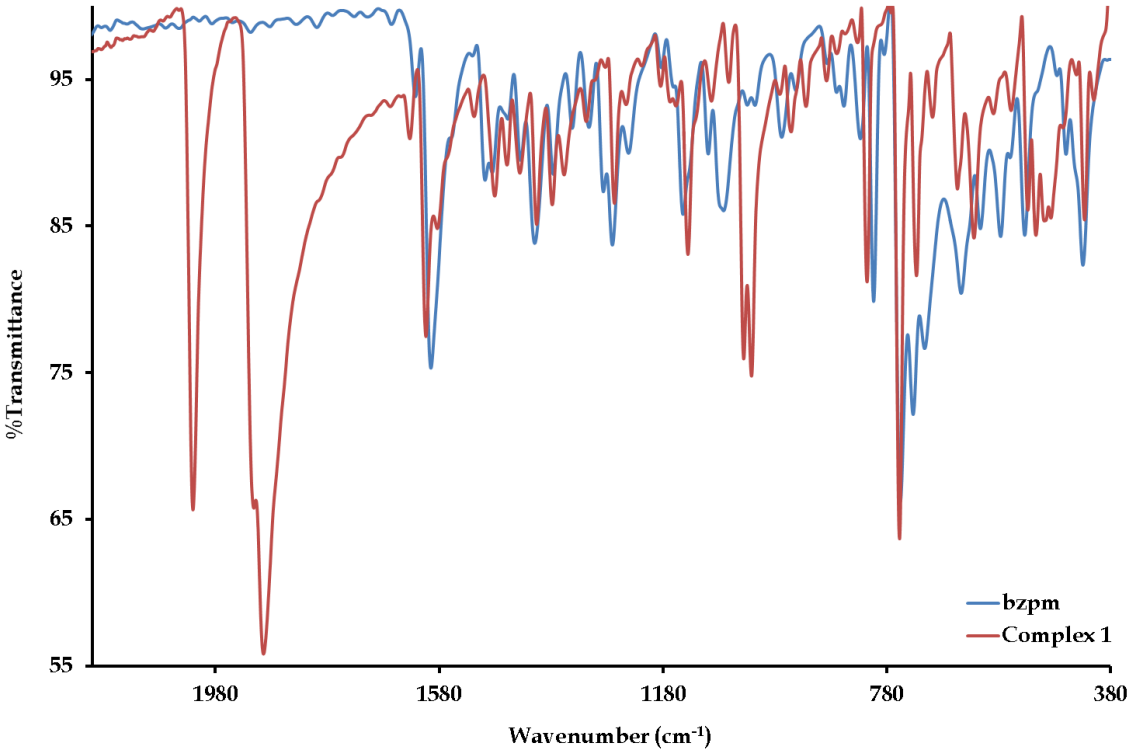

Fig 4.7: *Overlay IR spectra for bzpm and its metal complex **1** between 380 and 2200 cm^{-1}.*

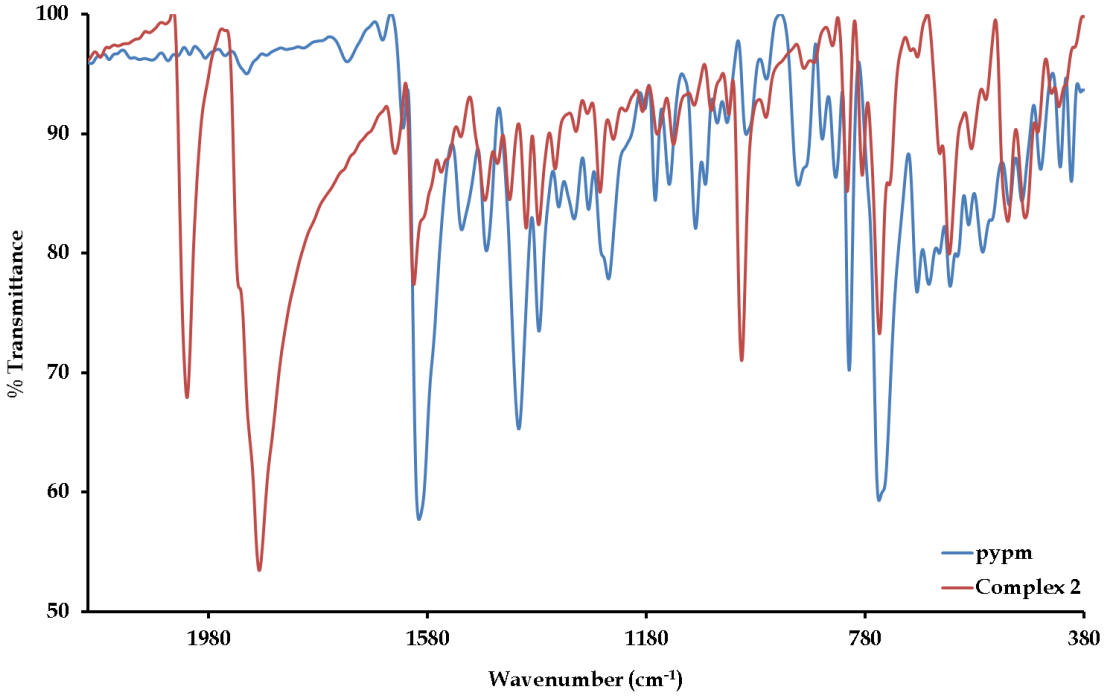

Fig 4.8: *Overlay IR spectra for, pypm and its metal complex* **2** *between 380 and 2200 cm-1.*

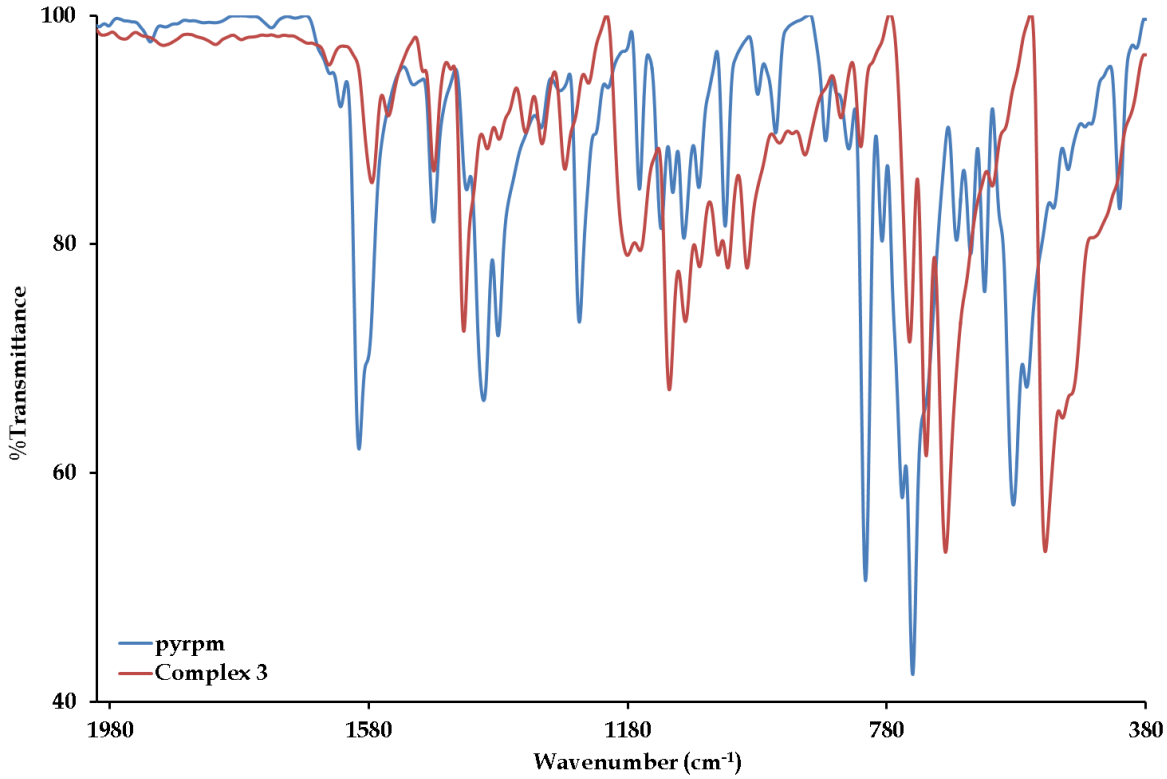

Fig. 4.9: *Overlay IR spectra for pyrpm and its metal complex* **3** *between 380 and 2000 cm-1.*

The electronic spectra of the free ligands and metal complexes spots numerous common intra-ligand π-π^* transitions below 400 nm. The more red-shifted electronic transitions are ascribed to metal-to-ligand (for **1** and **2**) (see **Figs. 4.10** and **4.11**) and ligand-to-metal (for **3**) (see **Fig. 4.12**) charge transfer bands. The absence of the expected metal-based *d-d* electronic transition for the rhenium(V) complex indicates that the presence of the pyrpn chelator increases the band-gap energy of **3,** which makes the metal-based electronic transition unfavourable.

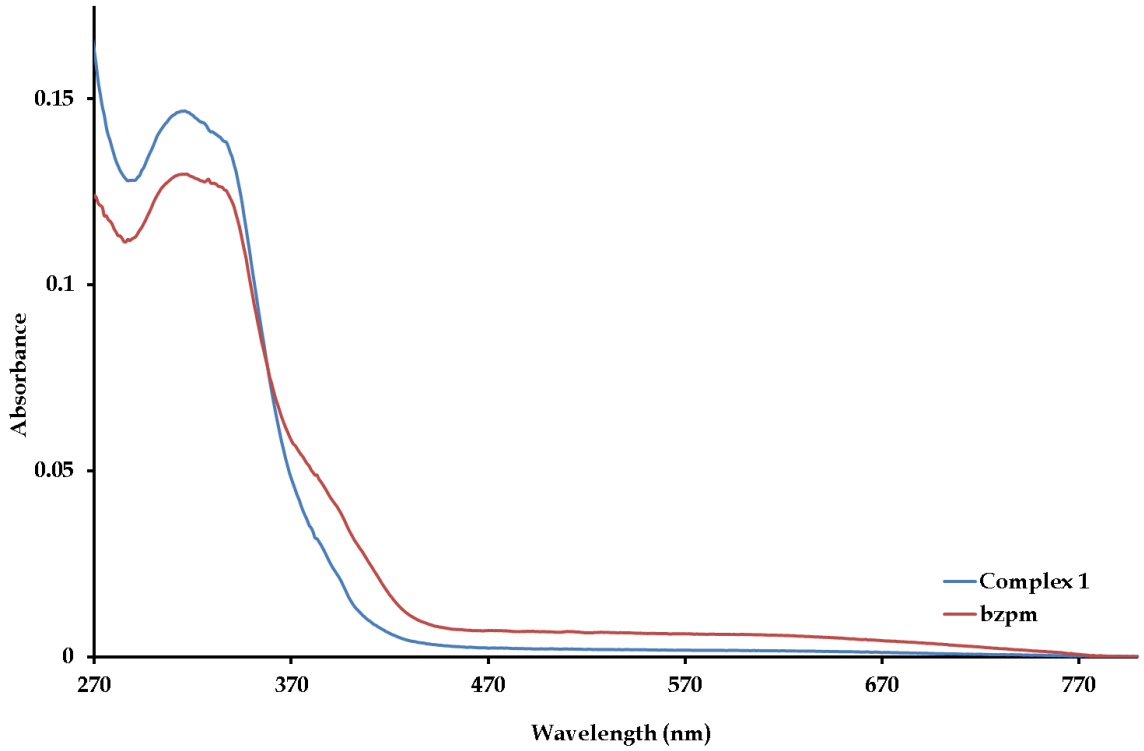

Fig. 4.10: *Overlay UV-Vis spectra of* ***1*** *and its free-ligand, bzpm.*

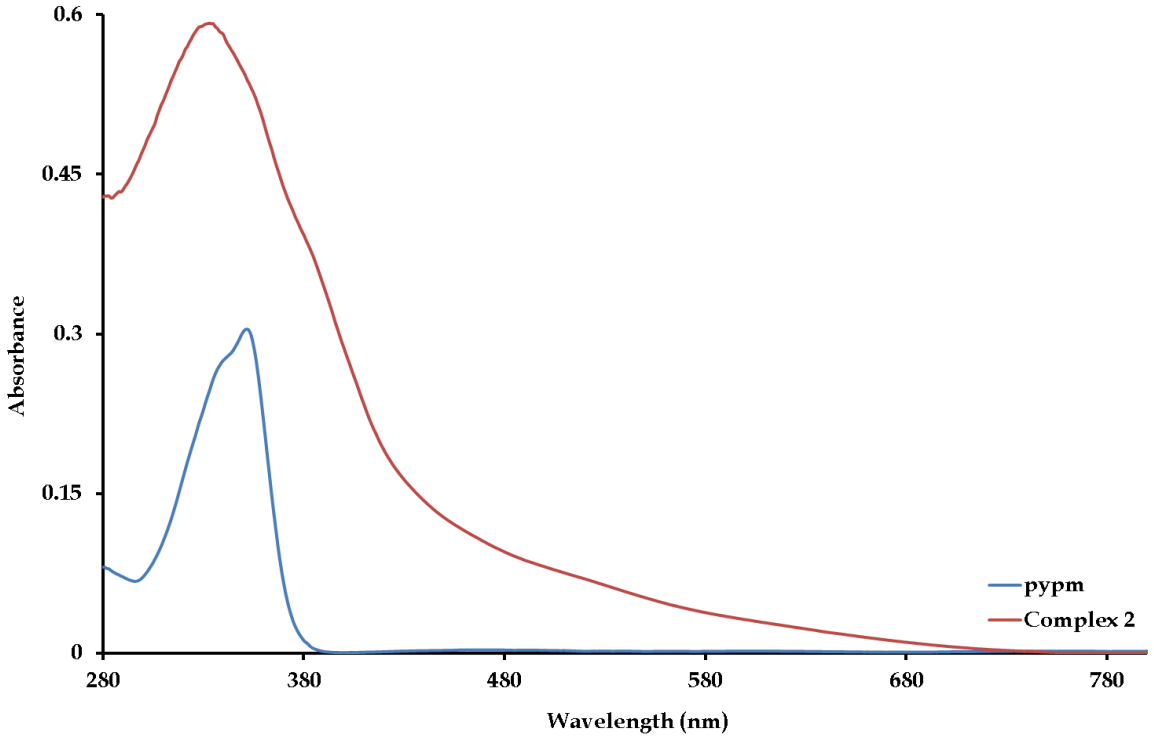

Fig 4.11: *Overlay UV/Vis spectra for pypm and complex* **2**.

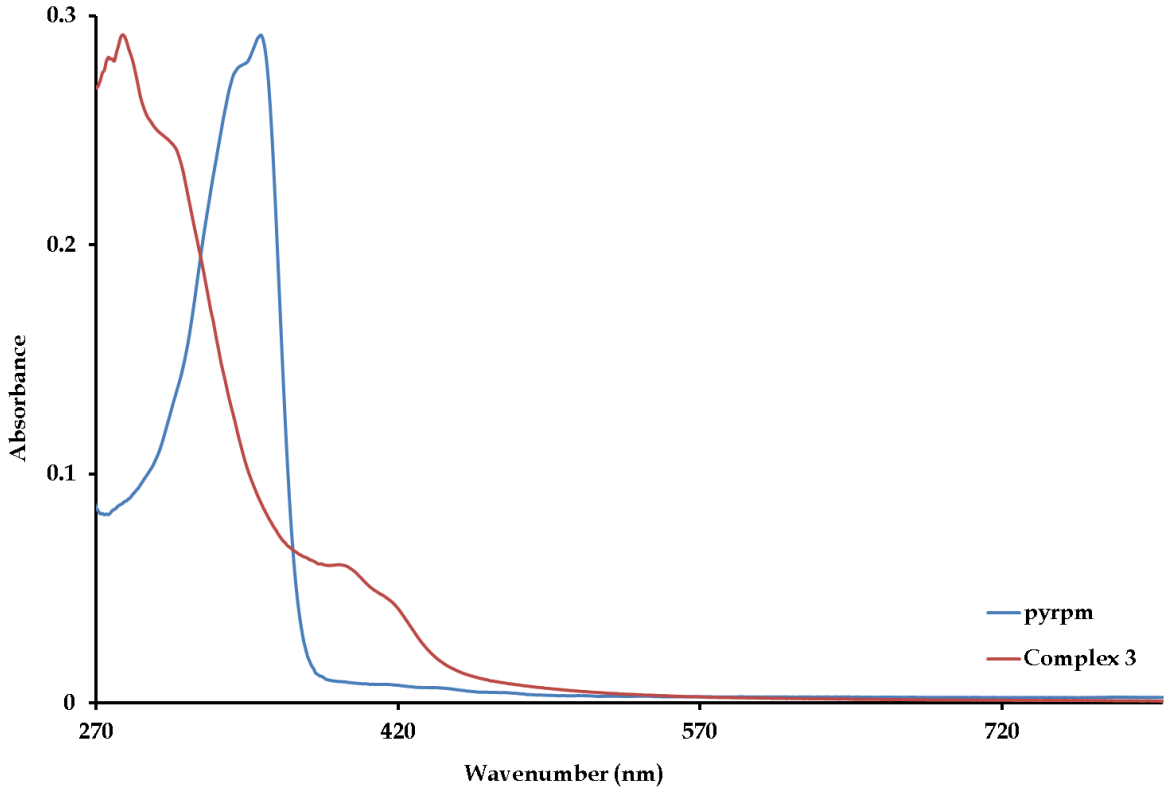

Fig 4.12: *Overlay UV/Vis spectra for pyrpm and complex* **3**.

4.4.2 DNA Binding Studies

UV-Visible molecular is an effective tool for determining the binding mode of metal to DNA including quantifying the metal complex to DNA interaction. This is achieved by calculating the intrinsic binding constants (K_b) of the metal complex [**30**]. The intrinsic binding constants (K_b) of **1** and **2** were calculated using equation (**A**) by monitoring the change in absorbance values of some selected π-π^* intraligand electronic transitions at 333 nm (for **1**) and 335 nm (for **2**):

$$[DNA]/(\varepsilon_a-\varepsilon_f) = [DNA]/(\varepsilon_a-\varepsilon_f) + K_b(\varepsilon_b-\varepsilon_f) \qquad \mathbf{A}$$

where [DNA] is the concentration of the molar DNA in base pairs, ε_a is the extinction coefficient of the observed absorbance value at the given DNA concentration, ε_f is the extinction coefficient of the complex free in solution and ε_b is the extinction coefficient of the complex when fully bound to the DNA. A plot of $[DNA]/(\varepsilon_a-\varepsilon_f)$ versus [DNA] gives a slope $1/[\varepsilon_a-\varepsilon_f]$ and the Y-intercept equals $1/K_b(\varepsilon_b-\varepsilon_f)$. The intrinsic binding constant K_b is the ratio of the slope to the Y–intercept [**31**].

Progressive decreases in the absorbance values of the intra-ligand electronic transitions accompanied with no significant stock shifts suggest the chelators are partially intercalated between the base pairs of the CT-DNA, see **Figs. 4.13** and **4.14**. In fact, these hypochromic effects are synonomous with many rhenium(I) compounds containing *pi*-conjugated chelators [**31**, **32**]. This is further supported by the fact that the calculated intrinsic binding constants of **1** (4.1×10^5 M^{-1}) and **2** (1.4×10^5 M^{-1}) are either within or close to the range [1.5×10^5 - 1.32×10^7 M^{-1}] of other rhenium(I) complexes that are classed as DNA interchelators and which exhibit hypochromism [**32-34**]. However for complex **3**, due to the presence of the bulky triphenylphosphine co-ligand, negligible change was noticed when the electronic

spectroscopy titrations. The triphenylphosphine co-ligand hindering DNA intercalation or groove binding of this metal complex to DNA.

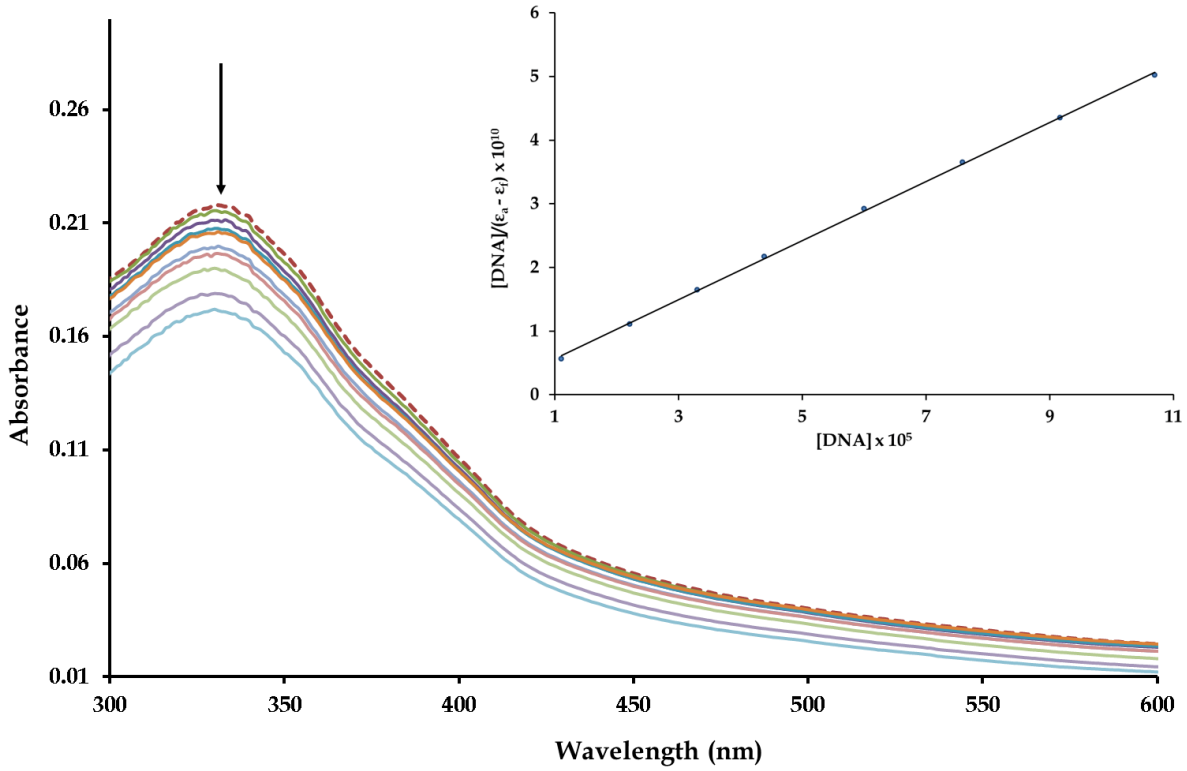

Fig. 4.13: *Overlay UV-Vis spectra of the CT-DNA (in pH 7.4 PBS buffer) titrations conducted with metal complex* ***1****. The UV-Vis spectrum with the dashed line is the initial spectrum without any CT-DNA added. The inset shows the plot of* $[DNA]/(\varepsilon_a-\varepsilon_f) \times 10^{10}$ *vs* $[DNA] \times 10^5$ *and its linear trend line.*

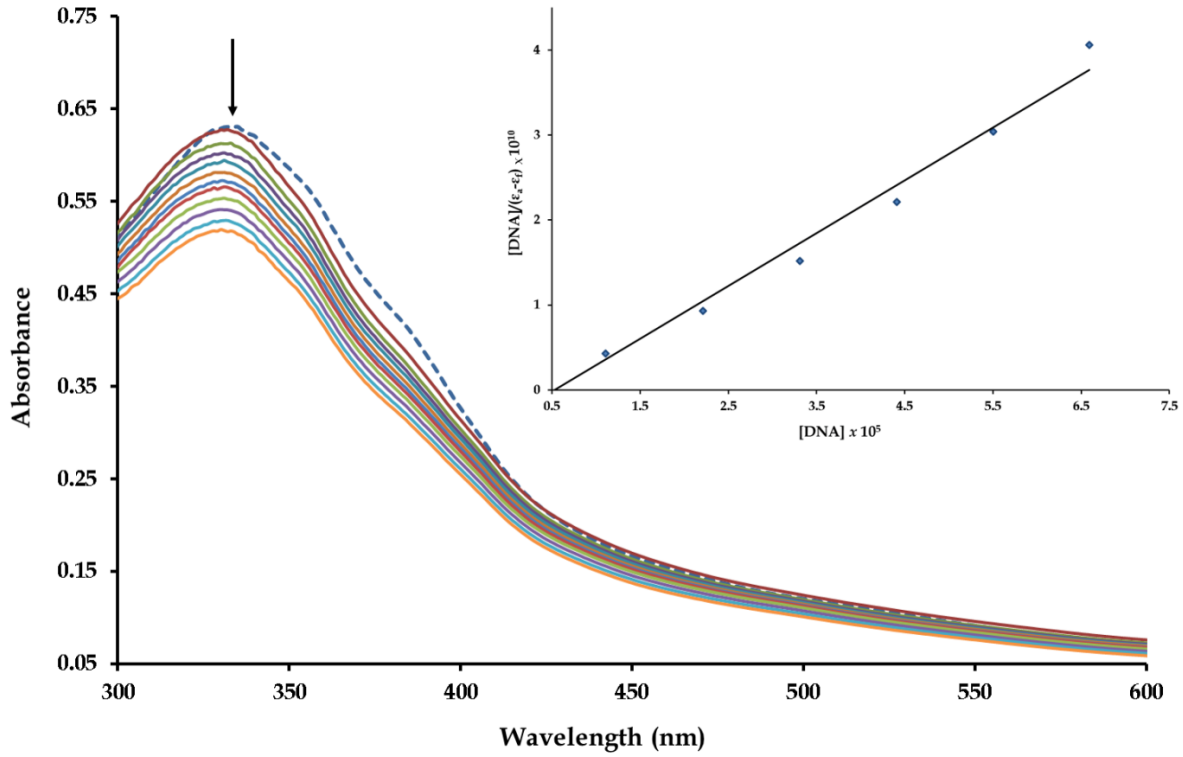

Fig. 4.14: *Overlay UV-Vis spectra of the CT-DNA titrations (in pH 7.4 PBS buffer) conducted with metal complex* **2**. *The UV-Vis spectrum with the dashed line is the initial spectrum without any CT-DNA added. The inset shows the plot of* $[DNA]/(\varepsilon_a-\varepsilon_f) \times 10^{10}$ *vs* $[DNA] \times 10^5$ *and its linear trend line.*

4.4 Crystallographic studies

Two monomers of **1** occupies its triclinic unit cell and each monomer forms dimers with another monomer in adjacent unit cell *via* classical hydrogen bonding interactions [N3-H3···BrA/N3A-H3A···Br = 2.85(3) Å], see **Fig. 4.15**. The crystal lattice of **1** is further stabilized by intermolecular between the benzothiazole and perimidine moieties and co-planar analogous moieties in neighbouring molecules of **1** with centroid to centroid distances of 3.859 Å and 4.133 Å, respectively, see **Figs. 4.16** and **4.17**. These intermolecular interaction at distances does not reflect π-π stacking as they are larger than 3.5 Å. The metal complexes **2** and **3** crystallizes out in respective $P2_1/n$ and *P-1* space-groups with their unit cells occupied by four and two molecules, respectively.

The solid-state structures of the metal complexes are distorted octahedrons induced by their constrained bite angles: N1-Re-N2 = 74.56(8)^{o} for **1**, N2-Re-N3 = 73.92(8)^{o} for **2**, N1-Re-N2 = 75.7(2)^{o} and N2-Re-N3 = 81.9(2)^{o} for **3**, see **Figs**. **4.18 - 4.20.** The difference in the Re-Br bonds of **3** [Re-Br1 = 2.5033(7) Å and Re-Br2 = 2.6008(5) Å] illustrates the variable *trans*-influence of the imino (N2) and pyrrole (N1) nitrogens imposed onto the Br1 and Br2 atoms, respectively. The rhenium(I) halide coordination bonds lengths of **1** [Re-Br = 2.6222(3) Å] and **2** [Re-Br = 2.6319(6) Å] are longer than the Re(V)-Br bonds of **3** which accounted to the higher acidic character of the complex **3**'s central metal atom. No rhenium to perimidine bonds could be found in the Cambridge Crystallographic Database Centre (CCDC) to compare the Re^{I}-$N_{perimidine}$ bonds of **1** [Re-N2 = 2.257(2) Å] and **2** [Re-N2 = 2.198(2) Å] with [**35**]. The difference in the aforementioned bond distances reflects that Re(I) metal in atoms 1 and 2 are bonded to nitrogen atoms of different hybridizations. Nearly equidistant are Re-$N_{benzothiazole}$ [2.207(2) Å] of **1** and Re-$N_{pyridine}$ [2.170(2) Å] bonds of **2** when compared to the *facial* tricarbonylrhenium(I) complexes: *fac*-[Re(Habt)$(CO)_3$Br] (Habt = 2-(2-aminophenyl)benzothiazole) with a Re-$N_{benzothiazole}$ bond of 2.227(2) Å and *fac*-[Re$(CO)_3$(adp)Br] (adp = 5-amino-1,3-dimethyl-6-[(pyridin-2-ylmethylidene)amino]pyrimidine-2,4(1*H*, 3*H*)-dione) Re-$N_{pyridine}$ bond of 2.166(2) Å [**36, 37**].

The organometallic Re-C bonds of **1** [Re-C1 = 1.914(2) Å, Re-C2 = 1.912(3) Å and 1.918(3) Å] and **2** [Re-C1 = 1.913(2) Å, Re-C2 = 1.904(3) Å and Re-C3 = 1.914(3) Å] were similar to other rhenium(I) compounds containing the *facial* tricarbonyl core [**38**]. For **3**, the N3 atom is a dianionic nitrogen which implies that Re-N3 [1.733(5) Å] is a bent imido bond and the latter bond is longer than the typical range [1.698(4) – 1.75(1) Å] of oxo-free rhenium(V) compounds containing linear phenylimido Re≡N bonds [**39-43]**. As expected, the neutral sp^2 N2 atom affords a longer rhenium coordination bond [2.150(2) Å] of **3** in comparison to the Re=N bent imido and the deprotonated Re-$N_{pyrrole}$ [2.092(5) Å] bonds. The Re-P bond length of **3** is 2.412(1) Å and has a comparable bond distance to *trans*-[Re(apd)Br(aor)$(PPh_3)_2$] (apd = 5-

imidopyrimidine-2,4-dione) (aor = 5-aminoorotic acid) with an Re-P bond length of 2.456(7) Å [**44**].

Evaluating the pyprm chelator of **2**, it can be clearly established that the bond order of the C14-N2 [1.315(3) Å] bond is the same as its cyclic C=N bonds of pyridine [C15-N3 = 1.357(3) Å and C16-N3 = 1.344(3) Å] and the imino bond of **3** [C5-N2 = 1.335(7) Å]. Furthermore, the flexibility of the N2-C11-N3 bond angle of **1** affirms that all the bonds connected to the C11 atom are single. Consequently, the benzothiazole and naphthalene moieties form a dihedral angle of 72.96°. In addition, the benzothiazole and naphthalene moieties lies out of the mean C1C3N2N1 basal plane by 21.51° and 73.76°, respectively. Indicative to **1**, the influence of the aliphatic imino moiety is emphasized by the deviation of the pyrrole and naphthalene moieties out of the mean Br1N3N2N1 basal plane by 11.90° and 8.85°, respectively while the aforementioned moieties form a dihedral angle of 20.15°.

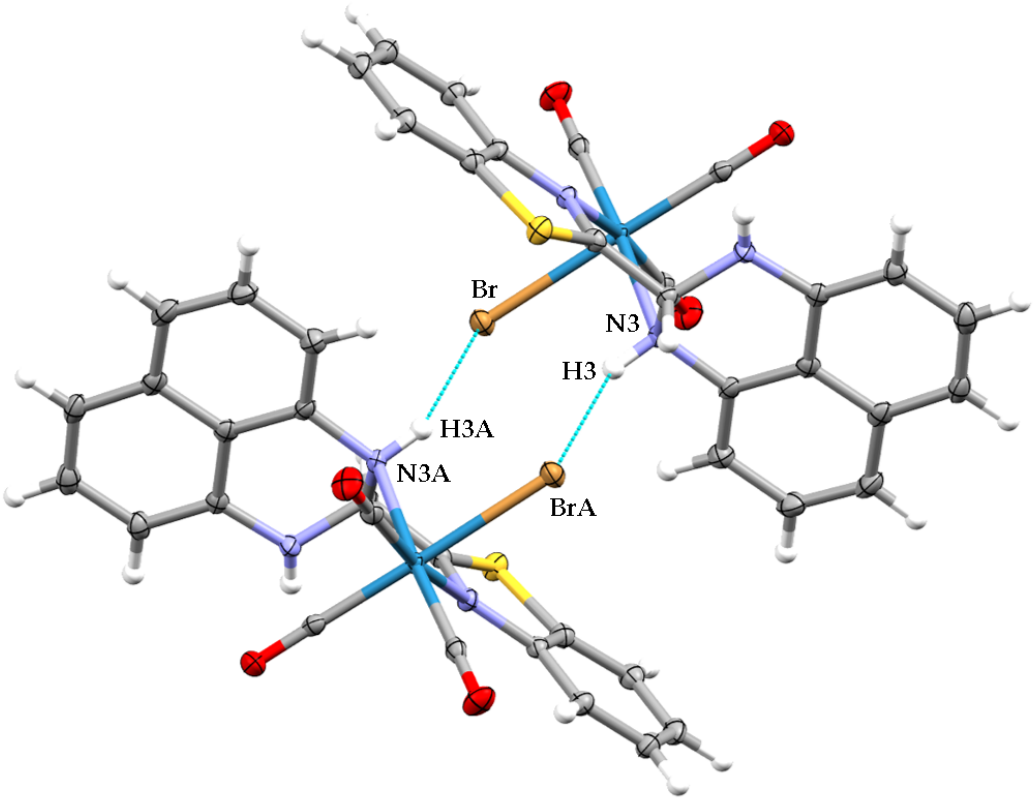

Fig. 4.15: *A perspective view of the dimer of* ***1*** *formed by hydrogen bonding interactions:*

N3-H3···BrA/N3A-H3A···Br = 2.85(3) Å.

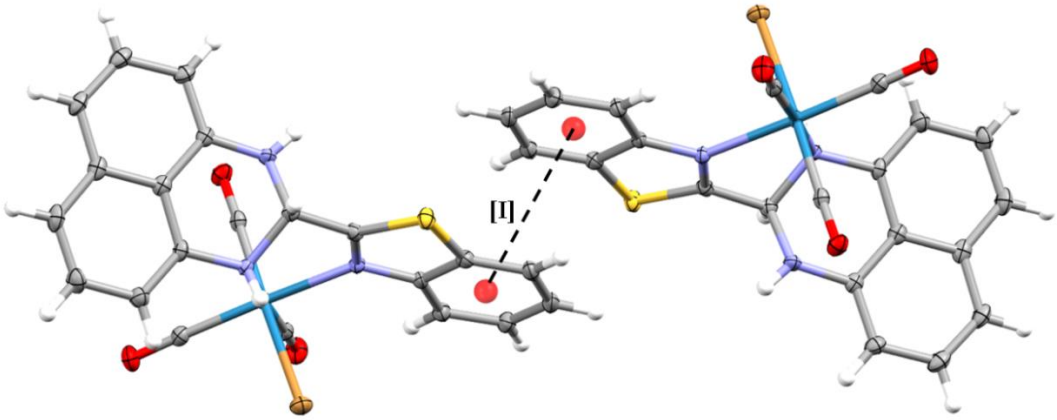

Fig. 4.16: *An illustration showing the nearly co-planar benzothiazole moieties of adjacent molecules with a centroid-to-centroid distance of 3.859 Å, denoted as* ***[I]****.*

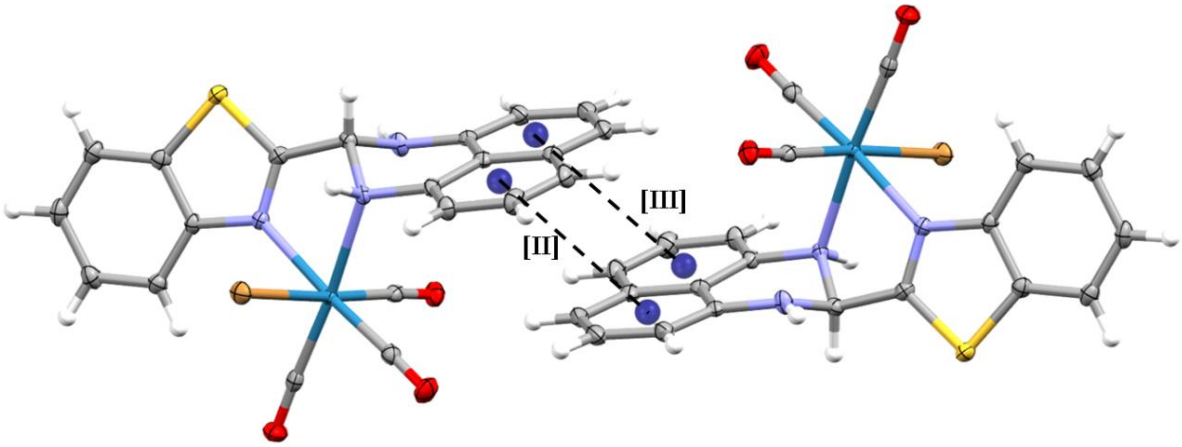

Fig. 4.17: *An illustration showing the nearly co-planar perimidine moieties of adjacent molecules with a centroid-to-centroid distance of 4.133 Å, denoted as* ***[II]*** *and* ***[III]****.*

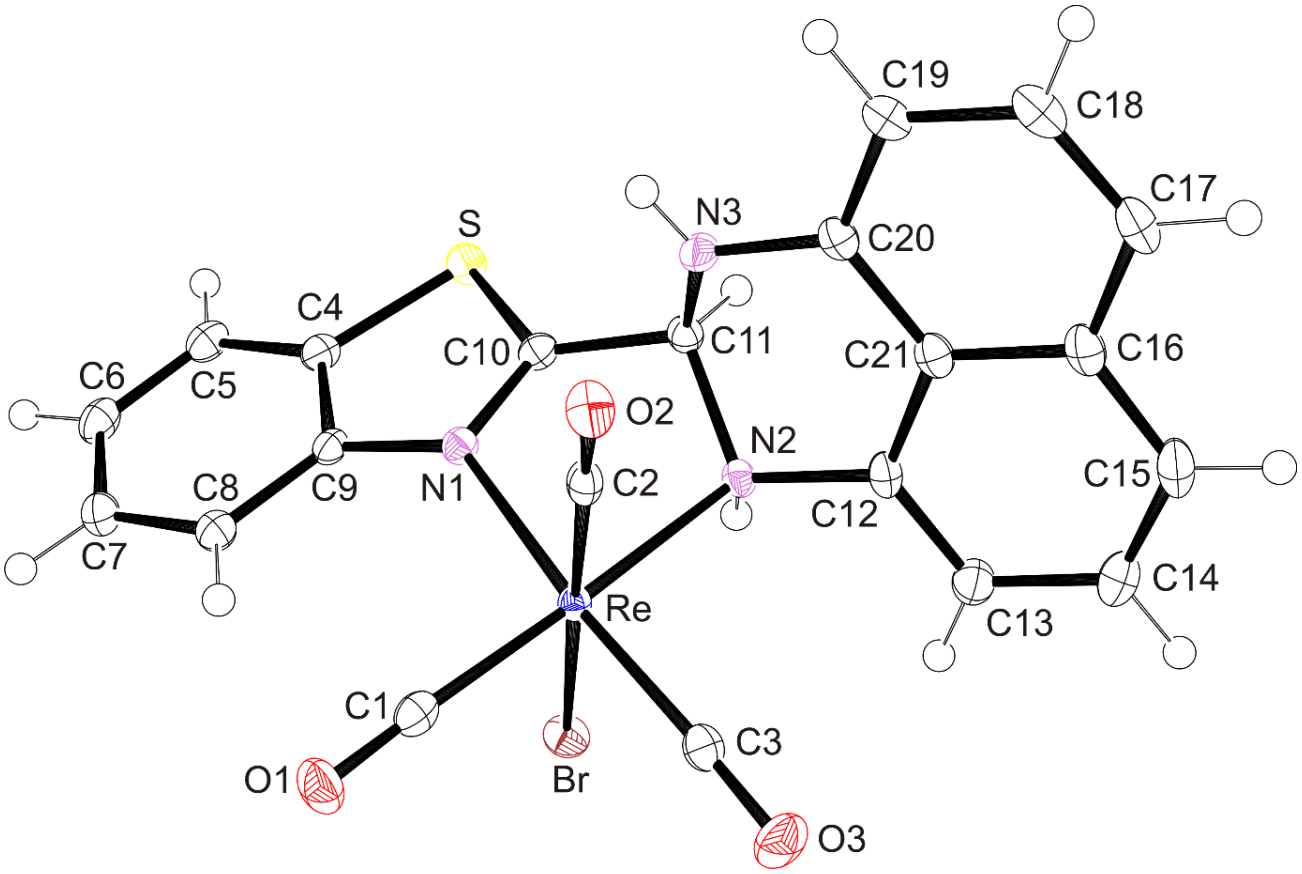

Fig. 4.18: *Thermal ellipsoid diagram (50% probability surfaces) and atom numbering scheme for the X-ray structure of fac-[Re(CO)$_3$(bzpm)Br](**1**).*

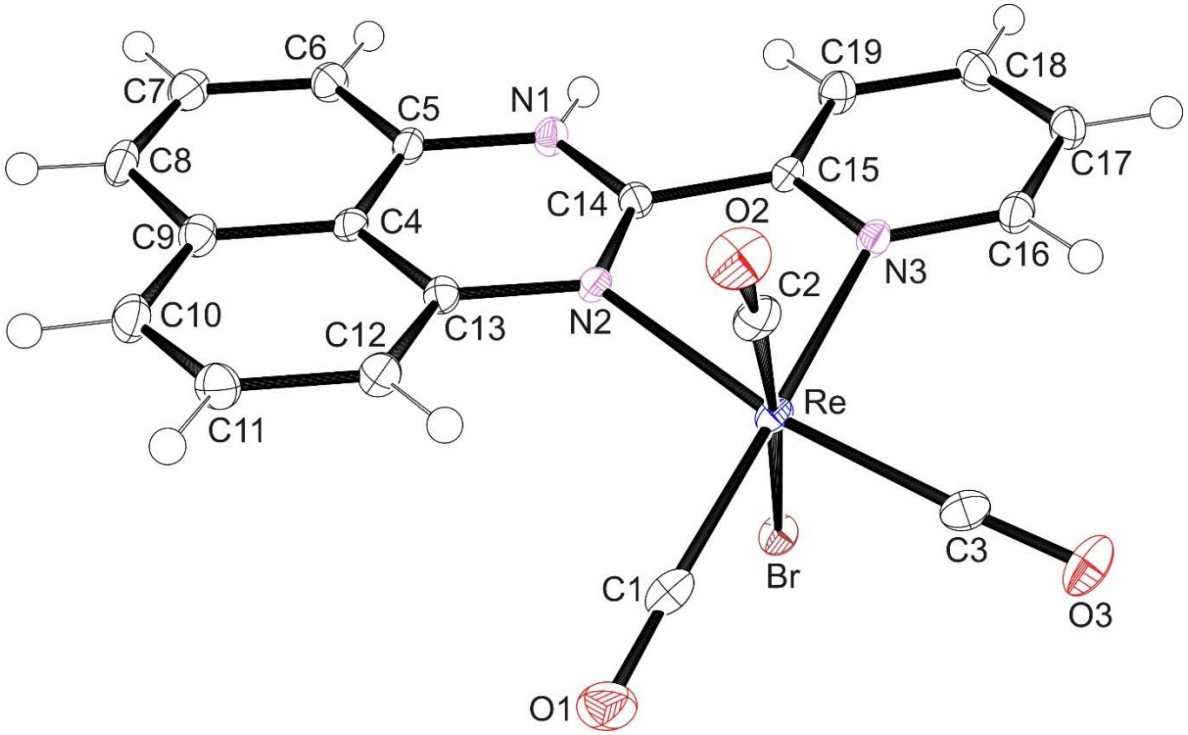

Fig. 4.19: *Thermal ellipsoid diagram (50% probability surfaces) and atom numbering scheme for the X-ray structure of fac-[Re(CO)$_3$(pypm)Br]*(**2**).

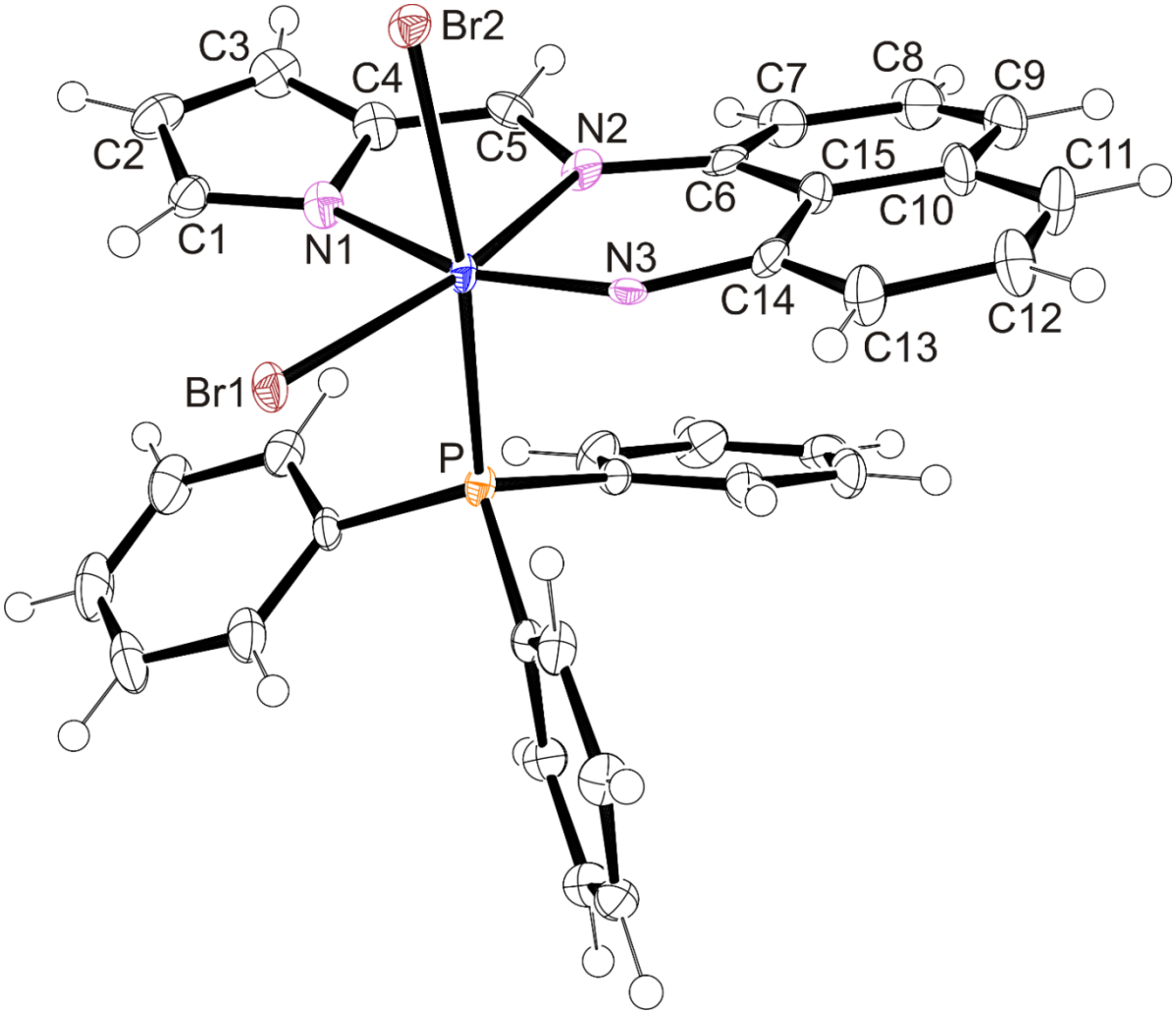

Fig. 4.20: *Thermal ellipsoid diagram (50% probability surfaces) and atom numbering scheme for the X-ray structure of cis-[Re(pyrnp)Br$_2$(PPh$_3$)]*(**3**).

4.5 References:

[1] Y. Junfeng, Y. Duanzhi, M. Xiaofeng, G. Zili, Z. Jiong, W. Yonxian, F.F. Knapp Jr, *Nucl. Med. Bio.* 26 (1999) 573.

[2] V. Sathish, E. Babu, A. Ramdass, Z. Lu, M. Velayudham, P. Thanasekaran, K. Lu, S. Rajagopal, *Talanta* 130 (2014) 274.

[3] J.R. Sorenson, *J. Met. Ions Biol.Syst.* Marcel Dekker: New York 14 (1976).

[4] R. Alberto, J.A. McCleverty, T.J. Meyer, Ionic Interactions in Natural synthetic Macromolecules, *Elsevier, Oxford* 5 (2004) 127.

[5] H. Ni, C. Yu, S. Chen, L. Chen, C. Lin, W. Lee, C. Chuang, C. Ho, C. Chih-Hsien, T. Lee, *Appl. Radiat. Isot.* 99 (2015) 117.

[6] L. Fuks, E. Gniazdowska, P.Kozminski, M.Lycziko, J. Mieczkowski, J. Narbutt, *Appl. Radiat. Isot.* 68 (2010) 90.

[7] M. Papadopoulos, C. Tsoukalas, I. Pirmettis, B. Nock, T. Maina, Z. Abedin, C.P. Raptopoulou, A. Terzis, E. Chiotellis, *Inorg. Chim. Acta* 285 (1999) 97.

[8] D.J. Hayne, A.J. North, M. Fodero-Tayoletti, J.M. White, L.W. Hung, A. Rigopoulos, C.A. Maclean, P.A. Adlard, U. Ackerman, H. Tochon-Danguy, V.L. Villemagne, K.J. Bamhamb, P.S. Donnelly, *Dalton Trans.* 44 (2015) 4933.

[9] J.W. Steed, D.A. Tocher, *Polyhedron* 13 (1994) 167.

[10] M. Hasanzandeh, N. Shadjou, *Mater. Sci. Eng. C*. 61 (2016) 1002.

[11] M. Azama, I. Warada, S.I. Resayesa, N. Alzagria, M.R. Khana, R. Pallepogub, S. Dwivedic, J. Musarratd, M. Shakire. *J. Mol. Struct.* 1047 (2013) 48.

[12] S.P. Singh, S. Seghal, *Indian J. Chem*. 27 (1988) 941.

[13] W. Wilkerson, R.A. Copeland, M. Covington, J.M. Trzaskos, *J. Med. Chem.* 38 (1995) 3895.

[14] H. Lee, J. Lee, S. Lee, S. Lee, Y. Shin, W. Jung, J.H. Kim, K. Park, K. Kim, H.S. Cho, J.S. Koh, *Bioorg. Med. Chem. Lett.* 11 (2001), 3069.

[15] R. Garamvölgyi, J. Dobos, A. Sipos, S. Boros, E. Illyés, F. Baska, L. Kékesi, I. Szabadkai, C. Szántai-Kis, G. Kéri, L. Őrfi, *Eur. J. Med. Chem.* (2016), doi: 10.1016/j.ejmech.2015.12.001.

[16] J.A.S. Smellie, R.M Paton, *Tetrahedron Lett.* 50 (2009) 4104.

[17] Bruker APEX2, SAINT and SADABS. Bruker AXS Inc. (2010) Madison, Wisconsin, USA

[18] R.H. Blessing, *Acta Cryst.* A51 (1995) 33.

[19] G.M. Sheldrick, *Acta Cryst.* A64 (2008) 112.

[20] L.J. Farrugia, *J. Appl. Cryst.* 45 (2012) 849.

[21] I.N. Booysen, M.B. Ismail, O.Q. Munro, *Inorg. Chem. Comm.* 30 (2013) 168.

[22] B. Terfassa, J.A. Schachner, P. Traar, F. Belaj, N.C. Mösch Zanetti, *Polyhedron* 75 (2014) 141.

[23] B. Machura, M. Wolff, E. Benoist, J.A. Schachner, N.C. Mosch-Zanetti, K. Takao, Y. Ikeda, *Polyhedron* 69 (2014) 205.

[24] B. Machura, M. Wolff, W. Cieslik, R. Musioł, *Polyhedron* 51 (2013) 263.

[25] A. Bhattacharya, J.P. Naskar, S. Majumder, R. Ganguly, P. Mitra, S. Chowdhury, *Inorg. Chim. Acta* 425 (2015) 124.

[26] P. Mayer, E. Hosten, T.I.A. Gerber, I. Booysen, *J. Iran. Chem. Soc.*, 7 (2010) 775.

[27] M.T. Ahmet, B. Coutinho, J.R. Dilworth, J.R. Miller, S.J. Parrott, Y. Zheng, *Polyhedron* 15 (1996) 2041.

[28] T.I.A. Gerber, D. Luzipo, P. Mayer, *J. Coord. Chem*. 59 (2006) 1149.

[29] T.I.A. Gerber, D.G. Luzipo, P. Mayer, *J. Coord. Chem*., 59 (2006) 1801.

[30] M. Sirajuddin, S. Ali, A. Badshah, *J. Photochem. Photobio. B* 124 (2013) 1.

[31] M. Kaplanis, G. Stamatakis, V.D. Papakonstantinou, M. Paravatou-Petsotas, C.A. Demopoulos, C.A. Mitsopoulou, *J. Inorg. Biochem.* 135 (2014) 1.

[32] T.E. Kydonaki, E. Tsoukas, F. Mendes, A.G. Hatzidimitriou, A. Paulo, L.C. Papadopoulou, D. Papagiannopoulou, G. Psomas, *J. Inorg. Biochem.* (2015) doi.org/10.1016/j.jinorgbio.2015.12.010.

[33] L.A. Mullice, R.H. Laye, L.P. Harding, N.J. Buurma, S.J.A. Pope, *New J. Chem.* 32 (2008) 2140.

[34] D. Ma, C. Che, F. Siu, M. Yang, K. Wong, *Inorg. Chem.* 46 (2007) 740.

[35] C.R. Groom, F.H. Allen, *Angew. Chem. Int. Ed.* 53 (2014) 662.

[36] I. N. Booysen, T.I.A. Gerber, P. Mayer, *Inorg. Chim. Acta* 363 (2010) 1292.

[37] K. Potgieter, P. Mayer, T.I.A. Gerber, N. Yumata, E. Hosten, I.N. Booysen, R. Betz, M. Ismail, B. Van Brecht. *Polyhedron* 49 (2013) 67.

[38] T.R. Hayes, B.B. Kasten, C.L. Barnes, P.D. Benny, *Dalton Trans.* 19 (2014) 6998.

[39] G. Bandoli, T.I.A. Gerber, J. Perils, J.G.H. du Preez, *lnorg. Chim. Acta* 278 (1998) 96.

[40] X. Schoultz, T.I.A. Gerber, E. Hosten, R. Betz, L. Rhyman, P. Ramasami, *Polyhedron* 96 (2015) 6.

[41] C.S. Masui, J.M. Mayer, *lnorg. Chim. Acta* 251 (1996) 325.

[42] B. Machura, I Gryca, *Polyhedron* 53 (2013) 8.

[43] T.I.A. Gerber, D.G. Luzipo, P. Mayer, *J. Coord Chem.* 2016 (59) 1515.

[44] J. Mukiza, T.I.A. Gerber, E.C. Hosten. *Inorg. Chem. Comm.* 57 (2015) 54.

Table 1: *Crystal data and structure refinement data.*

	1	**2**	**3**
Chemical formula	$C_{21}H_{13}BrN_3O_3ReS$	$C_{19}H_{11}BrN_3O_3Re$	$C_{33}H_{25}Br_2N_3PRe$
Formula weight	653.51	595.42	840.55
Temperature (K)	100(2)	100(2)	100(2)
Crystal system	Triclinic	Monoclinic	Triclinic
Space group	P-1	$P2_1/n$	P-1
Unit cell dimensions (Å, °)	a = 10.1444(7)	a = 15.262(5)	a = 10.2487(8)
	b = 10.9671(8)	b = 7.381(5)	b = 11.2932(8)
	c = 12.3715(8)	c = 19.557(5)	c = 15.0028(12)
	α = 100.677(3)	α = 90.000(5)	α = 89.578(3)
	β = 111.580(3)	β = 98.023(5)	β = 80.338(4)
	γ = 98.694(3)	γ = 90.000(5)	γ = 71.229(3)
V(Å^3)	1220.99(15)	2181.51	1620.9(2)
Z	2	4	2
Density (calc.) (Mg/m^3)	1.778	1.813	1.722
Absorption coefficient (mm^{-1})	6.72	7.42	6.29
F(000)	620	1120	808
θ range for data collection (deg)	1.8; 28.0	1.6; 30.1	1.4; 29.2
Reflections measured	19909	25474	29760
Observed reflections [I>2σ(I)]	5844	6387	8626
Independent reflections	5520	5651	7585
Data/Restraints/parameters	5520/0/279	5651/0/248	7585/0/361
Goodness of fit on F^2	1.015	0.989	1.066
Observed R, wR^2	0.018; 0.042	0.023; 0.052	0.054; 0.155
R_{int}	0.023	0.037	0.055

Table 2: *Selected bond lengths [Å] and bond angles [°] for* ***1****.*

Re-Br	2.622(2)
Re-C1	1.914(2)
Re-C2	1.912(3)
Re-C3	1.918(3)
Re-N1	2.207(2)
Re-N2	2.257(2)
N1-Re-N2	74.56(8)

Table 3: *Selected bond lengths [Å] and bond angles [°] for* **2***.*

Re-Br	2.6319(6)
Re-C1	1.913(2)
Re-C2	1.904(2)
Re-C3	1.914(3)
Re-N2	2.198(2)
Re-N3	2.170(2)
C14-N2	1.315(3)
C15-N3	1.357(3)
C16-N3	1.344(3)
N2-Re-N3	73.92(8)

Chapter 5
Conclusions and Futurework

In this research study, the coordination susceptibility of N-donor heterocyclic multidentate chelators incorporating various biologically relevant moieties (*viz.* chromone, benzothiazole, perimidine and pyrrole) have been explored towards either the *fac*-$[Re^{I}(CO)_3]^{+}$or $[Re^{V}O]^{3+}$ cores. The isolated metal complexes were characterized *via* NMR-, IR- and UV-Vis spectroscopy and conductivity measurements. Single crystal X-ray analysis provided definitive confirmations of the structural elucidations of the respective metal complexes. The coordination chemistry was complemented by DFT and DNA binding studies.

More specifically in chapter 3, reports the coordination chemistry of the ligands chret and chb to Re to afforded the di- and mononuclear rhenium(I) compounds: *fac*-$(Re(CO)_3Br)_2(\mu$-chret) (**2**) and *fac*-$[Re(CO)_3$(bzch)Br] (**3**) respectively. However, in an attempt to isolate the diimine, 3,5-*bis*-(3-methylimino-chromone)-1*H*-1, 2, 4-triazole (prchr) in the presence of trifluoro acetic acid; a novel ligand, chrpychr was inadvertently isolated. Subsequently, the 1:1 molar reaction between chrpychr and $[Re(CO)_5Br]$ led to the formation of the rhenium(I) complex, *fac*-$[Re(CO)_3$(chrpychr)Br] (**1**) in low yield. The interpretation of the IR spectra of the metal compounds (**1**-**3**) was supported by their simulated spectra data calculated at the DFT level of theory. X-ray studies concurred with the spectroscopic characterization, revealing the metal-induced transformation of the chb diimine into the bzch chelator (in **3**). It also affirmed the bidentate coordination modes of the, chrpychr (in **1**), chb (in **2**) and bzch (in **3**) to form new octahedral Re complexes. In addition, the 6-membered chelate rings of complex 1-3 had a significant influence on the octahedral geometries.

Furthermore in chapter 4, novel perimidine rhenium(I) and –(V) complexes were spectroscopically characterized and single crystal X-ray analysis revealed that their respective Re atom is in the centre of a distorted octahedrons for each complex imposed on by their individual constrained chelate bite angles. They form five-membered chelates in contrast to six-membered rings for complexes discussed in chapter 3.CT-DNA titrations conducted with *fac*-[$Re(CO)_3$(bzpm)Br](**1**) and *fac*-[$Re(CO)_3$(pypm)Br](**2**) suggested that they are partial DNA interchelators facilitated by *pi*-conjugated moeities within their respective chelators while the bulky triphenylphosphine co-ligand of *cis*-[Re(pyrnp)$Br_2(PPh_3)$](**3**) induced limited interaction between the CT-DNA and complex **3**.

It is envisage that this work will be expanded by utilizing different biological moeities appended to the 1, 3-dihydroperimidine core, see **Figure 6.1.** Plausible biologically relevant moeities could include the secondary metabolite, chromone and 1,3,7-trimethyllumazine which is a derivative of the enzyme, Lumazine synthase [**1**, **2**]. The scope of the research study will also be expanded by exploring the anticancer properties of the formulated metal complexes against various cancer cell lines. In addition, Gel Electrophorises and DNA binding studies will be conducted on all the metal complexes to provide insight into their modes of interactions with DNA.

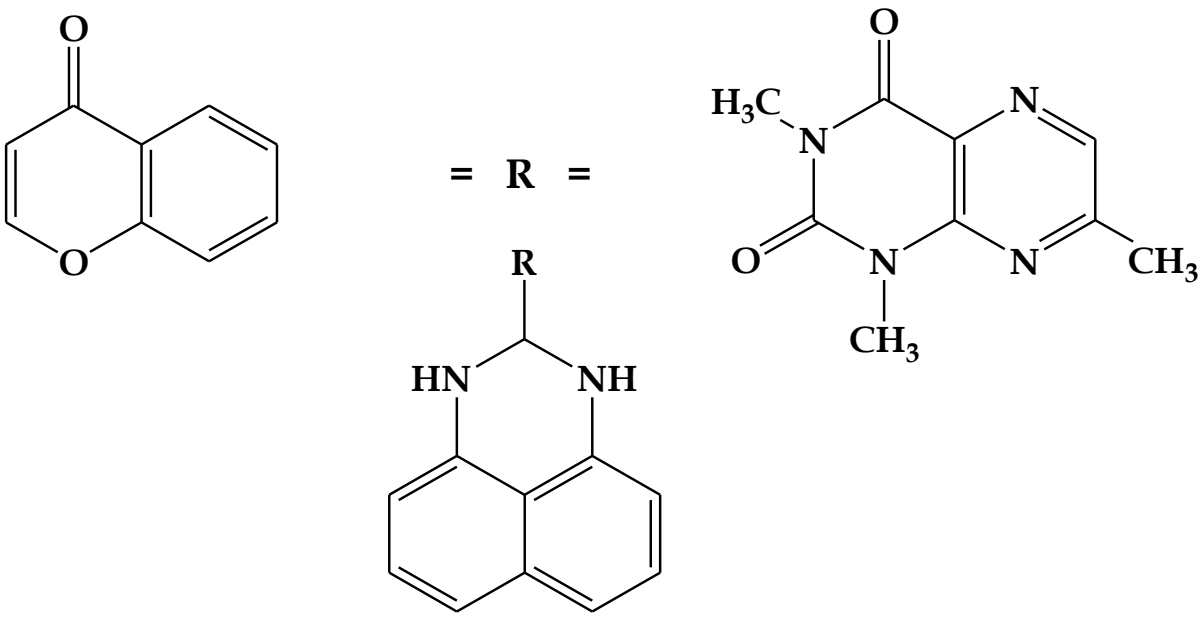

Figure 6.1: *Generic structure of the proposed new perimidine ligands where the appended **R** groups can be the biologically relevant moieties: chromone or 1, 3, 7-trimethyllumazine.*

References:

[1] Adewole L. Okunade, M. P. F. Elvin-Lewis, W. H. Lewis, *Phytochemistry* 65 (2004) 1017–1032.

[2] E. R. A. Cueva, R. Faure, S. B. Jimenez-Pulido, M. N. Moreno-Carretero, Tomas Pena-Ruiz. *J. Mol. Struct.* 697 (2004) 65–71.